Light propagation in tuneable nonlinear periodic photonic structures

A thesis submitted for the degree
of Doctor of Philosophy of
The Australian National University

Francis H. Bennet

August 2011

ANU

THE AUSTRALIAN NATIONAL UNIVERSITY

Light propagation in tuneable nonlinear periodic photonic structures

A thesis submitted for the degree
of Doctor of Philosophy of
The Australian National University

August 2012

Declaration

This thesis is an account of research undertaken in the Nonlinear Physics Centre, within the Research School of Physics and Engineering in the College of Physical Sciences and Mathematics at the Australian National University, between January 2007 and March 2011 while I was enrolled in the degree of Doctor of Philosophy. The research has been conducted under the supervision of Dr. Dragomir N. Neshev, Professor Wieslaw Z. Krolikowski and under advisement from Dr. Andrey A. Sukhorukov.

I declare that, unless specifically stated otherwise, the material presented within this thesis is my own and has never been submitted for any degree at this or any other institution of learning.

Francis Bennet

Francis H. Bennet August 2011

Refereed Publications

1. V. E. Lobanov , A. A. Kalinovich , A. P. Sukhorukov , **F. Bennet** and D. Neshev *"Nonlinear reflection of optical beams in the media with a thermal nonlinearity"* Laser Phys., **19**, 1112-1116, (2009)

2. P. D. Rasmussen, **F. H. Bennet**, D. N. Neshev, A A. Sukhorukov, C. R. Rosberg, W. Krolikowski, O. Bang, and Y. S. Kivshar, *"Observation of two-dimensional nonlocal gap solitons"*, Opt. Lett., **34**, 295-297, (2009)

3. **F. H. Bennet** and J. Farnell, *"Waveguide Arrays in Selectively Infiltrated Photonic Crystal"* Opt. Comm., **283**, 4096-4073, (2010)

4. **F. H. Bennet**, I. A. Amuli, A. A. Sukhorukov, W. Krolikowski, D. N. Neshev, and Y. S. Kivshar*"Focusing to defocusing crossover in nonlinear periodic structures"* Opt. Lett., **35**. 3213-3215, (2010)

5. **F. H. Bennet**, T. J. Alexander, F. Haslinger, A. Mitchell, D. N. Neshev, Y. S. Kivshar *"Observation of nonlinear self-trapping of broad beams in defocusing waveguide arrays"* Phys. Rev. Lett., **106**, 093901, (2011)

6. E. Zeller, **F. H. Bennet**, D. N. Neshev and A. Mitchell *"Laminated Air Structured and Fluid Infiltrated Polymer Waveguides"* Photon. Tech. Lett., accepted August 2011

7. **F. H. Bennet**, M. Molina *"Nonlinear light localization around the core of a 'holey' fiber"* Phys. Rev. A, submitted March 2011

Full Text Conference Proceedings

1. **F. H. Bennet**,, C. R. Rosberg, P. D. Rasmussen, A. A. Sukhorukov, O. Bang, D. N. Neshev, W. Krolikowski, Y. S. Kivhsar, *"Nonlocal gap soliton in liquid infiltrated photonic crystal fibres"*, ACOFT, Sydeny 2008, paper 619

2. **F. H. Bennet**,, P. D. Rasmussen, C. R. Rosberg, A. A. Sukhorukov, O. Bang, D. N. Neshev, W. Krolikowski, Y. S. Kivhsar, *"Nonlocal Gap Solitons in Infiltrated Photonic Crystal Fibres"*, Fronteers in Optics, Rochester, NY, USA 2008, OSA Technical Digest (CD) (Optical Society of America), paper FWL5

3. **F. H. Bennet**, J. Farnel, P. D. Rasmussen, A. A. Sukhorukov, O. Bang, W. Krolikowski, D. N. Neshev, Y. S. Kivshar, *"Nonlocal Gap Solitons in Fully and Selectively Liquid Infiltrated Photonic Crystal Fibres"*, Australian Institute of Physics annual Congress, Adelaide 2008, paper 209

4. **F. H. Bennet**, E. Zeller, T. Larter, A. Mitchell, D. N. Neshev, Y. S. Kivhsar, *"Light propagation in novel fluid infiltrated polymer waveguide arrays"*, CLEO Europe and EQEC 2009, Germany, Conference Digest, (Optical Society of America), paper CL_P13

5. E. Zeller, **F. H. Bennet**, D. N. Neshev, W. Krolikowski, Y. S. Kivhsar, A. Mitchell, *"Planar fluid infiltrated waveguide arrays in SU8 epoxy"*, ACOFT, Adelaide 2009

6. **F. H. Bennet**,, I. A. Amuli, D. N. Neshev, A. A. Sukhorukov, W. Krolikowski, Y. S. Kivshar, *"Observation of focusing to defocusing crossover in nonlinear two-dimensional periodic structures"*, ACOFT, Adelaide 2009, paper 224

7. **F. H. Bennet**,, P. D. Rasmussen. A. A. Sukhorukov, O. Bang, E. Zeller, A. Mitchell, D. N. Neshev, W. Krolikowski, Y. S. Kivhsar, *"Nonlocality in infiltrated 1D and 2D periodic structures"*, PECS, Sydney 2009

8. **F. H. Bennet**, I. A. Amuli, D. N. Neshev, A. A. Sukhorukov, W. Krolikowski, Y. S. Kivshar *"Switching from nonlinear beam focusing to defocusing in periodic structures"*, CLE QELSO US, San Jose, CA, USA 2010, OSA Technical Digest (CD) (Optical Society of America), paper QMC2

9. **F H. Bennet**, T. J. Alexander, F. Haslinger, A. Mitchell, D. N. Neshev and Y. S. Kivshar, *"Observation of truncated bloch wave solitons in $LiNbO_3$ waveguide arrays"*, Australian Institute of Physics Congress, Melbourne 2010, paper 1427

10. **F H. Bennet**, T. J. Alexander, F. Haslinger, A. Mitchell, D. N. Neshev and Y. S. Kivshar, *"Nonlinear self-trapping of broad beams in lithium niobate waveguide arrays"*, CLEO US, Baltimore, ML, USA 2011, paper QMD2

11. **F H. Bennet**, T. J. Alexander, F. Haslinger, A. Mitchell, D. N. Neshev and Y. S. Kivshar, *"Self-trapping of broad beams in defocusing nonlinear Lithium Niobate waveguide arrays"*, CLEO Europe, Münich, Germany, 2011, paper EF5.4

Other Refereed Publications

1. C. R. Rosberg, **F. H. Bennet**, D. N. Neshev, P. D. Rasmussen, O. Bang, W. Krolikowski, A. Bjarklev, and Y. S. Kivshar, *"Tunable diffraction and self- defocusing in liquid-filled photonic crystal fibers,"* Opt. Express **15**, 12145- 12150 (2007).

2. **F. H. Bennet**, C. R. Rosberg, D N. Neshev, P. D. Rasmussen, O. Bang, W. Z. Krolikowski, A. O. Bjarklev, Y. S. Kivshar, *"Temporal nonlinear beam dynamics in infiltrated photonic-crystal fibers"* SPIE Symposium on Microelectronics, MEMS, and Nanotechnology 5-7 December 2007 Australian National University 2007 Paper Number: 6801-60.

Acknowledgements

I would like to thank my supervisory panel, Dr. Dragomir Neshev, Professor Wieslaw Krolikowski, and advisor Dr. Andrey Sukhorukov for their support and encouragement throughout my student life with the Nonlinear Physics Centre. Professor Yuri Kivshar as head of this centre provides a clear and concise leadership as well as an abundance of cake to welcome and farewell new members and visitors.

Thanks to all the staff and students at the Nonlinear Physics Centre, who make working here a pleasure. The social atmosphere and casual interaction between staff and students allows for the flow of ideas and information throughout the centre. This environment nurtures creative problem solving and high quality research. I would like to thank Ms. Kathleen Hicks for her tireless efforts as our departmental administrator, without whom no conference would see a member from the Nonlinear Physics Centre.

Dr. Dragomir Neshev has provided a particularly nurturing environment for me during my time with NLPC, which dates over a year before I began my PhD. I would like to thank him for his continued support and acceptance of my often wildly creative approach to problem solving. I would like to thank Professor Wieslaw Krolikowski for his support through my experimental work through his continued encouragement of, and interest in, my work. Dr. Andrey Sukhorukov always provided a wealth of knowledge and support for numerical simulations, I am grateful for his patience and skill while helping me with the development of the algorithms without which this thesis would not be possible.

I would like to thank my predecessor Dr. Christian Rosberg, who helped begin my interest in nonlinear optics in periodic structures while he was supervising my undergraduate studies, as a PhD student himself. I would like to thank other students for their stimulating and insightful conversations, Ms. Kimberly Heenan, Mr. Wei Liu, Ms. Yue Sun, Dr. Steven Lade, Ms. Kirsty Hannam, and my office mate Dr. Alexander Minovich, who had to put up with my comics plastered on our office door.

I would like to thank my family for their love and support, my girlfriend Clair

Abstract

The action of light in periodic structures can be quite different to that in a homogenous medium. For example, while a nonlinear beam will spread out in a medium with a negative nonlinearity, in a periodic structure the beam is focused and a localised state is formed. In this thesis I will show my work on light propagation in tuneable nonlinear periodic photonic structures.

Nature provides us with dazzling displays of periodic photonic structures in the form of butterfly wings, peacock feathers, and opals. How these magnificent natural spectacles work has been a source of great scientific interest since we mastered the modern scientific method.

With new technologies we can utilise periodic photonic structures to control how light propagates, which wavelengths are transmitted or reflected, and how light moves between waveguiding structures. Coupled waveguides provide a platform in which to study the linear and nonlinear light propagation and interaction in periodic photonic structures. Nonlinearity in optics provides a feedback mechanism which allows one beam of light to influence the propagation of another, or even itself. Advancements in our understanding of how light propagates and interacts in nonlinear periodic photonic structures is leading us to new and interesting areas of Physics. It is hoped that one day photons and photonic components can be used in place of electrons in electronic components widely used today. This will propel our computing power and further advance our understanding of the physical universe.

In order to fully understand how light behaves in photonic structures and to make use of nonlinear features to allow light to control light, we first must understand the fundamental interactions of light in linear and nonlinear periodic photonic structures. We must be able to tune the properties of the system to investigate the fundamental behaviour of nonlinear beam propagation.

In this thesis I investigate light propagation in tuneable nonlinear periodic photonic structures. I begin by introducing relevant concepts and ideas necessary to understand my work (Chapter 1). Included in this introduction is theoretical and experimental work I conducted with two interacting beams in a bulk nonlinear liq-

uid (Sec. 1.4.6). I discover that a high power pump beam influences the nonlinear medium in a way which locally alters its refractive index. This alteration occurs due to a change in temperature of the medium caused by absorption of the pump beam and results in the reflection of a probe beam from the pump beam.

I then present my research on the development of two platforms in which liquid is used to guide light in a one-dimensional (1D) periodic array. The first platform is made from photolithographically defined air-filled channels in SU8 polymer (Sec. 2.1). These channels are infiltrated with an index matching oil and the linear diffraction is observed as the temperature of the platform is changed. I find that the discrete diffraction observed matches very well with an accompanying theoretical model of the system, and I am able to estimate the temperature of the liquid in the channels.

The second platform for light propagation in a 1D periodic array is developed using selectively infiltrated Photonic Crystal Fibres (Sec. 2.2). I use a simple method of blocking an inverse pattern with oil on one side of the fibre. The other end of the fibre is then submersed in a reservoir of the infiltrating liquid to fill any unblocked holes. I produce a 1D periodic array in a of coupled waveguides and demonstrate temperature tuneable linear diffraction, and nonlinear defocusing.

I then move on to present my observation of truncated nonlinear Bloch waves in Lithium Niobate waveguide arrays (Sec. 2.3). Such states are excited with a broad Gaussian input beam in a 1D array of coupled nonlinear waveguides. This state is different from well known solitons and nonlinear Bloch modes because it contains features of both: a constant phase across all guiding waveguides characteristic of a nonlinear Bloch wave, with sharp edges otherwise seen in gap solitons. This work is supported by theoretical modelling, and I am able to show that the width of the soliton is dependant only on the width of the input beam, in contrast to discrete or gap solitons who's width depends on the nonlinearity.

Chapter 3 then exhibits my work with liquid infiltrated Photonic Crystal Fibres as a two-dimensional (2D) periodic array of nonlinear waveguides. Firstly I show the existence and excitation conditions of nonlocal gap solitons (Sec. 3.1), where the properties of the system far from the light field influence soliton formation. I find that below a certain refractive index contrast these solitons are no longer excitable and the beam only defocuses. I then present my work on this crossover from focusing to defocusing in nonlinear periodic systems (Sec. 3.2). I show that the bandgap closes before the index contrast reaches zero, and that the system crosses from focusing to defocusing before the bandgap is fully closed.

I will finally discuss my theoretical and experimental work on vortex beams propagating around a surface in a nonlinear hexagonal array (Sec. 3.3). I use liquid infiltrated Photonic Crystal Fibres and propagate a vortex beam around the core

defect of the fibre. I find that nonlinear vortex modes of charge one are unstable and will focus to occupy a single waveguide on the surface of the core using the discrete model. A continuous model shows that linear and nonlinear charge one vortex modes are unstable and result in an asymmetric output. Linear charge three vortex modes show greater stability due to the staggered phase profile of the input beam, while nonlinear charge three vortex modes lose symmetry at the output due to a loss of this phase profile.

I will finish this thesis with conclusions about my work and ideas for future directions this work could take, including specific experimental ideas directly related to this work. I will include some ideas as to the future direction these ideas may provide.

Contents

CHAPTER 1

Introduction to Waveguiding, Periodic Media and Nonlinearity

1.1 Introduction

Light is fundamental to our existence. We experience it every day, use it to navigate, to entertain, to create and to destroy. We can't touch it, or manipulate it directly, but this doesn't mean we can't control its propagation and properties indirectly. We can create waveguides in which to confine light by using materials of differing refractive index. We can coax light to seep from one waveguide into a neighbouring one by placing them sufficiently close. By adding a periodic modulation to the refractive index of our waveguide(s) we can further control how light propagates. We can also use light to control light, which is known as a nonlinear interaction in which a propagating beam of light modifies the medium it is propagating through, which in turn modifies the beam.

Controlling the propagation of light with periodic refractive index modulation and nonlinearity allows us to explore new areas of optics which have analogies in other areas of physics, such as Bose-Einstein Condensates. In this thesis I explore control of light with nonlinear interactions in tuneable nonlinear periodic photonic structures.

The structure of this thesis is illustrated in Fig. 1.1. Physical concepts and previous works are introduced in Chapter 1. Chapter 2 discusses my development and investigation of linear and nonlinear waveguiding in novel 1D periodic arrays, including nonlinearity in Lithium Niobate. Similarly Chapter 3 shows my investigation into linear and nonlinear beam propagation in 2D periodic arrays in liquid infiltrated Photonic Crystal Fibres. Chapter 4 will draw final conclusions and offer an insight into what future directions this work could take.
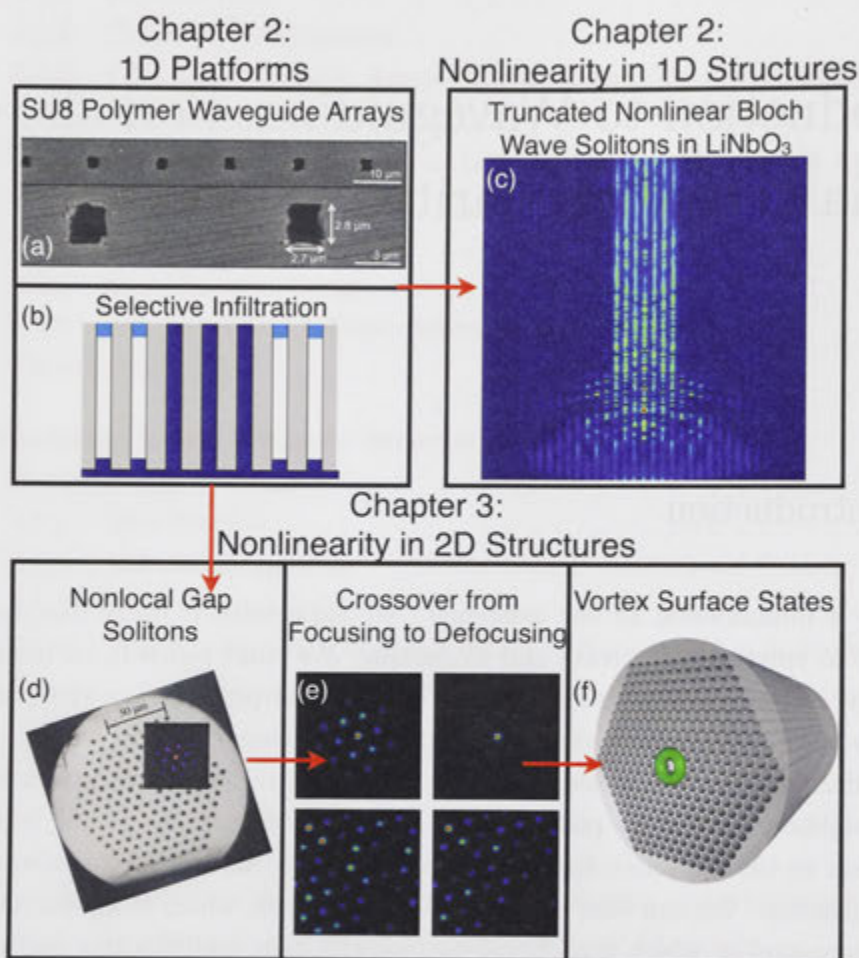
Figure 1.1: Illustration of thesis structure and layout. Chapter 2 discusses the development and testing of 1D platforms in (a) photolithographically defined waveguide arrays in SU8 polymer, and (b) selectively infiltrated Photonic Crystal Fibres. This chapter also presents (c) theoretical and experimental realisation of truncated nonlinear Bloch waves in Lithium Niobate waveguide arrays, as a nonlinear effect in a periodic 1D structure. Chapter 3 presents results from theoretical and experimental work with liquid infiltrated Photonic Crystal Fibres for (d) the observation of nonlocal gap solitons, (e) the crossover from focusing to defocusing nonlinearity, and (f) the investigation of vortex surface states.

1.2 The Physics of Waveguiding

In our everyday experience with light we see photons which are reflected from an object. These photons have traveled in a straight line (known as a ray of light) from an object into our eye. This is known as free space propagation in which light is propagating through a material of constant refractive index, for example air or water. Photons will only travel in a straight line until they are reflected from a surface, or refracted by a change in refractive index. We can hence modify the free space propagation of a ray of light and for example transmit a series of photons around a corner, by using a simple mirror. If we then introduce another mirror further along the path of the now reflected ray of light, we can again modify the propagation of the ray of light. We could have a large number of mirrors arranged such that the ray of light propagates in a circle, eventually returning to the point of origin. Here we have some control over the direction the ray of light, but only in a rudimentary sense: we cannot for example guide two rays of light with slightly different input angles, because they will constantly diverge as they propagate. The perturbed beam will eventually stray from our carefully arranged array of mirrors.

We can however come up with another way in which to guide light. A traditional mirror is made of a silvered metallic surface from which light will reflect. Light can also be reflected from the interface between two materials of differing refractive index. Light moving from one material of refractive index n_1 into another material of index n_2 will obey Snell's law where $n_1 \sin \theta_2 = n_2 \sin \theta_1$. From this equation we can see that an incident ray of light with angle θ_1 will be reflected from the surface when $\theta_2 > \pi/2$. This is known as a critical angle, after which light will be reflected from a surface between two media of refractive indices n_1 and n_2. The refractive index of a material is determined by its relative permittivity ϵ and permeability μ, $n^2 = \epsilon\mu$.

We can now imagine a slab waveguide in which a planar region of higher refractive index is between two regions of lower index. When a ray of light enters the region of higher index with an incidence angle larger than the critical angle it will be reflected from the interface between the higher and lower refractive index materials. The light will be reflected along the slab waveguide until the end and the light can exit. Such waveguides can be curved or even twisted, allowing us to control the propagation of light, and get light to bend around corners without the explicit use of mirrors.

We can now imagine strips of higher index material surrounded by lower index material, allowing us to confine light to an area of the same magnitude as the propagating light's wavelength. Such a device is known as a waveguide. A square or rectangular strip waveguide can be further improved by introducing a higher

3

degree of symmetry and producing a round waveguide, extruded into a cylinder. Such a device is known as an optical fibre, and forms the basis of most of our communications and information technology.

While guiding a coherent beam of light, a waveguide will guide the beam in a number of spatial modes determined by the dimensions of the waveguide and the wavelength of incident light [1]. If we consider a Gaussian beam with a profile $A(z) = A(0)e^{-i\beta z}$ propagating along the z axis of a fibre optic cable, we can determine how the amplitude and phase will vary with propagation by looking at the propagation constant β. In this thesis I only consider real values for β, indicating that we have negligible loss in our guiding systems. The propagation constant can be expressed in terms of effective index of a medium $\beta = n_{eff}k$, where $k = 2\pi/\lambda$ is the wavenumber and n_{eff} is the effective index of the propagating medium.

Light propagating along a waveguide will travel as a combination of bound modes, each mode having a discrete propagation constant [2]. The electric and magnetic components of a propagating mode will be invariant along the propagation direction for a uniform waveguide. A waveguide can support modes of light with different profiles, depending on the waveguide geometry and input conditions. The output of the waveguide will be a linear superposition of all supported bound modes in the waveguide. In this work I consider only the fundamental mode of the studied waveguides, although higher order modes may be mentioned.

Fibre optics guide light in a higher index core surrounded by a lower index cladding. They are thin and flexible, and are usually made from a silica glass. A recent development in fibre optics has yielded another breed of optical fibre, the Photonic Crystal Fibre (PCF). Such fibres consist of either a solid or hollow core surrounded by a periodic array of air filled holes. Light is guided by either the higher index core (index guiding), or by the photonic bandgap effect (bandgap guiding). The periodic nature of the cladding region allows for the study of light propagation in periodic photonic media.

1.2.1   Coupled Waveguides

A discrete mode propagating in a waveguide will extend beyond the waveguide, in the form of an evanescently decaying electric field. A mode in one waveguide will resonate and couple to another nearby waveguide when the propagation constant of the two modes is close enough [3]. A strongly coupled set of waveguides will allow coupling between modes of greater difference in propagation constant than weakly coupled waveguides. It is possible to strongly couple a single mode from one waveguide into another.

Mode coupling is not limited to coupling between two waveguides. By adding

more waveguides in a planar fashion we can create a one dimensional array of coupled waveguides. We can imagine more complicated structures for example two dimensional arrays with square or triangular lattices of coupled waveguides. The modal coupling will occur for any waveguide placed close enough to resonate with a propagating mode. A larger number of waveguides increases the complexity of the system. It is possible to derive a set of equations for the coupling between waveguides in an array in a simple fashion [3], which allows for the calculation of the coupling between modes in an arbitrary system of identical waveguides. If we arrange our waveguides carefully, the transverse refractive index profile will be periodic, further simplifying any coupled mode analysis.

1.3 Periodic Media

A periodic optical medium is one in which there is a periodic modulation of the refractive index in one, two, or three spatial dimensions. In this thesis I focus on one and two dimensional periodic optical media. I define the periodicity to be in the x, y plane, and light propagation to be along the z axis.

A periodic modulation of refractive index in an optical media is known as a photonic crystal, where the periodic nature of the optical properties is analogous to atomic periodicity in crystalline structures. It is logical then to borrow some concepts from solid state physics to describe and model a periodic optical media.

If we consider a set of waveguides in one dimension, we have a transverse refractive index profile, for example resembling a square wave in the x direction. Light entering a single waveguide will couple to the neighbouring waveguides (Sec. 1.2.1). This coupled light will be partially reflected from the surrounding waveguides. As light spreads through the array, reflections from each waveguide will add up in a linear superposition. The reflected rays of light will interfere constructively when their path length difference is an integer multiple of the wavelength. This is a well known phenomenum in solid state physics, and is known as the Bragg law [4]:

$$m\lambda/n_0 = 2d\sin(\theta), \tag{1.1}$$

where m is an integer, λ is the wavelength of light in a vacuum, d is the distance between waveguides, n_0 is the average refractive index, and θ is the incident angle of the input light beam. By tuning any of the properties of such a system one can achieve constructive or destructive interference after some propagation distance. Periodic optical media usually have fixed values for the distance between waveguides. We have ultimate control however over the wavelength of light used, and some control over its input angle. Some types of optical media have a tuneable refractive

index, but for simplicity we will first consider a fixed index contrast.

Light incident on a single waveguide in an array will couple to neighbouring waveguides. As the modes propagate, light will couple further into the array, spreading the light throughout the waveguides. This is known as *discrete diffraction*, and is illustrated in Fig. 1.2. The diffraction can be controlled in an array of waveguides by controlling the coupling between waveguides. Light couples back and forth between the waveguides in the array due to coupling between the individual waveguides and Bragg reflections. We can model a simple one dimensional system using a differential equation which uses the propagation constant (β) and coupling coefficient (C) to transfer light between the waveguides [5]:

$$i\frac{dA_n}{dz} + \beta A_n + C(A_{n-1} + A_{n+1}) = 0, \tag{1.2}$$

where A_n is the amplitude of the propagating mode in waveguide n, and the two neighbouring waveguides have amplitude A_{n-1} and A_{n+1}. β is the propagation constant for the mode being studied, and C is the coupling coefficient between the waveguides $n, n-1$, and $n+1$. We can see that as light propagates along z it will couple to the two neighbouring waveguides (Fig. 1.2). Light in these waveguides in turn couples to their neighbours and the light will eventually spread out to occupy the whole array (Fig. 1.2).

Such coupled mode theory assumes ideal conditions and waveguides, as well as low absorption of propagating waves. Modes excited with transverse electric or transverse magnetic polarisation may also be slightly different. In a real world setting coupled mode theory is only an approximation due to losses through radiation caused by higher order bandgap effects.

While the coupled mode theory (Eq. 1.2) may model simple systems with weak coupling, it becomes difficult to model the full system including bandgap effects, which result from the periodic nature of the material. We can expand our understanding of such a system by moving to a more complete description using the time independent wave equation in the form of the Helmholtz equation:

$$\nabla^2 u(r) - \frac{\omega^2}{c^2}\epsilon(r)u(r) = 0, \tag{1.3}$$

where u is a scalar function representing the components of the electric or magnetic field, c is the speed of light in the medium, ω is the angular frequency of the wave, and $\epsilon(r)$ is the positional dependant permittivity of the material. In a homogenous medium the eigenvalue solutions to this equation are in the form of a plane wave $U(\mathbf{r}) = U_0 \exp(i\mathbf{k} \cdot \mathbf{r})$, where $\mathbf{r} = (x, z)$ is the positional vector, $\mathbf{k} = (k_x, k_z)$ is the plane wave vector where $|\mathbf{k}| = k = 2\pi n/\lambda = n_0 k_0$. We can introduce a transverse wave vector κ to achieve $k^2 = \kappa^2 + \beta^2$, in order to get a diffraction relation $\beta =$
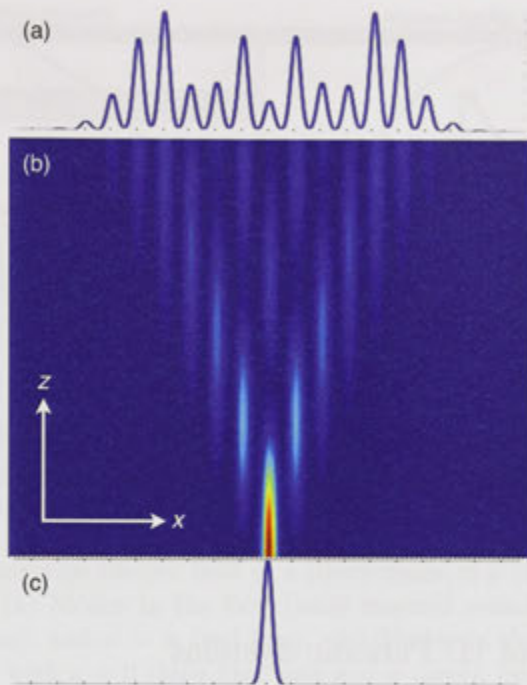
Figure 1.2: (a) Output of a beam having undergone (b) discrete diffraction in a 1D waveguide array. Bragg reflections cause the beam to periodically move through the lattice, causing the (c) input mode to diffract and spread to neighbouring waveguides.

$\sqrt{\kappa^2 + k^2}$. κ and β can now be seen as a basis for the wave vector $\mathbf{k}$ (Fig. 1.3 (a)). We can rearrange this to a more convenient form of the propagation constant using the paraxial approximation where $\kappa \ll k$, giving $\beta = k - \kappa^2/2k$. This is a quadratic relationship in which each corresponding value of β and k represents a plane wave solution with propagation direction and $\mathbf{k}$ normal to the diffraction curve (Fig. 1.3 (a)).

Periodic optical media exist in one, two or three dimensions. Many interesting linear phenomena have been observed in all such systems. For example recently Zhang *et al.* have shown enhancement of discrete diffraction in a 3D optically induced lattice [6], and Szameit *et al.* have shown polychromatic localisation in curved waveguide arrays [7]. Waveguide arrays have also been used as multichannel wavelength-division multiplexers and demultiplexers [8], in which wavelengths are combined or separated respectively, into a single waveguide. I will limit my discussion to relevant structures in one and two dimensions.

Figure 1.3: Illustration of the (a) diffraction relation $\beta(\kappa)$ for a homogenous medium (inset). Gaps appear in the (b) diffraction relation for a periodic optical media (inset), caused by Bragg reflections from the periodic modulation of refractive index.
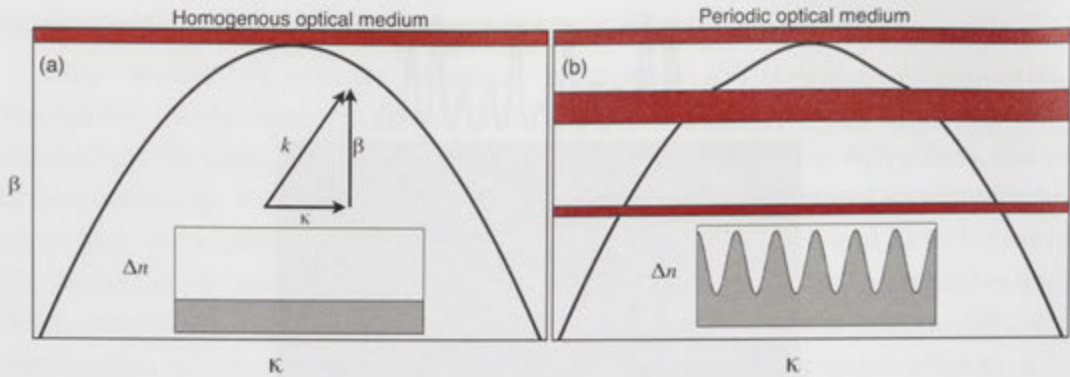
1.3.1 Properties of 1D Periodic Systems

In a 1D periodic optical medium with period (distance between waveguides) d, any eigenmodes of the system should be invariant to a coordinate transform along the axis of periodicity x. The amplitude of the mode, denoted $A_{\kappa_l \beta_l}(x)$ will be periodic such that $A_{\kappa_l \beta_l}(x) = A_{\kappa_l \beta_l}(x + d)$, where the index l denotes the band number. We can now see the eigenmodes of the system will take the form $U(\mathbf{r}) = A_{\kappa_l \beta_l}(x) \exp(i\kappa x + i\beta z)$. Such modes are known as *Bloch modes*, which come from the Floquet-Bloch theorem from solid state physics [4]. Such modes have an infinite spatial extent, and any mode of a periodic system can be expressed as a linear superposition of Bloch modes.

Using the eigenmodes of a 1D periodic system we can determine a diffraction relation $\beta(\kappa)$. Since κ is periodic we only need to look at the diffraction relation in the first Brillouin zone $(-\pi < \kappa < \pi)$ in order to fully understand the system. I define the first Brillouin zone as the region formed by the points which are closer to the origin than to any other vertex of the periodic lattice. When the diffraction relation is plotted one notices discrete jumps in β when κ is an integer multiple of π. These discontinuities correspond to photonic bandgaps, in which modes are forbidden to propagate (Fig. 1.3 (b)). This brings to mind a previous concept discussed in relation to coupling between waveguides (Eq. 1.1), and this is no coincidence! The origin of the photonic bandgaps is the Bragg reflections caused by the periodicity in the refractive index of the medium. If we consider two Bloch modes, with $A_{\kappa_l \beta_l}(x) = A_{\pm \pi_l \beta_l}(x)$, we can see they both propagate with the same wavenumber (π), but in opposite directions. From the Bloch theorem [4] these modes are identical, because they only differ by 2π. At the edge of the Brillouin

8

zone these two Bloch functions are inverted versions of each other, and so have distinct values of β. This leads to the discontinuities of the diffraction relation at the boundary of the Brillouin zone.
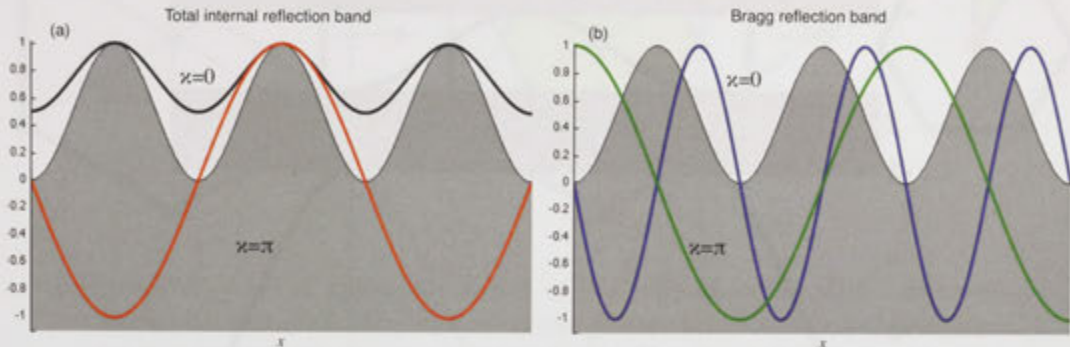

Figure 1.4: Transverse electric field of a Bloch mode in a 1D periodic array of waveguides. (a) Modes in the first (total internal reflection) band with $\kappa = 0$ (black line), and $\kappa = \pi$ (red line). (b) Modes in the second (Bragg reflection) band with $\kappa = 0$ (blue line) and $\kappa = \pi$ (green line). Grey shaded area indicates refractive index contrast.

Photonic bandgaps represent modes which are forbidden to propagate through the periodic system, due to destructive interference from Bragg reflections. There are bands of allowed Bloch modes, numbered 1, 2, 3, etc. Modes propagating in the first band can be described using the coupled mode theory from Eq. 1.2, and are hence the simplest propagating Bloch mode. Modes in the first band can exist with uniform or staggered phase profile. Higher order bands can not be easily modelled using coupled mode theory, and they introduce more complexity into the propagating modes, usually resulting in multimode beam propagation [9].

Fig. 1.4 shows the transverse electric field of modes propagating in the first (Fig. 1.4 (a)) and second band (Fig. 1.4 (b)) at the points $\kappa = 0$ and $\kappa = \pi$ (Fig. 1.5). In the first band (Fig. 1.4 (a)) Bloch modes have maxima in the high index waveguides. The mode at the centre of the band ($\kappa = 0$) has a constant phase across all waveguides and hence is never reduced to zero, meaning there is always some light even in between the waveguides. In contrast to this the mode at the edge of the band ($\kappa = \pi$) has a staggered phase profile, and hence will have a zero electric field component in between each waveguide where light does not exist. Higher order modes exist in the second band (Fig. 1.4 (b)) in a similar way. At the centre of the band ($\kappa = 0$) a second order mode with a zero electric field exists in phase across the waveguides, while at the band edge ($\kappa = \pi$) the mode again has a staggered phase, but in this case the mode also exists in between the higher index waveguides.

The band diagram for these modes in the first and second band is shown in
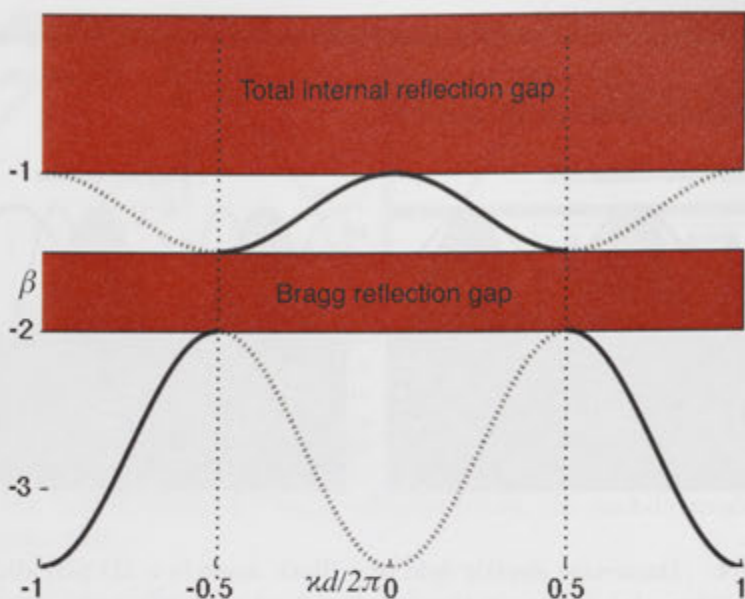
Figure 1.5: Illustration of a band diagram showing the linear diffraction relation $\beta(\kappa)$ in a 1D periodic photonic structure with period d. Shaded areas indicate a bandgap (only two gaps are shown). Transmission bands lie between the gaps, with modes indicated by solid black lines. Modes in the second band (black dotted lines) can be represented in the first Brillouin zone. Vertical dotted lines indicate the boundary of the first Brillouin zone.

Fig. 1.5. The Brillouin zone is indicated by vertical dashed lines. Modes within a transmission band are shown as solid black curves. Modes in the second (lower) band can be represented in the first Brillouin zone (black dotted line in the second band). Similarly modes in the first band can be represented past the Brillouin zone (dotted lines in the first band).

1.3.2 Properties of 2D Periodic Systems

When we introduce another dimension to our periodic structure we will add some more complexity to the system. Bloch modes can be expanded to the 2D case by adding another term for the periodicity in the y dimension and will have the form $U(\mathbf{r}) = A_{\kappa_x l \kappa_y l \beta_l}(x, y) \exp(i\kappa_x x + i\beta z) \exp(i\kappa_y y + i\beta z)$, where $A_{\kappa_x l \kappa_y l \beta_l}(x, y)$ is now periodic in two dimensions, and κ is split into x and y components.

This new dimension of periodicity introduces the possibility for partial bandgaps. Since a mode can now propagate with a new degree of freedom there will be some values for $\beta(\kappa_x, \kappa_y)$ under which a mode is permitted to propagate, while others where it is not. Complete bandgaps may still exist and can be a dominant feature
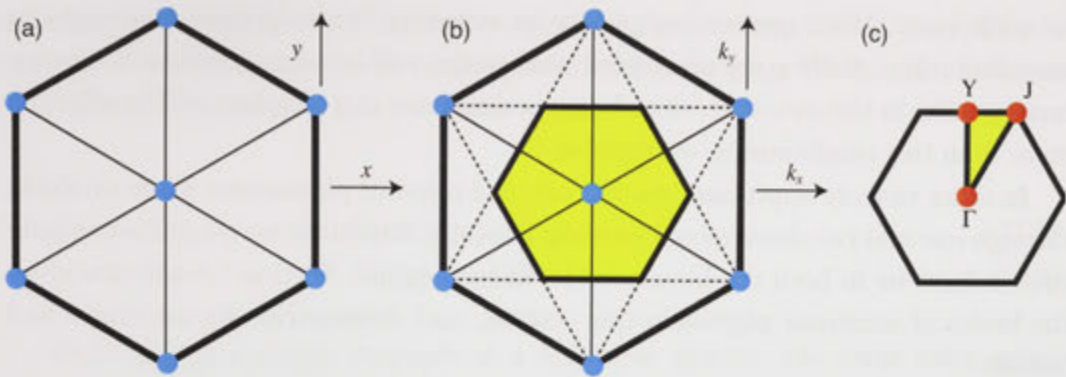
Figure 1.6: (a) A triangular lattice of periodic refractive index produces a hexagonal primitive. (b) The reciprocal lattice (black lines) and Brillouin zone (shaded yellow) are also hexagonal. (c) The irreducible Brillouin zone (shaded yellow) is formed by the triangle of reciprocal lattice points ΓYJ [1].

in some structures.

A common 2D periodic structure is a triangular lattice, making up a hexagonal array (Fig. 1.6(a)) which has the highest degree of symmetry for a 2D lattice. The Brillouin zone is a hexagon (Fig. 1.6(b)) with an irreducible Brillouin zone making up a triangle (Fig. 1.6(c)) from the points ΓYJ. Such symmetry promotes the formation of omnidirectional bandgaps, although partial gaps still exist. Fig. 1.7 shows an illustration of the diffraction relation for a hexagonal lattice. Red shaded regions are partial bandgaps, while the complete bandgap is shaded grey.
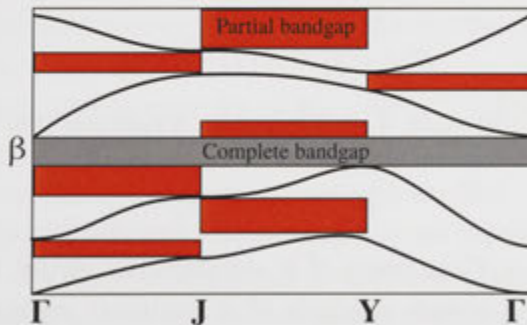
Figure 1.7: An illustration of the complete and partial bandgaps for modes in a hexagonal lattice. Partial gaps are shaded red, while the complete bandgap is shaded grey.

The added complexity of the 2D periodic lattice in comparison to a 1D lattice also introduces a wide range of rich physical phenomena, unavailable in a 1D lattice. Optical structures such as vortices only exist in 2D, and hence cannot be simplified

to a 1D case. With greater complexity in structure comes greater challenges in manufacturing. A 2D array of coupled waveguides will be more sensitive to any inhomogeneity in the structure, since beam propagation and coupling will be effecting more than two neighbouring waveguides.

In order to truly appreciate the full range of physical phenomena made available through one and two dimensional periodic photonic structures we should investigate their behaviour in both the linear and nonlinear regime. Section 1.4 will introduce the basics of nonlinear physics in this context, and demonstrate its usefulness and beauty.

1.4   Nonlinear Physics and Nonlinearity in Optics

Interest began in nonlinear systems in the 1950's with the pioneering work of Fermi, Pasta and Ulam [10], in which they studied the the evolution of particles connected by nonlinear springs. They expected the system to homogenise to a single energy, but instead found a wide variety of interesting dynamics. They found coupling between modes of the system, which is not possible in a linear system. This research sparked an intense interest in nonlinear physics and nonlinear dynamics of nonlinear systems.

A nonlinear system is a system in which a linear superposition no longer applies. A solution cannot be written as a linear combination of independent components. The output of a linear system F will be the simple sum of the individual response to each component of the input x and y:

$$F(x + y) = F(x) + F(y), \tag{1.4}$$

a linear equation will also scale if multiplied by a rational real number α:

$$F(\alpha x) = \alpha F(x). \tag{1.5}$$

A function $F(x) = C$ is linear if it satisfies the above two conditions, and nonlinear otherwise. A simple example of a nonlinear equation is the quadratic equation $x^2 + x - 1 = 0$. We can write $F(x) = C$, where $F(x) = x^2 + x$ and $C = 1$. If we adjust the input x by adding a constant term a we get:

$$F(x + a) = (x + a)^2 + x + a = 1 \tag{1.6}$$
$$F(x + a) = x^2 + a^2 + 2xa + x + a = 1. \tag{1.7}$$

Eq. 1.7 is not a linear superposition of $F(x) + F(a)$ because it contains a term

including both x and a, and hence the equation is nonlinear. A similar outcome is easily observed to result in the same conclusion when trying to scale the function by a rational real number α:

$$F(\alpha x) = (\alpha x)^2 + \alpha x = 1 \qquad (1.8)$$
$$F(\alpha x) = \alpha^2 x^2 + \alpha x = 1. \qquad (1.9)$$

While this is a simple example of a nonlinear system, the same rules apply for more complicated situations. This mathematical distinction gives a clear contrast between linear and nonlinear equations. Such clarity is not always possible in physical systems, which can often contain a combination of linear and nonlinear components. The linear physics used to describe many physical systems is often a first order approximation of a very complex physical system. These first order approximations are perfectly valid when any input or driving forces involved in such a system are small in amplitude. If x and a are sufficiently small such that $x^2 \ll x$ and $a^2 \ll a$ then $xa \ll x + a$, and from Eq. 1.7 and Eq. 1.9 :

$$F(x + a) = x + a = 1 \qquad (1.10)$$
$$F(\alpha x) = \alpha x = 1. \qquad (1.11)$$

This demonstrates a first order approximation when the input amplitudes (x, a, and α) are sufficiently small. If we increase these amplitudes we need to take the higher order and coupled terms (e.g. $2xa$, $\alpha^2 x^2$) into account to fully appreciate the physics in the system.

Nonlinearity adds to the complexity of the system by allowing independent inputs (or variables) to interact. This does more than add complexity to any mathematical model: it allows one variable to interact with another. Our modern day lives rely on electrostatic interactions between electrons in microprocessors and electronic systems. The output of a diode or transistor are inherently nonlinear, which is what makes them so useful. Can this concept of nonlinear interaction be translated to another field of physics, such as optics, and be as useful? Section 1.4.1 and onwards will introduce the concepts of nonlinear optics, in which noninteracting photons are coerced into interacting.

1.4.1   Nonlinearity in Optical Systems

Optics is the study of the propagation of light through optical systems. Light is made of photons, which are noninteracting particles. If they are noninteracting they

13

must be inherently linear, which is also the case with the equations which describe electromagnetic propagation, Maxwell's equations. Photons may not interact with each other, however they do interact with matter. Photons can be absorbed or emitted by an accelerating charge, adding or subtracting energy from the particle the photon interacts with.

The study of optics and optical effects was made possible by the invention of the laser [11]. The coherent light produced by a laster is far superior to other light sources for the study of optical waves and interactions. Nonlinear optics began quite soon after the invention of the laser [12, 13, 14] in the form of damage to silica glass by high intensity lasers. Interest was growing in the phenomena of optical self trapping [15]. Such phenomena require optical nonlinearity, whereby the large electric field of a high intensity laser beam interacts strongly with the atoms of the nonlinear medium through its polarisation density.

If we consider the dipole moment per unit volume of a material, its polarisation density $P(t)$, is defined by an applied electric field E:

$$P(t) = \epsilon_0 \chi^{(1)} E(t), \tag{1.12}$$

where ϵ_0 is the permittivity of vacuum, and χ is the linear electric susceptibility of the medium. This is a first order linear approximation of a more complex system, which can be expanded as a power series of the applied electric field $E(t)$:

$$P(t) = \epsilon_0(\chi^{(1)} E(t) + \chi^{(2)} E^2(t) + \chi^{(3)} E^3(t) + \chi^{(4)} E^4(t) + \cdots). \tag{1.13}$$

The values of $\chi^{(2)}$, $\chi^{(3)}$, and $\chi^{(4)}$ are the second, third, and fourth order susceptibilities, respectively. For simplicity the fields $P(t)$ and $E(t)$ have been taken as scalar quantities. It is possible to treat them as vectors, in which case $\chi^{(1)}$ becomes a second-rank tensor, $\chi^{(2)}$ becomes a third-rank tensor, etc [16]. We also assume that the polarisation at time t only depends on the instantaneous value of the electric field $E(t)$ at that point in time. This implies the medium is lossless and dispersionless. Fig. 1.8 graphically shows the difference between a linear and nonlinear dependance of the polarisation density P on the electric field E. At low values of E (low optical intensity) the linear and nonlinear values of P are identical. As E increases, the difference between the linear and nonlinear values of P increases.

Second order nonlinear optical phenomena are those which are produced by the second order susceptibility of a material. The second order susceptibility $(\chi^{(2)})$ dominates the nonlinear polarisation of non-centrosymmetric crystals [16], those without an inversion symmetry. Examples of second order nonlinear effects are the Electro-Optic effect, three-wave mixing, and second harmonic generation.

14
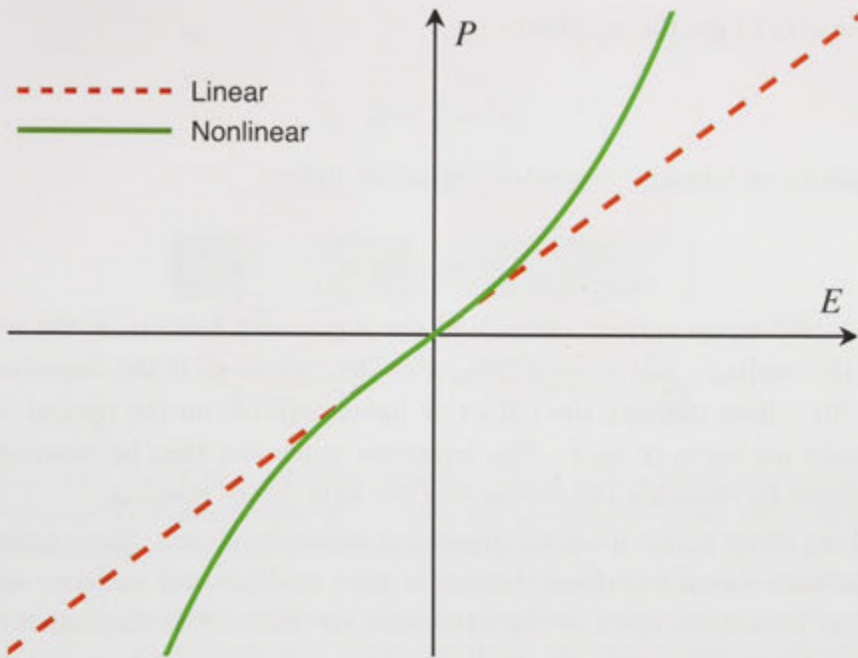
Figure 1.8: Linear (red dashed line) and Nonlinear (green solid line) relationship between the electric field E and polarisation density P.

Higher order nonlinear effects arising from the third order susceptibility ($\chi^{(3)}$) occur in media where the second order susceptibility no longer dominates. Such media are usually amorphous solids, liquids or gasses, since these materials display inversion symmetry, leading to vanishingly small or nonexistent $\chi^{(2)}$. Examples of third order nonlinear effects include the Kerr effect, third harmonic generation, stimulated Raman scattering, and four wave mixing. In this thesis I will limit my discussion to the concepts required to understand my work, the Kerr effect and intensity dependant refractive index change in liquids, as well as the consequences this has on propagating modes. I will also discuss a nonlinearity in Lithium Niobate which can achieve similar nonlinear effects.

1.4.2 The Kerr Effect

A Kerr medium is one in which the third order susceptibility ($\chi^{(3)}$) dominates, and the nonlinear polarisation can be defined as:

$$P_{NL}(t) = \epsilon_0 \chi^{(3)} E^3(t). \tag{1.14}$$

We can use the relation of relative permittivity $\epsilon/\epsilon_0 = 1 + \chi$ and the refractive

index $n^2 = \epsilon/\epsilon_0$ to get the equation:

$$n^2 = 1 + \chi, \tag{1.15}$$

which leads to an intensity dependent refractive index:

$$n = n_0 + n_2 I, \tag{1.16}$$

where $I \sim |E|^2$ is the optical intensity of the input light field, n_0 is the refractive index of the medium, and $n_2 = \chi^{(3)} 3\eta_0/n^2\epsilon_0$ [16], where η_0 is the impedance in a vacuum. In a Kerr medium the refractive index depends on the optical intensity of a propagating beam of light. The refractive index can thus be controlled to a certain degree by changing the intensity of the light in the medium.

The Kerr effect is this intensity dependent refractive index. As a result of this a high intensity beam travelling through a Kerr medium will undergo self-phase modulation, a nonlinear effect in which the refractive index of the medium is changed by a beam of light (Fig. 1.9). Physically the high intensity light beam modifies the polarisation of the medium, leading to a change in the refractive index (Eq. 1.14-1.16) [16]. This modification of the medium in turn alters the optical path length the beam of light experiences, resulting in a phase shift at the output. This is a key feature of the Kerr effect: feedback. A beam of light interacts with the medium, changing the optical properties of the medium. This change in turn changes the propagation of the beam. Such feedback loops can drive some interesting nonlinear phenomena, such as self focusing (Fig. 1.9(b)) and self defocusing (Fig. 1.9(a)), which are both a result of this self phase modulation.

The Kerr effect is a local change in refractive index. The fundamental output of a laser beam will have a Gaussian profile, with a high intensity central region. Hence the centre of a high intensity laser beam propagating in a Kerr medium will produce a locally higher (Fig. 1.9(b)) or lower (Fig. 1.9(a)) refractive index than other parts of the beam.

1.4.3 Positive and Negative Nonlinearity

In a Kerr medium the nonlinear coefficient is n_2. It is convenient to introduce a general nonlinear coefficient γ, which can be used to describe a nonlinearity regardless of its origin. For a Kerr medium $\gamma \propto n_2$. The value for γ can be either positive or negative. A positive γ will increase the refractive index of the medium for a high intensity beam of light, while a negative γ will decrease the refractive index under the same conditions. Fig. 1.10 shows the effect a high intensity Gaussian laser beam will have on a background refractive index of $n = 1.46$ for positive and negative γ.
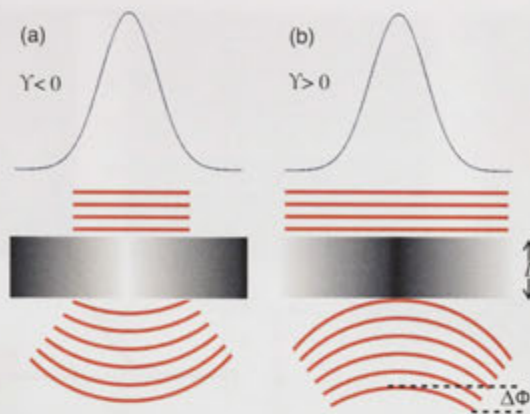
Figure 1.9: (a) A high intensity Gaussian beam with uniform phase profile incident on a nonlinear material of length L with negative nonlinearity causes a phase shift $\Delta\phi$ resulting in the beam defocusing. (b) the same beam incident on a nonlinear material with positive nonlinearity causes a phase shift $\Delta\phi$ resulting in the beam focusing. Blue lines indicate input beam profile, red lines indicate wave fronts of the beam, greyscale indicates change in refractive index caused by the incident beam, white is a lower index than black.

Fig. 1.10(a) and (b) show the Gaussian laser beam mode shape and profile. Fig. 1.10 (c) shows the induced refractive index profile of a nonlinear material with a positive nonlinearity ($\gamma > 0$). The induced refractive index profile is inverted (Fig. 1.10 (d)) for a material with a negative nonlinearity ($\gamma < 0$).

Positive and negative nonlinear coefficients γ give rise to a range of often complimentary and inverse effects. One key example of such inverse behaviour is the phenomena of self focusing and self defocusing in homogenous media. Self focusing is a nonlinear phenomena which occurs in mediums with a positive nonlinearity. The high intensity light of a Gaussian beam causes a local increase in the refractive index (Fig. 1.10(c)). This high index region then acts as a high index waveguide, trapping light. The opposite effect occurs when the nonlinearity is negative. High intensity regions of the beam cause a local *decrease* in the refractive index (Fig. 1.10(d)) which causes the beam to diffract, or defocus, faster than it would in a linear regime.

Fig. 1.11 shows a numerically simulated beam propagating in a nonlinear material. Self trapping (Fig. 1.11(a)) is achieved when the linear diffraction of the beam is balanced by the nonlinear focusing. Fig. 1.11(d) shows how the high intensity regions of the beam cause a local increase the refractive index of a medium with positive nonlinearity ($\gamma > 0$). The beam is then trapped in the high index region it created. Fig. 1.11(f) shows how the high intensity regions of the input beam cause a local decrease in the refractive index of a medium with negative nonlin-
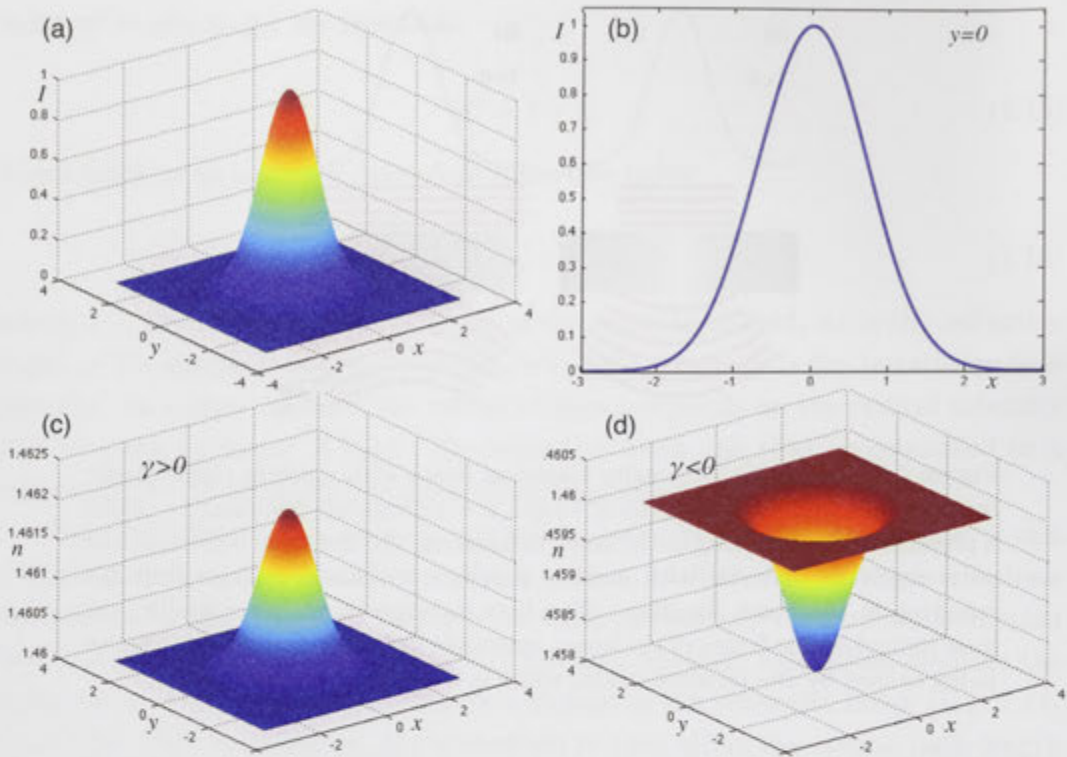
Figure 1.10: (a) A Gaussian laser beam has an intensity $I = \exp(-x^2)$ (b) profile. Such a beam increases the refractive index proportionally to its intensity for a (c) positive nonlinearity, and (d) decreases the refractive index locally for a negative nonlinearity.

earity ($\gamma < 0$). The beam is then repelled from this low index region, diffracting faster (Fig. 1.11(c)) than it otherwise would in a linear medium (Fig. 1.11(b)). Fig. 1.11(e) compares the input ($z = 0$) beam (black line) with the output ($z = 120$) for nonlinear media with positive nonlinearity (red line), negative nonlinearity (green line), and no nonlinearity (blue line).

The origin of self focusing and self defocusing is the intensity dependent refractive index $n(I)$. When passing through a Kerr medium a Gaussian beam with uniform phase will experience self phase modulation in proportion to the intensity of the beam. A Gaussian beam thus experience different phase shifts across the profile of the beam (Fig. 1.9), due to the nonuniform intensity. The phase shift will be $\Delta\phi = (2\pi/\lambda)Ln(I)$, for a beam of wavelength λ propagating through a medium of length L. A beam incident on a medium with negative nonlinearity (Fig. 1.9(a)) will experience a negative phase shift ($n_2 = \gamma < 0$), resulting in the beam defocusing. A similar beam incident on a medium with positive nonlinearity (Fig. 1.9(b)) will experience a positive phase shift ($n_2 = \gamma > 0$), resulting in a focusing of the beam.

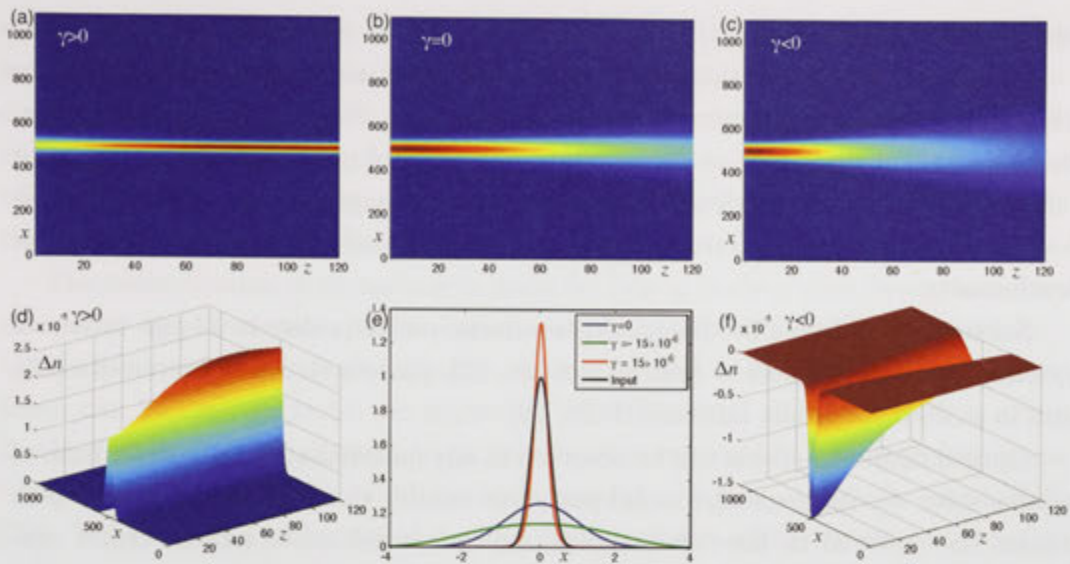Figure 1.11: Propagation of a Gaussian input through a nonlinear medium when γ is (a) positive, (b) zero (a linear medium), and (c) negative. The high intensity light modifies the refractive index, increasing the index (d) when $\gamma > 0$, and decreasing the index (f) when $\gamma < 0$. (e) Output profiles show the difference between the input and the outputs from (a),(b), and (c), where $\gamma = 15 \times 10^{-6}$, $\gamma = 0$, and $\gamma = -15 \times 10^{-6}$ respectively.

It is clear that the sign of the nonlinearity has a drastic effect on the output beam. When a medium has a positive nonlinearity, a high intensity beam propagating through it will experience *self focusing*. In Fig. 1.11(e) it is obvious that the output of such a beam has a higher peak than the input. This does not break any conservation of energy rules because the integral of both curves is in fact identical. Each output has the same integral as the input, as one would expect in a closed system such as this. When the nonlinear focusing exactly balances the linear diffraction otherwise experienced by a propagating beam, the beam can propagate as a *spatial soliton*, in which the profile of the beam doesn't change as it propagates.

The general concept of a soliton was developed when nonlinearity balances linear dispersion of a wave in 1965 [17]. The concept of a soliton has been known since the 1830's when John Scott Russell observed a well defined water wave travelling down a canal without changing its shape. Soliton propagation on bulk nonlinear materials has been observed in nonlinear liquids [18] and silica glass [19], although the high optical intensity required to form the soliton limits any practical application. Pulsed laser and slab waveguides were used to achieve the optical intensity and effective 1D geometry favourable to soliton formation [18, 19]. Spatial optical solitons supported by mutual focusing of a second beam have been studied for Kerr-type [20] and

anisotropic optical media [21].

On the other hand optical solitons in silica fibres received much focus in the 1970's and 1980's for telecommunication purposes [22, 23]. Guided modes are confined to a small silica core and thus require lower total power to achieve nonlinear effects than in a bulk medium. Long propagation lengths of an optical fibre allow for dispersion compensation over a very long distance even with relatively low nonlinearity.

Solitons are indeed a fundamental phenomenon which exists in a large variety of systems, from Bose-Einstein condensates [24, 25], protein chains in biophysics [26], and in periodic photonic lattices [27, 28, 29].

Optical nonlinear effects can be observed in any material with the correct form of nonlinearity. Centrosymmetric solid materials exhibit the Kerr nonlinearity which causes the material to have an intensity dependent refractive index. Other centrosymmetric materials such as liquids and gasses can exhibit the same behaviour without a fundamental Kerr nonlinearity n_2. In these cases the nonlinearity arises from thermal effects.

Materials not exhibiting centrosymmetry can be susceptible to photorefractive nonlinearity, where an applied electric field can produce a charge distribution in the material, locally altering the refractive index.

I utilise materials with both Kerr-type and photorefractive-type nonlinearity. I use liquids with thermal Kerr-type nonlinearity to investigate tuneable periodic photonic structures, and Lithium Niobate to investigate soliton propagation in waveguides with photorefractive nonlinearity.

1.4.4 Photorefractive Nonlinearity

Photorefractive media are usually non-centrosymmetric crystalline materials, and contain a high concentration of weakly bound charge carriers (electrons). These charge carriers can be excited to become mobile by the electric field of a sufficiently high intensity incident light beam. These photo-excited charge carriers non-uniformly redistribute throughout illuminated areas, creating an electric field and altering the local refractive index by Δn through the electro-optic effect $\Delta n = -0.5n^3 r_P E$ for a space-charge electric field E caused by the separation of charges, refractive index n, and Pockels coefficient r_P [1].

Lithium Niobate (LiNbO$_3$) is such a photorefractive crystal, and is widely used in Nonlinear Optics for this reason [30, 31, 32]. Other materials include Potassium Niobate (KNBO$_3$), and Strontium Barium Niobate (SBN). Dopants in these crystals provide a source for mobile charge carriers in the form of donor electrons of acceptor sites for charge recombination. These dopants absorb incident light and generate

mobile electrons, which migrate through the crystal in response to the electric field associated with the illuminating beam. These mobile electrons will eventually re-combine with a dopant centre away from illuminated areas. This constant transfer of charge away from illumination leads to the generation of an electric field inside the crystal. This causes a change in refractive index in regions under illumination, through the electro-optic effect.

The redistribution of charges can remain for long periods of time (hours to days), even after the illuminating beam has been turned off. Since only high intensity beams have a strong enough influence on the medium to mobilise charges, a weak beam can be used to probe the refractive index structure of such a crystal. This has lead to devices which serve as an optical memory, where a high intensity beam 'writes' a refractive index profile into the crystal, which a probe can later 'read' [33]. The memory can be erased by illumination of the whole crystal, resulting in redistribution of charges throughout the crystal.

1.4.5 Nonlinearity in Liquids

The refractive index of many materials (particularly liquids and gases) depends on its density, which in turn depends on the temperature of the material. This is known as the thermo-optic effect, which governs the material's change in refractive index due to a change in temperature ΔT [16]:

$$ n = n_0 + \left(\frac{dn}{dT} \right) \Delta T, \tag{1.17} $$

where n_0 is the refractive index of the material before any temperature change, and T is the temperature of the system. dn/dT is known as the thermo-optic coefficient, which can be either positive or negative and depends on the material. Liquids for example usually have a negative thermo-optic coefficient because of their relation between density, temperature, and refractive index. Liquids typically display an order of magnitude higher thermo-optic coefficient of around 10^{-4} K^{-1} when compared to solids which often exhibit a thermo-optic coefficient around 10^{-5} K^{-1} [16].

The refractive index of a bulk volume of liquid can be controlled globally by changing the temperature of the whole volume, or locally by introducing a local heat source. One way of introducing a heat source is to illuminate part of the liquid with a beam of laser light, of a wavelength which will be slightly absorbed by the liquid. The temperature of the illuminated liquid will be increased due to absorption of a fraction of the propagating light. For the purposes of this thesis I will look at liquids which absorb light with a constant fraction. This is common for many liquids until a very high light intensity, at which point the absorption can

saturate.

Higher intensity regions of a Gaussian beam will result in more photons absorbed, which will lead to a higher change in temperature than lower intensity regions of the beam. This leads once again to an intensity dependent refractive index, since the change in temperature is a function of the intensity $\Delta T(I)$:

$$n(I) = n_0 + \left(\frac{dn}{dT}\right)\Delta T(I), \tag{1.18}$$

where I is the intensity of the propagating beam, n_0 is the refractive index in the absence the beam, and dn/dT is the thermo-optic coefficient.

The intensity induced temperature change $T(I)$ is governed by the heat transport equation:

$$(\rho_0 C)\frac{\partial T}{\partial t} - \kappa_T \nabla^2 T = \alpha I, \tag{1.19}$$

where $\rho_0 C$ is the heat capacity per unit volume, κ_T is the thermal conductivity, α is the linear absorption coefficient, I is the intensity of the propagating light, t is time, and ∇ denotes the partial derivative in each relevant spatial coordinate. While an incident Gaussian laser beam may only heat the liquid locally, this heat will spread through the liquid over time t as defined by Eq. 1.19. For most liquids this heat transport is a relatively slow process, occurring over a timescale of microseconds to milliseconds. Pulsed laser beam will thus be just as effective in heating a liquid along the propagation direction as a continuous wave laser beam. When using a pulsed laser beam the pulse energy will determine the amount of heating in the medium [16].

Such heat transport leads to a refractive index change in regions where the heating laser beam is not present. This is known as a *nonlocal* effect, in which the properties of the system far from the heat source are still under its influence. Nonlocal effects can have a significant impact on a beam propagating in such a medium [34, 35]. These nonlocal effects can be used to create an indirect interaction between two laser beams, allowing one photon to influence another through the use of a nonlinear medium.

1.4.6 Nonlinear Beam Interaction in Bulk Liquids

The interaction between a high intensity beam and an absorbing liquid opens up the possibility for one laser beam to directly influence another. When propagating in a vacuum, photons have no mechanism with which to interact. If however one laser beam modifies a medium for example with a thermal interaction (Eq. 1.19), a second laser beam propagating through the modified medium will be effected by

the first. I investigated this nonlinear interaction for two beams propagating in a bulk liquid, both experimentally and theoretically.

I looked at the interaction between two continuous wave laser beams with wavelengths 532 nm (pump) and 633nm (probe), in a bulk liquid with a negative thermo-optic coefficient. The pump beam generates the nonlinear effect in the liquid, while the probe beam allows us to investigate this induced refractive index change. The liquid used is ethanol, doped with Iodine to absorb 45.5% of 532 nm CW laser light over a distance of 5 cm to enhance the a defocusing nonlinearity of this liquid.

Theoretically I consider the steady-state propagation of two paraxial beams with different frequencies. I and employ a system of equations for slowly-varying amplitudes of optical waves with weak absorption, intensity induced thermal self-action (Eq. 1.18), and heat-conduction equation (Eq. 1.19) which account for the wave-induced heating of the medium with a temperature profile $T(x, y)$:

$$\frac{\partial A_1}{\partial z} + iD_1\Delta_\perp A_1 = -ik_1\frac{dn_1}{dT}(T - T_0)A_1 - 0.5\delta_1 A_1, \tag{1.20}$$

$$\frac{\partial A_2}{\partial z} + iD_2\Delta_\perp A_2 = -ik_2\frac{dn_2}{dT}(T - T_0)A_2 - 0.5\delta_2 A_2, \tag{1.21}$$

$$\kappa_T\Delta_\perp T = \delta_1|A_1|^2 - \delta_2|A_2|^2, \tag{1.22}$$

where z is the longitudinal coordinate, $\Delta_\perp$ is the Laplacian in terms of transverse coordinates x and y, $A_j(x, y, z) = \sqrt{\epsilon_0 c_0 n_j}E_j(x, y, z)$ is the normalised amplitude of the electric field (E_j) of the pump or probe beam, where c_0 is the speed of light in a vacuum, ϵ_0 is the permittivity of vacuum, and n_j is the refractive index of the medium for the corresponding wavelength. $D_j = 1/(2k_j)$ is the diffraction coefficient for wavenumber $k_j = 2\pi/\lambda$. δ_j is the linear absorption of the corresponding wavelength of light, κ_T is the thermal conductivity, and dn_j/dT is the thermo-optic coefficient of the medium.

For simplicity I consider a medium with weak absorption, where $\delta_{1,2} \approx 0$. I consider two propagating beams with incident conditions $A_1 = E_1\exp(-x^2/w_1^2 - y^2/w_1^2)$ and $A_2 = E_2\exp(-(x - d)^2/w_2^2 - y^2/w_2^2 + ik_2\theta_2 x)$, where d is the initial distance (at $z = 0$) between the pump and probe beams, which are propagating with an initial angle θ_2 (Fig. 1.12), w_1 and w_2 are the widths of the pump and probe beams. The temperature is held at a constant of T_0 on the boundaries of the system. The refractive index is modified by an amount $\Delta n_j(x, y, z) = dn_j/dT[T(x, y, z) - T_0]$. This refractive index difference results in the defocusing of both the beams, and a modification of the propagation profile of the probe beam. Several interesting effects were observed, the most prominent are: reflection of the probe beam from the pump; thermal defocusing; and nonlinear
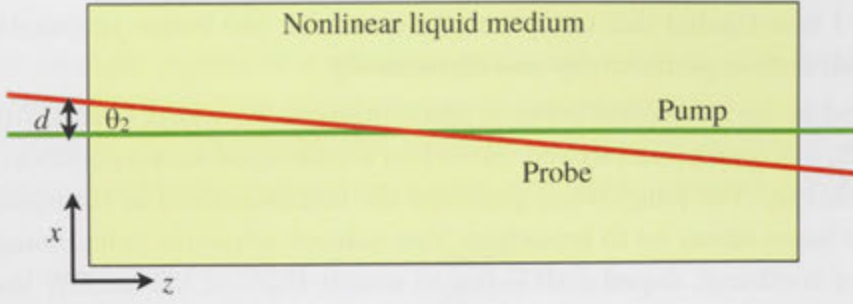
23

Figure 1.12: Schematic showing linear pump and probe beam propagating through a nonlinear liquid medium with initial distance between the beams d and initial angle between the beams θ_2.

reflection. To begin I look at the nonlinear interaction resulting in reflection of the probe beam from the pump.

The probe beam trajectory was characterised using Snell's law [36], $n_2(x)\cos(\theta_2(x)) = n_2(d)\cos(\theta_2(d))$, and the approximation that the angle between the two beams is small ($\theta_2(x) \approx \pi/4$), and weak inhomogeneity ($n_2(x) - n_2(d) \ll n_2(d)$). This gives a simple relation:

$$\theta_2^2(x) = \theta_2^2(d) + 2[n_2(x) - n_2(d)]/n_{02}, \qquad (1.23)$$

where n_{02} is the refractive index in the absence of radiation, and d is the initial distance between the two beams. As the probe beam becomes parallel to the pump beam, the distance between the two beams will be a minimum with a distance of $d_{min} = n_{02}\theta_2^2(d)/2$.

There is a maximum initial angle between the beams θ_c after which total internal reflection of the probe from the pump induced refractive index profile will not occur.

$$\theta_c = \sqrt{2[n_2(d) - n_{02}]/n_{02}}. \qquad (1.24)$$

The thermal profile can be determined from (Eq. 1.22) with a Gaussian energy source:

$$T(r) = T_0 + \frac{\delta_1 P_1}{4\pi\kappa_T}[H(R/w_1) - h(r, w_1)], \qquad (1.25)$$

where the total power of the beam is $P_1 = 2\pi \int_0^\infty |A_1|^2 r dr = \pi\epsilon_0 c_0 n_1 E_1^2 w_1^2/2$, and the temperature distribution function:

$$H(\varsigma) = \int_0^{2\varsigma^2} dt(1 - e^{-t})/t = C_e + l(2\varsigma^2) - Ei(2 - \varsigma^2), \qquad (1.26)$$

where $C_e = 0.5772156649$ is the Eula constant and $Ei(-\varsigma)$ is the integral exponential function. If $d/w_1 \gg 1$ we can use the asymptotic expression $H(d/w_1) \approx 2\ln(1.8874d/w_1)$. The temperature profile is plotted in Fig. 1.13.
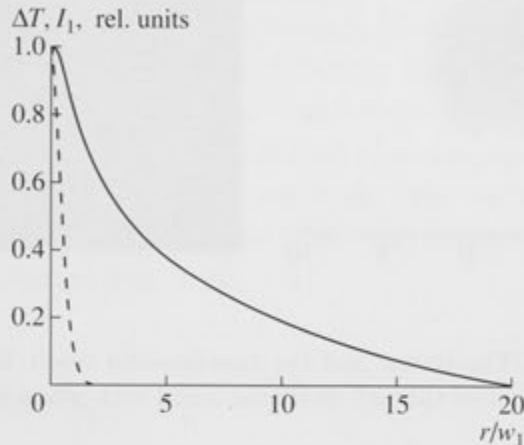

Figure 1.13: Transverse distribution of (solid line) the normalised temperature difference between the given point and the boundary of the liquid. (dashed line) The normalised intensity of the Gaussian pump beam for liquid contained in a cuvette of radius $R = 20w_1$.

Using (Eq. 1.25) and (Eq. 1.26) we can find the critical angle in terms of pump intensity:

$$\theta_c = \sqrt{\frac{2}{n_{02}}\left|\frac{dn_2}{dT}\right|[T(0) - T(d/w_1)]} = \sqrt{\frac{\delta_1 P_1}{\pi \kappa_T n_{02}}\left|\frac{dn_2}{dT}\right|\ln(1.8874d/w_1)}. \quad (1.27)$$

From these equations we can see that the critical reflection angle depends on the pump intensity and the initial distance between the beams d. This is due to the nonlocal character of the thermal nonlinearity. Such behaviour is not seen in other nonlinear media (e.g. quadratic or cubic nonlinear crystals) because they lack nonlocal interactions. A thermal nonlinearity is inherently nonlocal because of the diffuse nature of heat flow, where regions of the medium far from the heat source (the pump beam in this case) effects the propagation of the probe. I simulate the nonlinear reflection using numerical solution to equations Eq. 1.20, 1.21, and 1.22. Fig. 1.14(a) shows a calculated profile of propagated beams, compared to experimental realisation (Fig. 1.14(b)).

Next I look at the nonlinear beam interaction resulting in thermal defocusing and nonlinear reflection of the probe from the pump. As we have seen the negative thermal nonlinearity results in the reflection of the probe beam from the pump.
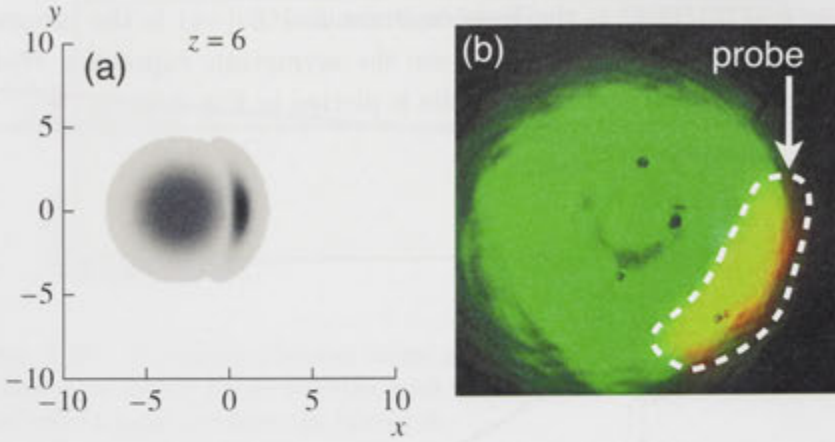
Figure 1.14: (a)Theoretical and (b) experimental result for a pump and probe beam propagated through nonlinear liquid with pump power $P_1 = 21.4$ mW, $\theta_2/\theta_c \approx 0.7$.

This reflection becomes more complicated at higher input power due to defocusing of the pump beam. To estimate the defocusing analytically I use the aberrationless approximation [37], in which the normalised width of the beam $w(z)$ satisfies the equation:

$$\frac{d^2 w}{dz^2} = L_{diff}^{-2} w^{-3} + L_{def}^{-2} w^{-1} \exp(-\delta_1 z),\tag{1.28}$$

where $L_{diff} = k_1 w_1^2/2$ is the linear diffraction length and

$$L_{def} = w_1 \sqrt{\frac{\pi \kappa_T}{2\delta_1 P_1 dn/dT}}\tag{1.29}$$

is the defocusing length. In the case where the defocusing is stronger than the diffraction, nonlinear broadening of the beam is observed up to $z \approx L_{def}$, and the beam has a divergence angle which is independent of the initial beam width:

$$\theta_{def} = \sqrt{\frac{\delta_1 P_1 dn/dT}{\pi \kappa_T n_0}}.\tag{1.30}$$

Comparing Eq. 1.27 and Eq. 1.30 we can see that the critical angle of total reflection roughly coincides with the divergence angle of the defocusing beam. These two effects are easily distinguished due to differing wavelengths of the pump and probe beams.

1.4.7 Nonlinear Beam Interaction in Bulk Liquids: Experimental Observations

Iodine (I_2) crystals were dissolved in ethanol to a concentration of approximately 10 mg per 100 ml. Iodine was chosen because of its absorption profile (highly absorbing at 532 nm, low absorption at 632.8 nm). This liquid was place in a glass cuvette with dimensions $50 \times 20 \times 20$ mm. Two laser beams (the pump with $\lambda = 532$ nm, and probe with $\lambda = 632.8$ nm) were aligned to co-propagate through the liquid, with an adjustable initial displacement and angle. The output was imaged, using a combination of polarising beam splitter (PBS) and filters to distinguish between the probe and pump beams (Fig. 1.15).
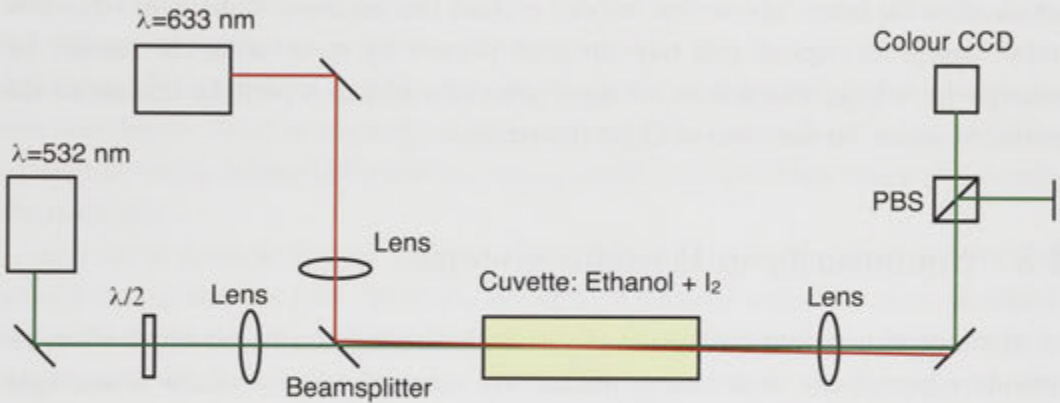
Figure 1.15: Experimental setup: a 532 nm CW laser beam (pump) is polarised with a $\lambda/2$ wave plate before being focused and combined with a 633 nm focused laser beam (probe). These two beams are co-propagated at an angle using a beamsplitter through a 50 mm long cuvette containing 0.1 mg/mL of Iodine dissolved in Ethanol. The probe and pump beams are imaged with a colour CCD.

The pump beam has optical power between $0 - 30$ mW, while the probe beam has a fixed power of 0.71 mW. The probe power is reduced by the beamsplitter used to combine the two beams, resulting in a power of 0.056 mW propagating in the liquid. The linear absorption of the liquid at 532 nm was measured to be 45.5% over 50 mm. Each beam is independently focused with a lens. The output is imaged with a lens onto a CCD camera. The waist of the pump beam is 18.7μm. I experimentally study the reflection at several pump power levels and intersection angles and positions inside the liquid.

Using Eq. 1.27 we can estimate the critical angle for beam reflection under the experimental conditions: $P_1 = 21.4$ mW, $dn/dT = 4 \times 10^{-4}$ deg^{-2}, $\kappa_T = 1.7 \times 10^{-3}$ W cm^{-1}deg^{-1}, $n_2 = 1.36$, $\delta = 0.12$ cm^{-1}, and $d/w_1 = 5$ we get $\theta_c \approx 0.018$ rad,

which agrees qualitatively with the experimental measurement of $\theta_2 = 0.008$ rad. θ_c is measured physically using trigonometric relations between the two laser beams, over the propagation distance. This manifests itself in the shape of the probe beam, where the pump is acting like a convex nonlinear mirror (Fig. 1.14).

We can see that in bulk material's nonlinearity has a very large effect on propagating beams. The nonlocal character of the thermal response cause the nonlinear effect to spread beyond the propagating pump beam. These nonlinear effects show how the pump beam can effect the propagation of the probe. This interaction comes from the influence of the pump beam on the medium. Without the medium the two beams would not interact at all. This is a key point about nonlinear interactions: they must occur in a nonlinear medium. While there are many bulk nonlinear media which allow for beam interaction, we can expand this intensity dependant refractive index change to explore rich new areas of physics by structuring the media, for example by adding waveguides, or more generally adding a periodic change to the refractive index, in one, two or three dimensions.

1.5   Nonlinearity in Periodic Systems

A range of new and interesting physical phenomena can be observed when we introduce periodicity to nonlinear media. We can take what we know about light propagation in periodic media (Sec. 1.3) and combine it with what we know about light propagating in nonlinear media (Sec. 1.4).

Interest in nonlinearity in periodic photonic structures began in 1988 when Christodoulides and Joseph showed that discrete solitons in an array of coupled nonlinear waveguides could exist [27]. Such solitons were observed a decade later with high power femtosecond pulsed laser and planar Aluminium Gallium Arsenide waveguide (AlGaAs) array [38]. Waveguide arrays can favour the formation of solitons because the diffraction can be controlled by the coupling between the waveguides (Sec. 1.3), resulting in lower power required for soliton formation when compared to a bulk medium. Nonlinearity in periodic systems also allows for other important effects such as soliton formation in self-defocusing media [39], and many other interesting phenomena.

Light propagating in discrete periodic optical media can be studied theoretically using coupled mode theory [3][27], and the tight binding approximation from solid state physics [4]. We can modify the coupled mode theory we already have (Eq. 1.2) for a 1D array of coupled waveguides, to include a nonlinear term [27]:

$$i\frac{dA_n}{dz} + \beta A_n + C(A_{n-1} + A_{n+1}) + \gamma |A_n|^2 A_n = 0, \tag{1.31}$$

where A_n is the amplitude of the propagating mode in waveguide n, and the two neighbouring waveguides have amplitude A_{n-1} and A_{n+1}. β is the propagation constant for the nonlinear mode, C is the coupling coefficient between the waveguides $n, n-1, n+1$, and γ is the nonlinear coefficient.

Just as we have with the linear case, we can get a more complete understanding of the system in both one and two dimensions by expanding this model of the system to the full continuous wave equation. In this case we use the nonlinear Schrödinger Equation, written in a time independent form:

$$i\frac{\partial A}{\partial z} + D\left(\frac{\partial^2 A}{\partial x^2} + \frac{\partial^2 A}{\partial y^2}\right) + F(x, y, z, |A|^2)A = 0, \tag{1.32}$$

where $A(x, y, z)$ is the normalised electric field amplitude, $D = z_0\lambda/(4\pi n_0 x_0 y_0)$ is the diffraction coefficient, λ is the wavelength of light in a vacuum, n_0 is the refractive index of the medium, x and y are the transverse coordinates, z is the propagation coordinate which is normalised to x_0, y_0 and z_0 respectively. $F(x, y, z, |A|^2)$ is a function which defines the refractive index profile and nonlinear response through the material.

In a linear periodic system we have a fixed refractive index contrast, determined usually during manufacture. With the intensity dependant refractive index provided by nonlinearity we can now study periodic media which contain a *defect*, where one or more of the waveguides are slightly different (or even nonexistent!) to the otherwise uniform periodic change in refractive index.
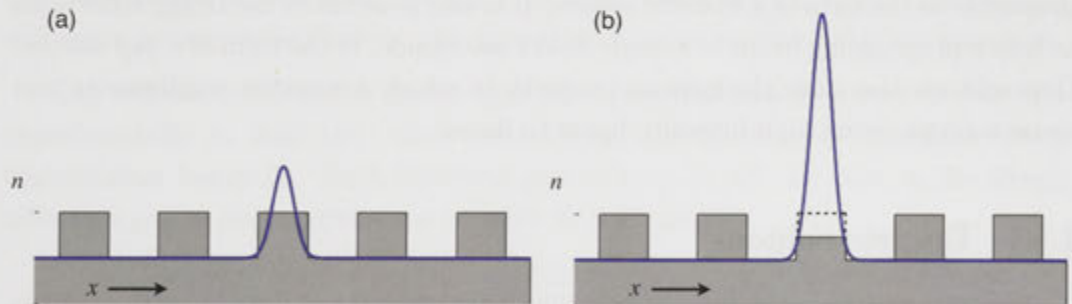
Figure 1.16: (a) refractive index of a periodic nonlinear medium (shaded grey) with a low intensity input Gaussian mode (blue line). (b) The same periodic medium with a high intensity input Gaussian mode (blue line) causes a local change in the refractive index on the input waveguide when the nonlinearity of the material is negative. Dashed lines indicate liner refractive index profile for comparison.

Fig. 1.16 shows how a nonlinear defect in a periodic structure is formed when the nonlinearity is negative. Fig. 1.16(a) shows the case when we have an array

of square waveguides with a low intensity Gaussian input. If we input a high intensity Gaussian mode into a single waveguide (Fig. 1.16(b)), that waveguide will experience a reduction in refractive index because of the nonlinearity. If the nonlinearity were positive the refractive index in that waveguide would increase.

Nonlinearity in such periodic structures forms defects, and allows us to study nonlinear *defect modes*. A defect is any irregularity in an otherwise uniform periodic array. A defect mode is a mode which resonates with such a defect, and can only exist because of it. These modes include discrete solitons and gap solitons, and can often display counterintuitive properties such as localisation of a beam under a defocusing nonlinearity. These properties do not show up in bulk media: they are due to the periodic nature of the material, and the nonlinearity causing the defect.

In a homogenous medium with a positive Kerr (-like) nonlinearity an increase in the intensity of a beam can be seen as an increase in the propagation constant β, which pushes the diffraction relation (Fig. 1.3(a)) into the total internal reflection gap at $\kappa = 0$. Such a beam is decoupled from the linear diffraction relation (Fig. 1.3(a)) and so can propagate in the form of a spatial soliton, which does not change its shape as it propagates. It follows that when a homogenous medium has a negative nonlinearity the propagation constant would be reduced, leading to increased spreading.

Self trapping is possible in periodic media in a similar way to homogenous media when the nonlinearity is positive. The propagation constant is increased for a single waveguide, trapping the light in the high index waveguide, allowing a beam to propagate in the form of a *discrete soliton*. It is also possible to use Bragg reflections to trap a propagating beam in a single defect waveguide, in the form of a *gap soliton*. Gap solitons also have the curious property in which a *negative* nonlinearity can cause a propagating high intensity beam to focus.

1.5.1 Discrete Solitons

Discrete solitons occur in periodic (discrete) photonic structures with positive ($\gamma > 0$) nonlinearity. A high intensity beam coupled into a single waveguide in a 1D array will cause a local increase in the refractive index of the input waveguide. The light will localise in this high index defect and can propagate as a soliton. While most of the light is confined to the input waveguide, coupling between close neighbours can still occur.

Discrete solitons were first observed in planar waveguide arrays [38]. Their dynamics were studied [40] and further control of the solitons was investigated through diffraction management [41]. Discrete solitons and self-defocusing effects were also observed [42] in the same periodic medium. Discrete solitons, dipole solitons, and

soliton chains have also been observed in optically induced structures [43, 44, 45, 46]. Martin *et al.* also showed that discrete solitons in partially coherent photonic lattices lead to a range of new interesting phenomena such as lattice dislocation and the formation of polaron-like structures [47].

A soliton mode in this configuration will not continue to couple further into the array, and will maintain its intensity profile as it propagates. This is due to the increase in propagation constant β resulting from the high index defect. This shifts the mode into the total internal reflection gap at $\kappa = 0$ (Fig. 1.17(a)), where it is decoupled from modes associated with linear discrete diffraction.

1.5.2 Gap Solitons

Periodic media with a negative nonlinearity will not experience the same focusing in this case. A high intensity mode will push β down, and since the total internal reflection gap always occurs at higher propagation constant than the first band (Fig. 1.5), such a medium can never enter this region.

Gap solitons occur when the propagation constant of a mode is pushed into the Bragg reflection gap in the diffraction relation. Previously observed discrete solitons only exist in the total internal reflection gap. For periodic media with a positive nonlinearity this occurs in the second band when $\kappa = \pi$ (Fig. 1.17(a)). Such beams will again propagate as solitons, this time with a more complicated phase structure.

Gap solitons in waveguide arrays with a focusing nonlinearity were first observed experimentally in 2003 [48], after the excitation of Bloch waves in higher order transmission bands [9]. Such observed gap solitons [9, 48, 49] exist in the Bragg reflection gap, a phenomenon not possible in bulk media.

Somewhat surprisingly a periodic medium with a negative nonlinearity can also experience self focusing in the form of a gap soliton. Discrete solitons can not be achieved with such a nonlinearity because the total internal reflection gap always has a higher β than the mode, and the nonlinearity will reduce β. This reduction in β can push a mode into the Bragg gap however, at the edge of the band where $\kappa = \pi$ (Fig. 1.17(b)). This results in the mode decoupling from the discrete diffraction band, and the formation of a gap soliton [43, 44, 50, 51]. The phase structure produced is staggered: each waveguide is out of phase with the neighbouring waveguide. This results in points of zero energy in between the waveguides, which has become a signature of the formation of gap solitons in periodic media with negative nonlinearity.
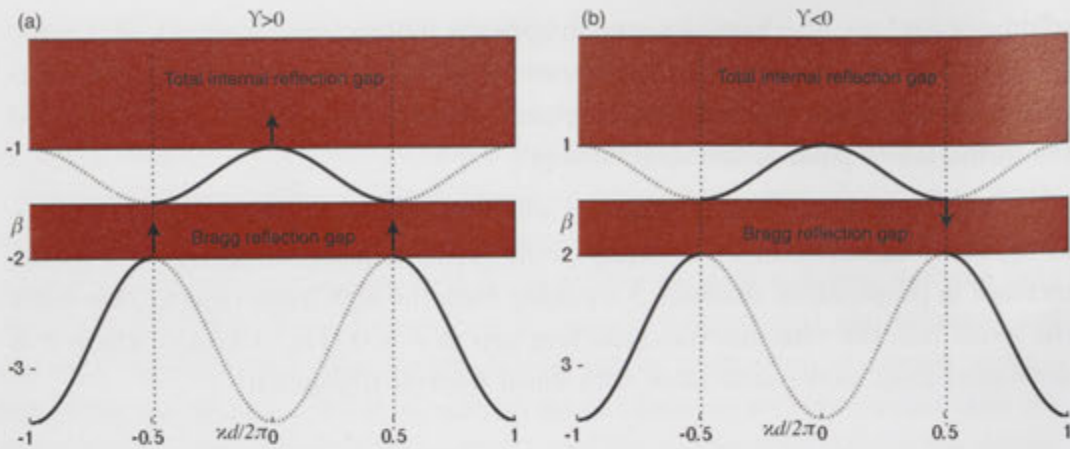
Figure 1.17:   (a) Discrete solitons occur in periodic media with period d with $\gamma > 0$ when the propagation constant of a mode is increased into the total internal reflection gap at $\kappa = 0$. Gap solitons occur in the same media when modes in the second band are pushed up into the Bragg reflection gap. (b) Gap solitons occur in periodic media with $\gamma < 0$ when the propagation constant of a mode is decreased into the Bragg reflection gap at $\kappa = \pi$. Modes in higher order bands can be excited into higher order bands in a similar way.

1.5.3   Other Nonlinear Effects in Periodic Photonic Structures

Many other interesting nonlinear effects in periodic photonic structures have been observed. Optically induced waveguide arrays [52, 53] are a common medium for the observation of such nonlinear features because of their reconfigurability. Effects such as discrete vortex solitons [31, 29, 54, 55, 56], two dimensional surface solitons [57], and necklace-like solitons [58] have all been observed in optically induced structures. Vortex solitons can be stabilised by a nonlinear medium [59], and have been shown to create stable waveguides in a nonlinear medium leading to second harmonic generation [60]. Anisotropic solitons in 2D square lattices occur when the effects of total internal reflection and Bragg reflection are combined [61].

1.6   Nonlinearity in Liquid Infiltrated Periodic Photonic Structures

In this thesis I study spatial nonlinear effects in periodic photonic structures. My approach is to use liquid infiltrated periodic microstructures as a scaffold in which to investigate spatial nonlinear effects. I chose to use liquid as a nonlinear waveguide because of its temperature tuneable refractive index (Sec. 1.4.5) and thermal nonlinearity (Sec. 1.4.6).

Using such periodic arrays of nonlinear waveguides I study tuneable nonlinear waveguide arrays in one-dimensional and two-dimensional periodic arrays, such as temperature tuneable discrete diffraction, nonlinear defocusing, and truncated non-linear Bloch-wave solitons. I then study spatial nonlinear effects such as nonlocal gap solitons, the crossover from discrete to homogenous systems, and surface vortex states in two-dimensional arrays. I study the majority of these systems in liquid infiltrated Photonic Crystal Fibres.

1.6.1 Photonic Crystal Fibres

Photonic crystal fibres (PCFs) are glass or polymer fibres with a photonic microstructure along their length. Such a microstructure is usually provided by an array of air filled holes (known as the cladding region) surrounding a solid core (Fig. 1.18). The size and arrangement of these holes can be tuned to give a wide variety of optical phenomena such as endlessly single mode index guiding [62], and photonic bandgap guiding [63].

The periodic nature of the refractive index profile gives rise to bandgap effects in PFCs. These bandgap properties are determined by the exact structure of the cladding region, and can be tuned with subtle variations of the structure.
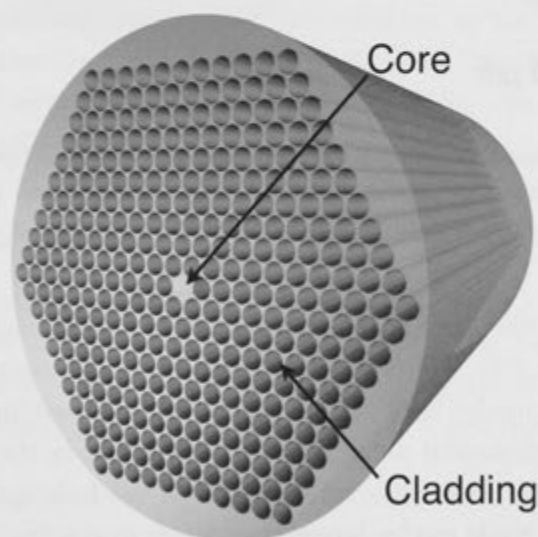

Figure 1.18: A Photonic Crystal Fibre is made up of a core and a periodic change in refractive index for the cladding.

Photonic crystal fibres were first suggested in 1976, as a cylindrical Bragg waveguide, where a periodic refractive index is arranged around a low index central core [64]. Another approach was taken by Knight et al. [65], whereby silica capillaries

are formed by drilling a bulk preform of silica glass. This is then heated and drawn down (Fig. 1.19) to form a fibre optic cable, in which the profile of the drilled preform is maintained. The cladding region of the first PCFs provide a region of lower index around a solid core, even though the fibre is made from a single material. Light is guided in the higher index core region via total internal reflection due to this refractive index difference. Bandgaps were not possible in these early fibres due to small hole size, and low filling fraction [66].
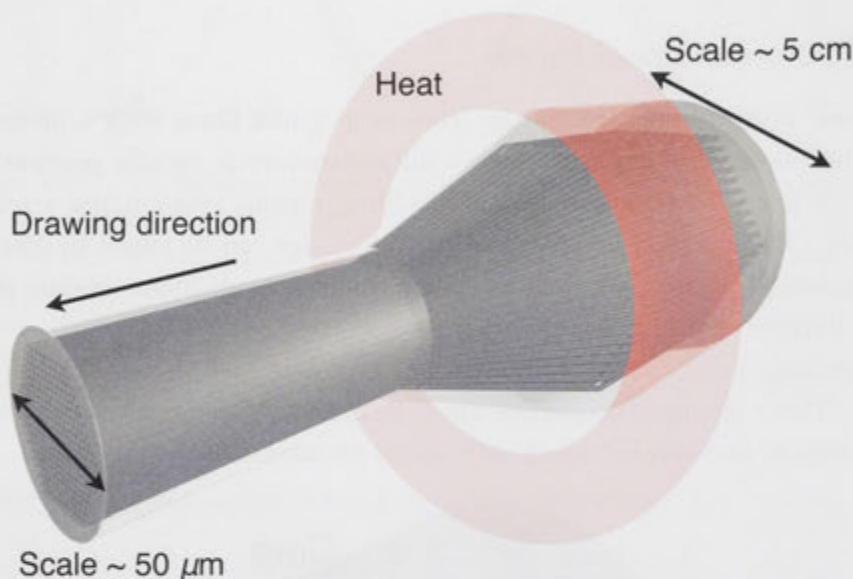

Figure 1.19: Heat is applied to a PCF preform which is then drawn down to the desired size. The profile of the preform is maintained through careful drawing process, over significant change in diameter.

These PCFs had the extraordinary property of being single mode for a wide range of wavelengths [62]. This was understood to be a property of the structure, whereby higher order modes 'leak' from the core into the cladding due to their mode profile, while the fundamental mode is always contained in the core [62]. Features in the profile of a mode with a size on the order of the hole spacing will be filtered out by the structure, while modes larger than the hole spacing will be contained in the core. By choosing the geometry it is possible to select which modes are guided.

The cladding structure can also be used to tune the dispersion properties of a PCF [67], and even to produce broadband near-zero dispersion [68]. This can be used for supercontinuum generation and nonlinear optics [69]. More exotic structures such as dual core fibres can be used as directional couplers [70] or polarisation splitters [71]. If the fibre itself is made from a nonlinear medium the core can exhibit nonlinear properties [72].

Photonic crystal fibres can also guide light using the photonic bandgap effect, where the periodic structure of the cladding region acts as a Bragg reflector. This allows for fibres with a *hollow core* to guide light [63]. Theoretical modelling of bandgaps in a PCF can take the form of coupled mode theory [73], the multipole method [74, 75], or more recently as layered inclusions [76].

While it is possible to engineer fibres to control dispersion, select guided modes, and even guide light in a hollow core, all of these properties mush be determined and engineered into the fibre structure. Every time one wishes to test another property a new fibre must be produced. As suggested by Monro *et al.* [77] the cladding of a PCF can be filled with a liquid or gas, to influence the guiding of light and enhance the interaction between infiltrating liquid or gas and light. This allows for the possibility of using such fibres for sensing applications [77, 78, 79]. The introduction of another medium into a PCF allows for dynamic tuning of the structure and hence its optical properpties [80, 81, 82, 83, 84] as well as the enhancement of nonlinear effects [85, 86, 87, 88]. Such devices have recently been shown as ultra-sensitive refractive index sensors [89].

We can utilise the cladding region of a PCF (Fig. 1.18) by displacing the air in the cladding structure. If we use a medium with a higher refractive index than the material of the fibre itself the cladding region will guide light instead of the core. In order to achieve infiltration of the capillaries making up the cladding region, it is important to chose a medium which can easily displace the air in these capillaries. A simple method of infiltration is to use a liquid, which can spontaneously fill a capillary through capillary action.

1.6.2 Liquid Infiltration

Liquid fills a thin capillary through liquid-capillary-air interaction known as *capillary action*. The contact angle of the liquid with the capillary allows for an imbalance in the surface tension forces in the liquid, resulting in the liquid 'climbing' the walls of the capillary. The height of the liquid h is governed by the equation:

$$h = \frac{2\xi \cos(\theta_c)}{\rho g r} \tag{1.33}$$

where ξ is the liquid-air surface tension, θ_c is the contact angle between the liquid and the capillary, ρ is the density of the liquid, g is the local gravitational field strength, and r is the radius of the capillary. From this equation one can see that a larger filling height can be achieved with a smaller radius capillary, lower density, smaller contact angle, or larger surface tension. It is also possible to offset the gravitational force by tilting the capillary on its side, or applying a negative pressure to aid in capillary action.
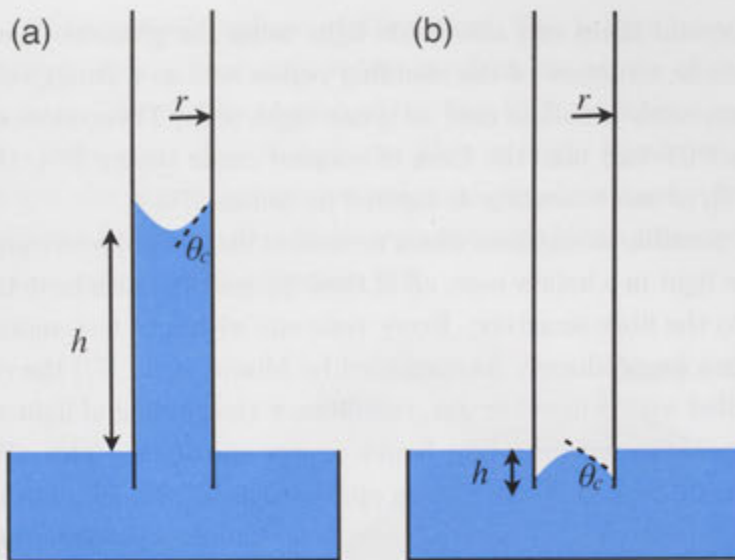
Figure 1.20: Capillary action for a liquid with an interface which: (a) produces a concave meniscus ($\theta_c < \pi/2$) results in liquid being drawn up the capillary by a distance h; (b) produces a convex meniscus ($\theta_c > \pi/2$) leads to a reduction of the height of the infiltrating liquid in a capillary.

A liquid-solid interface can result in either a concave, or convex meniscus. A concave meniscus has a contact angle $\theta_c < \pi/2$, resulting in a positive capillary action where h is increased (Fig. 1.20(a)). A convex meniscus has a contact angle $\theta_c > \pi/2$, resulting in a negative capillary action (Fig. 1.20(b)).

Capillary action can easily be used to fill the holes of the cladding region of a PCF due to their small radius. Many liquids (some oils, aqueous solutions) produce a concave meniscus at an air-glass interface, which provides us with a wide range of liquids to use in the infiltration of silica glass PCFs. Not only do liquids commonly display nonlinearity, but their refractive index is often tuneable by varying the temperature of the liquid (Sec. 1.4.5).

By infiltrating the cladding region of a PCF it is possible to guide light in the high index liquid filling each hole. The coupling of light between the holes can be tuned by varying the refractive index contrast between the infiltrating liquid and the glass or polymer making up the PCF (Sec. 1.3.2). This gives us a tuneable array of nonlinear waveguides, in which we can propagate light in the form of cladding modes along the length of an infiltrated PCF. The nonlinearity of the liquid provides an opportunity to investigate nonlinear beam propagation in these periodic structures. Many liquids also exhibit low absorption of a variety of wavelengths available in high-power lasers [90], both simplifying theoretical simulations of these systems

and allowing us to achieve nonlinear interaction over a greater distance.

A selective filling approach has been shown to introduce dynamically tuneable birefringence into an infiltrated PCF [91]. Selective filling of holes allows for the realisation of other waveguide geometries in a single fibre. In-fibre absorptive polarisers [92], ultra-sensitive refractive index sensors [89], and even direct measurement of the bands have been demonstrated [93].

1.6.3   Assumptions and Experimental Conditions

I have listed for convenience the experimental apparatus and conditions. Unless otherwise stated explicitly in a particular work these are the conditions under which experimental and theoretical studies are carried out.

Photonic Crystal Fibre

For my studies I used three different fibres from Crystal Fibre (LMA-15(5), LMA-15(7), and F-SM15). I measured the properties (hole size, spacing, core size etc.) of each fibre using a microscope and calibrated image. Several other fibre types were also tested for completeness and as such are also listed in Table 1.1.

Liquids

In my experimental research I used castor oil and Cargille Series A liquids for infiltration. Liquids used in the experiments and their properties are listed in Table 1.2. Measurements ate for ambient temperature of 25°Cand 1 Atmosphere pressure.

Liquid Infiltration

I infiltrated fibres by sitting one end inside a small reservoir of the infiltrating liquid, with the other end open to the air (Fig. 1.21). This is achieved by sitting one end of a fibre in a small syringe, in which the infiltrating liquid occupies the tip, leaving the other end of the fibre exposed. Capillary action is quite strong with such small capillary radii (Table 1.1), leading to simple and effective infiltration of all capillaries in a PCF. The length of fibre the liquid will fill can be estimated using Eq. 1.33 with a density of 863 kg/m^3, a surface tension of 0.03 N/m, and a capillary radius of 2.5μm. This gives a height for Series A 14800 oil in LMA 15 of $h = 2.83\cos(\theta)$m. Even for a small contact angle of 85° this is a significant length of fibre ($h = 0.25$m).

I utilise this concept of liquid infiltration to investigate light propagation in tuneable nonlinear periodic photonic structures. I begin by developing platforms for the study of linear and nonlinear beam propagation in 1D periodic structures.

Table 1.1: Photonic crystal fibres used for experiments. Λ is the pitch (distance between the centre of two holes), d is the diameter of a single hole, d/Λ is the relative hole diameter, d_c is the diameter of the core.
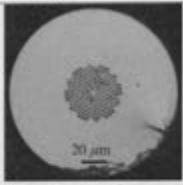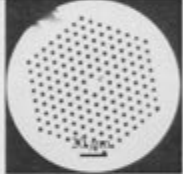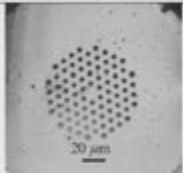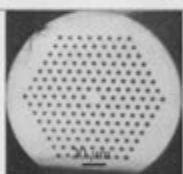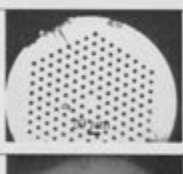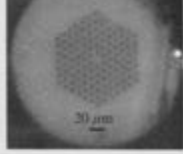
Name	Λ (μm)	d (μm)	d/Λ	d_c (μm)	Image of Fibre
LMA-5	2.85	1.12	0.423	5	
LMA-10	7.18	3.35	0.466	10	
LMA-15 (5)	9.78	4.46	0.456	15	
LMA-15 (7)	9.81	4.88	0.498	15	
LMA-20	13.22	6.32	0.478	20	
F-SM15	10	5	0.5	15 $\pm$5	

Table 1.2: Liquids used in experiments and their properties. n is the refractive index, $\frac{dn}{dT}$ is the thermo-optic coefficient. ρ is the liquid's density, and ξ is the liquid-air surface tension.

Name	n 25°C(532 nm)	$\frac{dn}{dT}$ (K^{-1})	ρ 25°C(kg/m^3)	ξ 25°C(N/m)
Castor Oil	1.46	-2.5×10^{-4}	unknown	unknown
Series A 14700	1.476	-3.92×10^{-4}	848	0.029
Series A 14800	1.484	-3.95×10^{-4}	863	0.030

This is achieved using new techniques for the fabrication of 1D waveguide arrays in SU8 polymer, and by developing a method for the selective infiltration of PCFs. I then move on to discuss more fundamental mode propagation in 1D periodic arrays with my observation of truncated nonlinear Bloch-wave solitons in Lithium Niobate waveguide arrays.

I then move to investigating nonlinear cladding modes in liquid infiltrated PCFs. I observe nonlocal gap solitons and discover the point at which such a system switches from focusing to defocusing. Finally I theoretically explore surface states of vortex modes propagating around the core of a liquid infiltrated PCF, and take the first steps to experimental realisation of this phenomena.

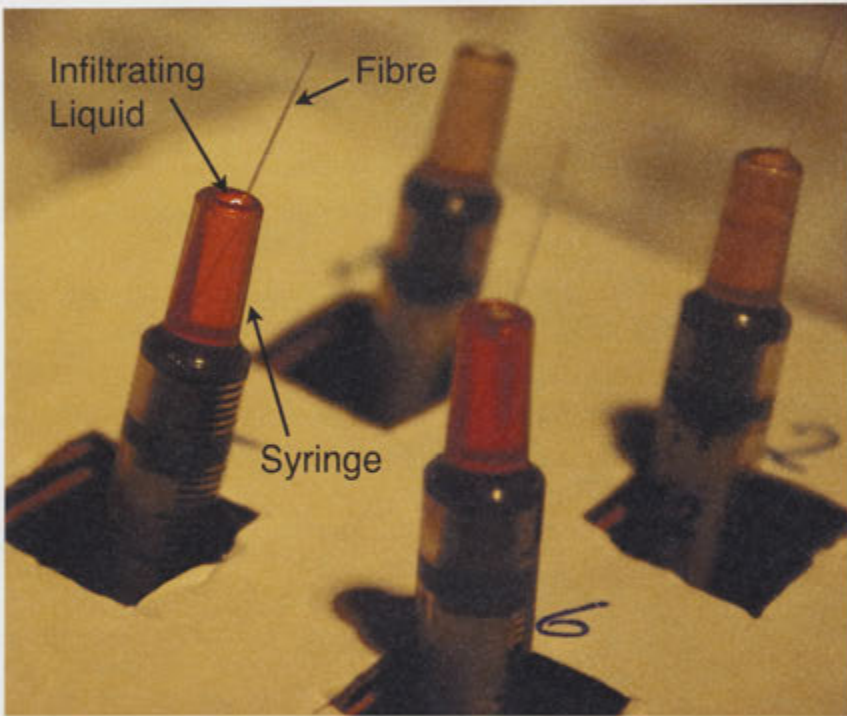Figure 1.21: Fibres being infiltrated with a liquid. A fibre sample is placed in a reservoir of the infiltrating liquid occupying the tip of a syringe. One end of the fibre is left exposed to the ambient atmosphere.

Light Propagation in 1D Periodic Arrays

In order to study light propagation in tuneable nonlinear periodic photonic structures one first needs a platform to produce a tuneable nonlinear array of waveguides. Many fundamental nonlinear effects in periodic photonic structures have been demonstrated in 1D periodic arrays of coupled nonlinear waveguides. It is therefore logical to begin by looking at 1D periodic arrays of liquid waveguides, the tuneable refractive index of liquids allows for highly tuneable coupling between the waveguides, while the nonlinearity enables us to study nonlinear beam propagation.

Typical waveguide size ($1-10 \, \mu$m) for single mode guiding at visible wavelengths are ideal for liquid infiltration. Capillary action will be strong for many liquids, even with low contact angle oils, for infiltration of waveguides with a length larger than the coupling length between waveguides. While single capillaries are common, periodic arrays of such small capillaries in high quality periodic arrays are not easily obtained.

I start by looking for a platform on which we can imprint or construct a periodic array of air filled capillaries which can be infiltrated. A simple method of photolithographically defined capillaries in an epoxy polymer (SU8) is used to create a high quality periodic structure in 1D. The liquid infiltrated waveguides are characterised in the linear regime, as the coupling between waveguides is tuned using an external heat source. I then move to selectively infiltrating the capillaries of a Photonic Crystal Fibre in order to expand our understanding of these systems by looking at nonlinear propagation, and develop a method of controlling light propagation in more complicated 1D structures without the need for expensive or time consuming platform development. I then investigate new fundamental nonlinear effects in well known periodic nonlinear waveguides in Lithium Niobate in the form of truncated nonlinear Bloch waves.

2.1 Platform: Polymer Waveguides

2.1.1 Introduction

The advent of air structured fibre initiated an entire field of photonic investigation [66]. The ability to realise periodic structures with high index contrast enables flexible dispersion engineering and strong optical confinement providing ideal conditions for studying nonlinear optical phenomena.

More recently, researchers have explored the use of air structured fibre as a platform for fluid infiltration [80]. For example, air structured fibres have been infiltrated with fluids to study tuneable and nonlinear propagation in two dimensional waveguide arrays [85] where the high thermo-optic nonlinearity of fluid can be exploited. The ability to infiltrate air structured fibres with fluids also suggests applications as refractive index sensors with many elegant designs being demonstrated [89].

However, the propagation of light in two-dimensional (2D) arrays of waveguides is highly sensitive to imperfections of the structure, because the light in each waveguide couples to more than two neighbouring waveguides. Thus, in 2D arrays there is always more than one path for light to couple from one waveguide to another. Small differences in these multiple coupling paths can degrade the coherence of a diffracting beam and thus typically, beam diffraction experiments in 2D arrays are limited to one or two coupling lengths making it difficult to observe subtle optical phenomena. For 1D arrays there is only a single path for coupling between adjacent waveguides and thus coherent discrete diffraction can be sustained over many coupling lengths. Hence, 1D infiltrated waveguide arrays can provide an excellent platform for the investigation of periodic behaviour enabling experimental observation of fundamental physical phenomena and also suggesting significant opportunities for photonic sensors.

It would be a great advantage to introduce lithographically defined longitudinal variations to these air structured waveguides to enable investigation of a wider variety of nonlinear optical phenomena [94] and also to realise more practical optofluidic sensors [95] that could be monolithically integrated with planar microfluidics to form fully integrated lab-on-chip systems [96].

In this section, I present a rapid and low-cost technique for the realisation of planar air structured waveguides using the SU8 family of polymers, standard photolithography and simple dry-film lamination. I confirm the utility of this platform by demonstrating temperature tuneable coupling of light in an array of closely spaced liquid-infiltrated channels.

2.1.2 Platform Development

Fig. 2.1 presents a schematic outlining the fabrication method. This method is similar to a recently reported microfluidic fabrication technique [97] but on a much smaller scale. Table 2.1 summarises the process parameters.

Table 2.1: SU8 Process Parameters

SU8 Film Thickness	3 μm	10 μm	50 μm
SU8 Product	SU8-2002	SU8-2005	SU8-2025
Spin Speed / rpm	1700	700	1000
Acceleration / rpm/ s	300	300	300
Spin Time / s	30	30	30
Soft Bake Time / min	2 at 95°C	1 at 65°C/ 10 at 90°C	3 at 65°C/ 6 at 95°C
Exposure energy / mJ	90	600	600
Post Exposure Bake Time / min	2 at 95°C	3 at 95°C	1 at 65°C/ 6 at 95°C
Development / s	60	n/a	n/a
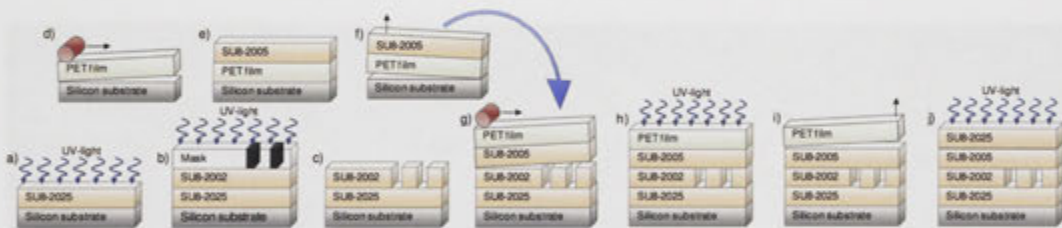
Figure 2.1: Fabrication Process: a) deposit and cure SU8 buffer; b) deposit, pattern and cure core; c) develop core; d) laminate PET film; e) deposit and soft bake SU8 sealing layer; f) peel carrier film and sealing layer; g) laminate sealing layer over core, h) cure sealing layer, i) remove carrier film; j) apply protective SU8 cover.

A 50 μm buffer layer of SU8-2025 was deposited on a 3 inch diameter silicon wafer using a Karl Süss RC-8 spin coater and UV flood exposed on a Karl Süss MA-6 mask aligner as shown in Fig. 2.1a). The cured SU8 film was then oxygen plasma treated for 2 minutes to promote adhesion. A 3 μm SU8-2002 layer was then spin coated, patterned by contact photolithography (Fig. 2.1 b)) and then cured and developed to reveal open channels (Fig. 2.1 c)). This layer was also plasma treated to promote adhesion to the sealing layer.

The sealing layer was formed using a 50 μm-thick Adhesives Research Aclear 8932 polyethylene terephthalate (PET) film consisting of two layers (carrier and substrate) which were weakly bonded with a strong adhesive applied to the substrate face. This PET film was laminated onto a silicon wafer, substrate side down, using a SSI FL-12HR laminator (Fig. 2.1 d). A 10 μm film of SU8-2005 was spin coated onto the PET film and soft baked (Fig. 2.1 e)).

The carrier PET film was then peeled from the substrate, inverted laminated onto the open channels at 45°C(Fig. 2.1 g)). The laminated stack was UV exposed and cured (Fig. 2.1 h)) After curing, the PET carrier was peeled off easily (Fig. 2.1 i)). Finally, the wafer was coated with a 50 μm-thick SU8-2025 protective cover (Fig. 2.1 j)). The laminated wafer was diced into 10 × 10 mm pieces using a Disco DAD 321 dicing saw.

The diced samples were inspected using a FEI Quanta 200 ESEM. Fig. 2.2 presents two of these ESEM images. These show that the channels remained open and had relatively straight sidewalls. The dimensions of the channels were 2.7 × 2.8 μm which were slightly different to the nominal 3 × 3 μm dimensions, but were well within the fabrication tolerance of SU8. More accurate lithography may be possible if required. Particles were evident at the openings of the channels. These may be silicon dust generated during dicing and should not affect the waveguide properties within the sample.

Figure 2.2: SEM micrographs of the cross-section of the diced (a) waveguide array and (b) two waveguides from the array.

2.1.3 Temperature Tuneable Discrete Diffraction

Having demonstrated fabrication of hollow channels with micron scale dimensions, we may now explore whether these channels can be used as fluid infiltrated optical waveguides.

For relatively short waveguides, distinguishing guided and scattered light can be difficult. Thus to test the waveguiding properties, I chose to examine discrete coupling of light within arrays of fluid infiltrated channels.

The refractive index of SU8 was measured to be 1.572 at 1.55 μm using a Metricon 2010/M prism coupler at room temperature. I chose Cargille Series A 1.64 as the infiltration fluid, which had a room temperature refractive index of 1.608 at 1.55 μm. Full wave finite element simulation was used to find the propagating modes of a 3×3 μm Cargille fluid core surrounded by SU8. Only the fundamental mode was found to propagate.

The optical properties of both the SU8 and Cargille fluid can be tuned thermally. The thermo-optic coefficients (dn/dT) of SU8 and Cargille fluid are -9.6×10^{-5}/K [98] and -4.59×10^{-4}/K, respectively. The thermo-optic coefficient of SU8 polymer was determined using the prism coupler and heater attachment. dn/dT was also measured at 532 nm and 1310 nm, the results are summarised in Table 2.2. Since the thermo-optic coefficient of the Cargille fluid is greater than that of SU8, temperature may be used to tune the index contrast of the waveguide. This will particularly impact coupling of light between waveguides in an array. The greater change in refractive index of the infiltrating liquid with increased temperature will lead to greater coupling between the waveguides due to the reduced refractive index contrast.

Table 2.2: Refractive index n and thermo-optic coefficient dn/dT of SU8 polymer for wavelengths of 532, 1310, and 1550nm.

Wavelength (nm)	n at 25°C	dn/dT (K^{-1})
532	1.601	-5.376 $\times 10^{-5}$
1310	1.573	-7.952 $\times 10^{-5}$
1550	1.572	-9.6 $\times 10^{-5}$

A 3D beam propagation method (BPM) was used to predict the temperature dependent coupling in an array of fluid infiltrated waveguides. Each waveguide was a 3×3 μm Cargille fluid core, surrounded by SU8. An array of 21 waveguides with 9 μm centre-to-centre separation and 10mm length was simulated. The output optical profile was analysed and the width containing 70% of the optical power was recorded as a function of temperature as presented in Fig. 2.3. Discrete steps are evident at $\Delta n = 0.028$ and 0.027, where the beam occupies 3 and 5 adjacent waveguides respectively. These jumps are typical for discrete diffraction.

Fig. 2.3 also presents the distribution of light as it propagates through the coupled waveguides. Fig. 2.3 (i)-(iv) presents the optical distributions from output

face of the sample in the experiment and correspond to temperatures of 55, 45, 40, and 35°C, respectively. As the temperature increases, the mode profile widens as the light couples to more waveguides in the array as it propagates. Fig. 2.3 (i) shows coupling resulting in the a dark central waveguide at the output. This feature is characteristic of discrete diffraction [99]. Fig. 2.3 (v)-(viii) present numerical results of a propagated beam in the theoretical system. The mode profile matches very well to the observed experimental outputs. The index contrast used for the theoretical calculations are $\Delta n = 0.025, 0.027, 0.03, 0.031$ respectively.
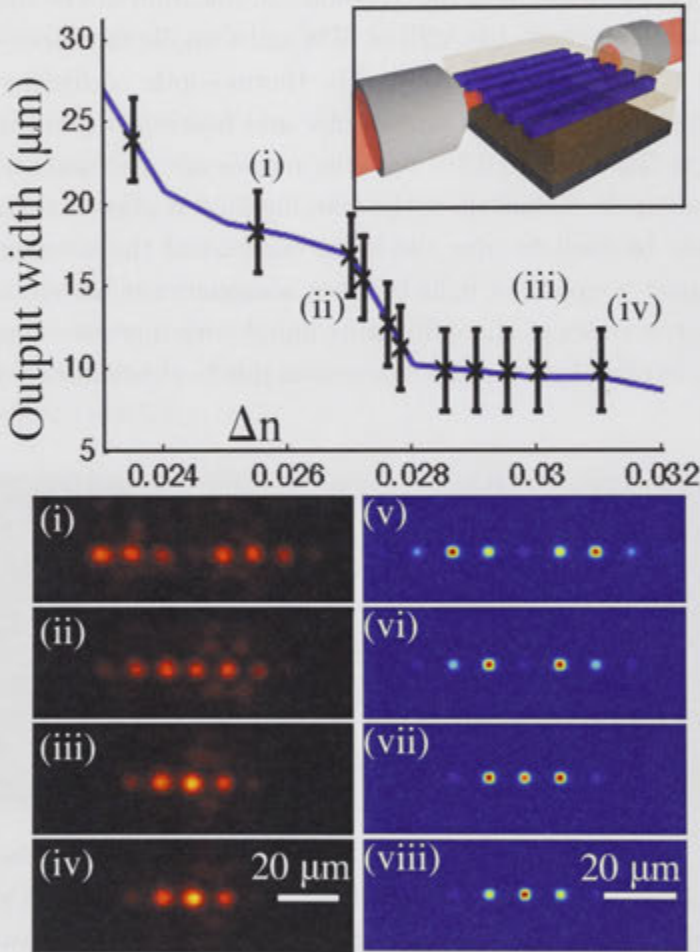
Figure 2.3: Comparison between width of output beam from experiment and simulation. Experimental images (i-iv) are matched to theoretical simulations (v-viii) to determine experimental index contrast Δn. Light is coupled into a single waveguide, and the output is imaged (inset). Δn for theoretical images are: (v) 0.025, (vi) 0.027, (vii) 0.030, (viii) 0.031, which correspond to estimated temperatures of 55, 45, 40, and 35°C± 1°Crespectively.

From my simulations we can conclude that fluid infiltration of this platform should provide temperature tuneable optical coupling between the waveguides. To experimentally test whether the structure depicted in Fig. 2.2 could provide this behaviour, a channel array with 3×3 μm air channels and 9 μm centre-to-centre separation was infiltrated with Cargille Series A 1.64 refractive index fluid. The small dimensions of the hollow waveguides enabled infiltration by capillary force through submerging one end of the sample in the Cargille liquid. Glass slides were clamped to either end of the sample to define the end facets.

The sample was tested by focusing a 10 ps pulsed laser light with at a carrier wavelength of 1.55 μm into one of the fluid waveguide cores using a 40$\times$ microscope objective. The light emerging from the exit facet was imaged onto a CCD camera using a 10$\times$ objective. The sample was heated to 60°C and a sequence of images were recorded as the sample cooled to room temperature.

Fig. 2.3 (i)-(iv) present the measured optical distributions corresponding to temperatures of 55, 45, 40 and 35°C respectively. These compare well to the predicted results of Fig. 2.3 . In particular the coherent cancellation of light in the central waveguide observed in Fig. 2.3 (i) could only be achieved if the waveguides are single mode and if the coupling is symmetric indicating that the fluid infiltrated channels are indeed behaving as a coupled waveguide array.

It should be noted that in the experiment, the pulsed laser had a spectral bandwidth of 0.3nm. This finite bandwidth would result in some loss of coherence when compared to the single wavelength assumption made in theoretical simulations.

48

2.2 Platform: Selective Infiltration of Photonic Crystal Fibres

While it is useful to produce custom structures in SU8 epoxy, we can expand on these waveguide arrays by utilising existing arrays of capillaries in Photonic Crystal Fibres. While these capillaries are two dimensional by design, I have developed a technique for selectively infiltrating these structures. This allows for more advanced structures to be produced using existing technology.

2.2.1 Introduction

1D periodic photonic structures provide a platform on which to study a rich variety of physical phenomena such as discrete diffraction, optical bandgaps and discrete solitons [28]. Waveguide arrays were first studied in Gallium Arsenide (GaAs) as a first step in producing optical circuits and switches [100]. It was observed that light would couple between waveguides as had been theoretically predicted several years earlier as discrete diffraction [101]. While it was unclear how to use or suppress this discrete diffraction, the idea of nonlinear optical effects began to take hold, with the prospect of nonlinear focusing balancing the diffraction caused by light coupling to neighbouring waveguides.

Spatial solitons formed in this manner were later observed in waveguides etched into Aluminium Gallium Arsenide (AlGaAs) [47]. Further advances led to laser written waveguides [102] which provide faster production of waveguide arrays than traditional etching techniques, allowing the investigation of more exotic 1, 2 and 3D structures. While the waveguides are of high quality, they can not be dynamically tuned, and are limited to relatively short lengths.

Lithium niobate (LiNbO$_3$) has also been utilised for planar optical waveguides, in order to take advantage of its relatively high photorefractive nonlinear response. Such waveguides can be used to demonstrate discrete diffraction and gap solitons [103, 51]. Lithium niobate introduces the possibility of dynamically tuning the coupling between waveguides in an array through the electro optic effect, in which an electric field can influence the refractive index of a material. This was furthered by the application of liquid crystals to 1D waveguide arrays [104], where tuneable breather states were demonstrated in arrays of waveguides with nematic liquid crystals. Although this provided a highly tuneable, periodic nonlinear platform, it is restricted to 1D planar waveguide arrays.

Optically induced lattices have been investigated in strontium barium niobate (SBN) crystals for applications in nonlinear effects such as soliton formation [44][45][47]. Such induced lattices can be extended to 2D arrays to provide a wider

range of physical phenomena to study, such as discrete vortex solitons [29]. Optically induced lattices provide tuneable 1, 2 and 3D waveguide arrays, but are only available for a small variety of geometries over short lengths.

In this section I present my work on the development of a new platform for waveguide arrays. By selectively infiltrating specific holes in a pre-existing array structure we can make waveguides which are tuneable, can be formed into complex network structures, and can be made in both 1 and 2D. I selectively infiltrate a photonic crystal fibre to achieve such waveguides and present it as a platform tuneable 1D waveguide arrays and demonstrate linear tuneability and nonlinear discrete diffraction. Such selectively infiltrated fibres provide orders of magnitude more interaction length than previously studied waveguide arrays, allowing for more sensitive measurements [84].

Photonic crystal fibres (PCFs) are a recent development in fibre optics in which a periodic array of air filled holes surrounds a solid core. The arrangement and size of holes can be tuned to give a wide variety of optical phenomena, such as endlessly single mode index guiding [62], and photonic bandgap guiding [63]. Phenomena such as the photonic bandgap effect arise from the periodic nature of the refractive index profile in PCFs. The optical properties of a PCF can be changed by altering the structure of the cladding. This has the effect of changing the bandgap properties, which determines how light is transmitted through the fibre.

It was suggested that the cladding structure of these fibres could be controlled by an external parameter such as temperature to provide a tuneable core mode [80]. Such a device would have the ability to dynamically control the optical properties of the medium using an existing platform, rather than develop a single platform for the study of a single optical phenomena. Liquid infiltrated PCFs were shown to have a tuneable photonic bandgap [105], and have been used to study linear and nonlinear effects [85, 106].

The added complexity of discrete diffraction in 2D requires high precision manufacturing and quality control to ensure symmetric coupling when using the infiltrated cladding of a PCF. Any slight irregularities in the size or spacing of the infiltrated holes will result in asymmetries in the output [85].

We can reduce the reliance on technical tolerances such as precise hole spacing by infiltrating a selected one dimensional area of the cladding structure in a PCF. The reduced complexity of the coupling in a 1D system is less reliant on the precision manufacturing of the PCF. While this may at first appear to be a platform similar to previous 1D systems, the selective infiltration can be considered as a new platform. The infiltrating liquid providing part of the periodic structure and/or waveguides can be selected from a wide range of exhaustively studied liquids and even polymers [91]. These infiltrating liquids can be doped to enhance nonlinear

response or increase absorption. In addition it is also possible to use the same platform and techniques developed here to create new structures which give a wide range of applications. The selective infiltration of a single cladding site in a PCF has been shown to be ultra sensitive to refractive index changes in the infiltrating liquid [89].

2.2.2 Platform Development

The air filled cladding of a PCF is easily infiltrated using capillary action. The small hole diameter results in capillary action capable of drawing up viscous liquids such as oil. By immersing one end of the fibre in a reservoir of the infiltrating liquid, the air is displaced by the liquid and the fibre is infiltrated. While the time it takes to fill depends on the liquid used, I observed a filling time of about 5 minutes per cm for a silica glass fibre with holes of diameter around 5 μm using a Cargille index matching oil of $n = 1.47$ and $n = 1.48$. Such liquids have a negative thermo-optic coefficient, close to $dn/dt \approx -3.9 \times 10^{-4}$ K^{-1}, resulting in a reduction of the refractive index of the oil as it is heated. Specifically the fibres I used were commercially available from Crystal Fibre as LMA-20 and LMA-15 (7). They consists of 7 hexagonal rings of air filled holes. LMA-20 has a measured hole diameter of 6.3 μm and hole spacing 13.2 μm. LMA-15 has a measured hole diameter of 4.9 μm and hole spacing of 9.8 μm.

In order to infiltrate only selected waveguides I took the approach of blocking an inverted infiltration pattern on one end. The unblocked end is then placed into the infiltrating liquid reservoir for infiltration (Fig. 2.4). Holes which are blocked at one end will not infiltrate more than a few mm, due to air pressure inside the cavity (Fig. 2.4). It is conceivable that the blocking compound is pushed out by the capillary action of the infiltrating liquid, but I did not find this to be the case with the blocking and infiltrating liquids.

I tested several different blocking compounds and techniques including epoxies, UV curable optical cement, and several oils. I applied the blocking liquid using an applicator made by tapering a conventional single mode fibre using a butane torch. The fibre is placed in the flame and tension is applied to either end of the fibre until it tapers to a small point. It is then broken at the taper under a shear stress. This forms the applicator for the blocking liquid, and is fixed to an x, y, z stage for manipulation (Fig. 2.5).

The PCF is held vertically in a clamp, with a microscope focused on the upper end of the PCF. The tapered applicator is held at an angle relative to the top face of the PCF on an x, y, x stage (Fig. 2.5). The fibre is fixed at an angle such that either the tip of the applicator can deposit a single drop on the PCF, or the shaft
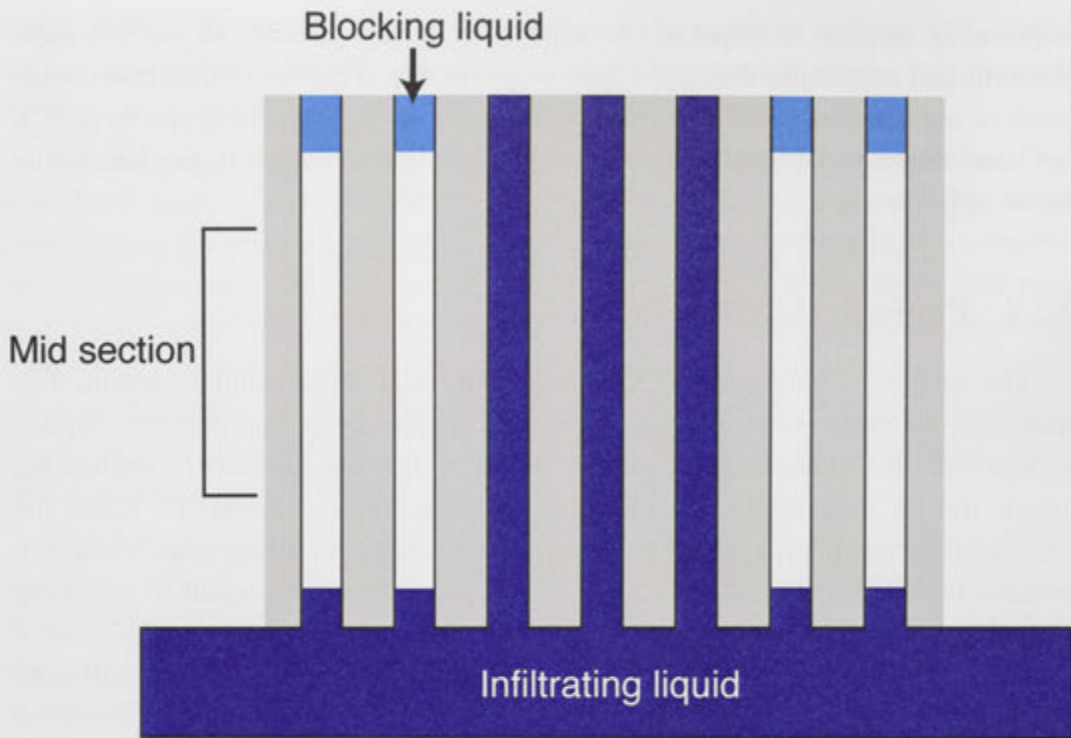
Figure 2.4: The unblocked end of the PCF is placed in a reservoir of the infiltrating liquid. Air pressure inside the blocked channels prevents them from completely filling. The ends of the sample are cleaved leaving the mid section of the fibre as a selectively infiltrated PCF sample.

of the applicator lies parallel to the end face of the PCF. This allows for either a single droplet of blocking liquid, or a row of droplets, to be deposited on the PCF in a controlled fashion. The PCF is illuminated from either above or below to best highlight the location of blocking liquid.

The first blocking technique tested was to apply a drop of blocking liquid to one area of the fibre and manipulate this drop to form the desired pattern [107]. The second technique involved drawing the applicator through a reservoir of liquid, forming small droplets along the length. Each droplet is then addressed to a specific hole or set of holes to block them. I found that castor oil was both the easiest to apply directly, and the most effective at blocking the holes. The glues were difficult to address to specific holes and were too viscous to move effectively. The castor oil was applied to the tapered fibre such that small drops are formed along the length of the taper. The range of drop sizes allows for the covering of single holes, or small groups of holes with high accuracy.

Fig. 2.6 shows an example of the progressive application of small droplets of
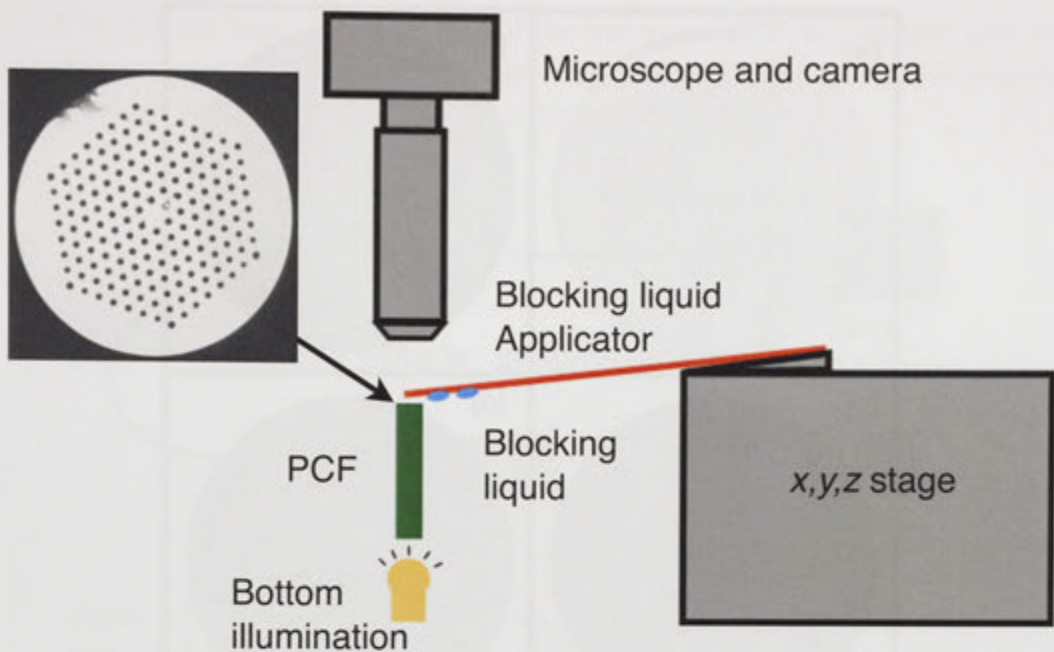
Figure 2.5: The PCF (top left) is held vertically under a microscope. A tapered fibre has blocking liquid applied to the tip, and is mounted on an x, y, z stage. The sample is illuminated to provide the best contrast between blocked and unblocked holes.

castor oil to specific holes on the PCF. Fig. 2.6(a) shows an unblocked PCF. The contrast and lighting used for imaging is adjusted to provide the maximum contrast between blocked and unblocked holes. In this example droplets are first applied to the top of the fibre (Fig. 2.6(b)). Blocked regions are enclosed by the red dashed line in Fig. 2.6. Unblocked holes are easily distinguished from blocked, as they retain their round shape and hexagonal pattern (Fig. 2.6(b)). Further droplets are applied (Fig. 2.6(c)) to cover more of the top region, and some of the bottom region. The final unblocked pattern of a single line is achieved with careful placement of the final droplets (Fig. 2.6(d)).

The sample is then placed in a reservoir of infiltrating liquid such that the blocked end is open to air (Fig. 2.4). Once any unblocked holes are filled both ends of the fibre are cleaved off leaving the mid section of the fibre with liquid only filling the selected holes (Fig. 2.4). The typical final sample PCF was ~ 2 cm in length.
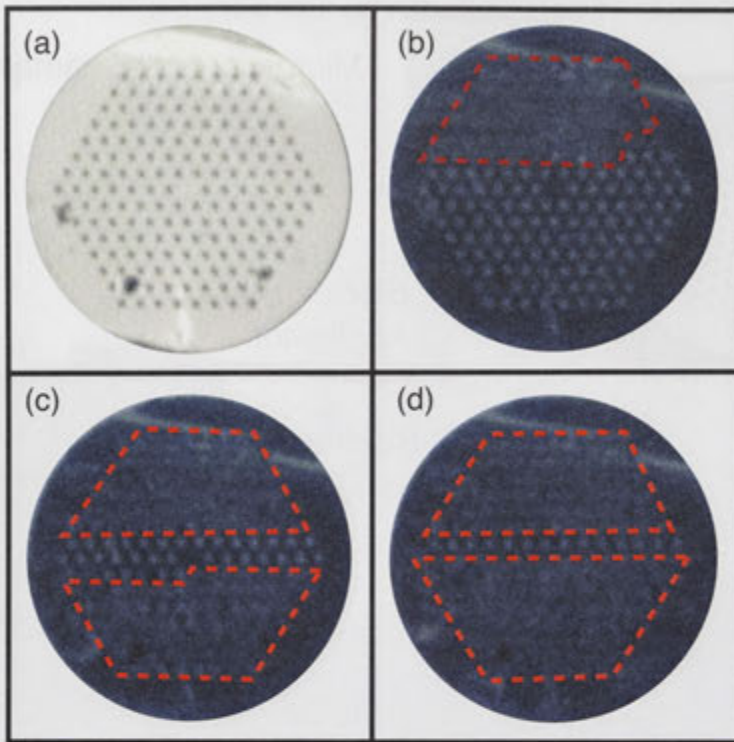
Figure 2.6: (a) An unblocked PCF has oil applied to one end to block specific holes. (b) The red dashed line indicates regions that are blocked with oil. (c) More oil is applied to specific holes until (d) the desired pattern for infiltration is reached: in this case a single line of holes is left unblocked.

2.2.3 1D Liquid Periodic Array: Linear Diffraction and Nonlinear Defocusing

In order to demonstrate and example the tuneable and nonlinear properties of this platform I first characterise the optical properties by first observing discrete diffraction [101] in the array in the linear regime for a variety of temperatures. I then observed nonlinear defocusing while the fibre was held at a single temperature and the input power was increased.

These observations were achieved by placing the the selectively infiltrated PCF inside a temperature stabilised oven. To ensure further stabilisation of the temperature the fibre is encased between two brass plates. The fibre sits in a square cut groove and is in contact with the lower brass plate. The temperature of the apparatus was allowed to reach an equilibrium before measurements are taken. The oven was mounted on an x, y, z stage. Light was butt coupled into a single infiltrated hole from a single mode polarisation maintaining fibre carrying light from a Verdi

V-5 CW 532 nm laser. The end face of the infiltrated PCF was imaged with an objective and camera (Fig. 2.7). The input fibre and oven were mounted separately to allow light to be coupled into any specific infiltrated hole.
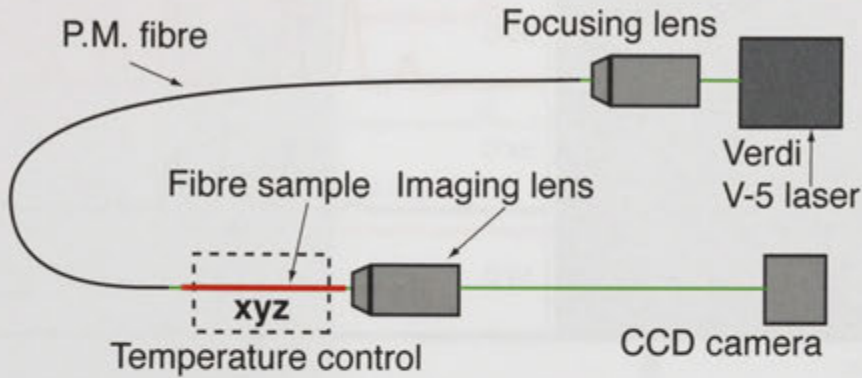

Figure 2.7: Light is addressed to a single infiltrated hole by butt-coupling with a polarisation maintaining fibre. The infiltrated sample is mounted in a temperature controlled oven. The output is imaged with an imaging objective.

In order to observe linear tuneable discrete diffraction, a selectively infiltrated PCF (LMA-20) was prepared as described above with a single row of holes infiltrated with $n = 1.47$ Cargille index matching oil. Light was injected into the center of the infiltrated 1D array to achieve symmetric coupling between the waveguides. I observed coupling between the waveguides as the temperature was raised to 53°C at which point the refractive index contrast between the infiltrating oil and silica cladding is close to 2×10^{-3}. Fig. 2.8 shows the output image and associated profile of the PCF as the temperature is increased. Each image and profile is normalised separately, to provide the best contrast. At 53°C there is very little coupling from the input waveguide to the neighbouring sites. When the temperature was raised to 54°C I observed significant coupling from the input waveguide to the two neighbouring sites. As the temperature was raised further to 55°C I observed nearly all the light coupling symmetrically out of the input waveguide into the array up to three sites away. At 56°C I observed a loss of symmetry and some higher order modes as the light reached the edge of the waveguide array. In this sample I was only able to selectively infiltrate 14 holes in the PCF. At 56°C some of the light has reached the edge of the array, resulting in less symmetric coupling. I observe a slight but consistent asymmetry across the profiles between 53°C-55°C. The first waveguide to the left of the input has slightly more light than the first waveguide to the right of the input. This is most likely due to a slightly inhomoganeous structure due to the consistent nature of the asymmetry.
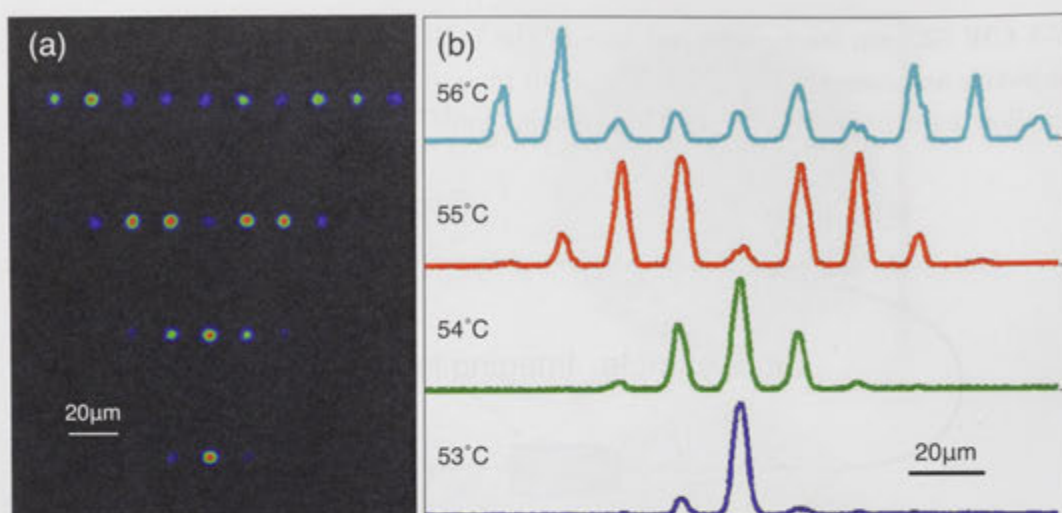
Figure 2.8: Demonstration of linear discrete diffraction as the fibre temperature is increased at (a) the fibre end face, and (b) profile of the end face images.

A new sample was prepared from LMA-15 fibre, infiltrating a single line with $n = 1.48$ Cargille index matching oil to investigate nonlinear effects in this system. Light was again injected into a site near the the center of the infiltrated 1D array which provided the best linear coupling. The temperature of the fibre was raised to 76°C until coupling was observed to occupy approximately three sites. At this temperature the index contrast between the infiltrating oil and silica cladding is close to 3×10^{-3}. This larger index contrast provides roughly the same linear coupling as seen in Fig. 2.8 53°C due to the closer spacing of the waveguides in LMA-15 used in this experiment. The temperature of the fibre was held constant while the intensity of light coupled into the input channel was increased. Fig. 2.9 shows images of the fibre end face as the input power is increased, and the associated profile of each image. I observed increased coupling of light from the input hole, even though the temperature of the whole fibre remained unchanged. At low power (0.3 mW) I saw very little coupling from the input waveguide to the two neighbouring sites. As the power was increased to 30 mW the coupling increases slightly. As the power was raised to 70 mW the coupling was observed to again increase. Equal amounts of light were observed in the input waveguide and the two neighbouring sites as the power was increased to 110 mW. As the power was increased further to 150 mW I observed nearly all of the light couple out of the input waveguide. I believe this occurs because the input waveguide is heated by absorption of the input light. This reduces the refractive index of the liquid in this waveguide, causing light to couple
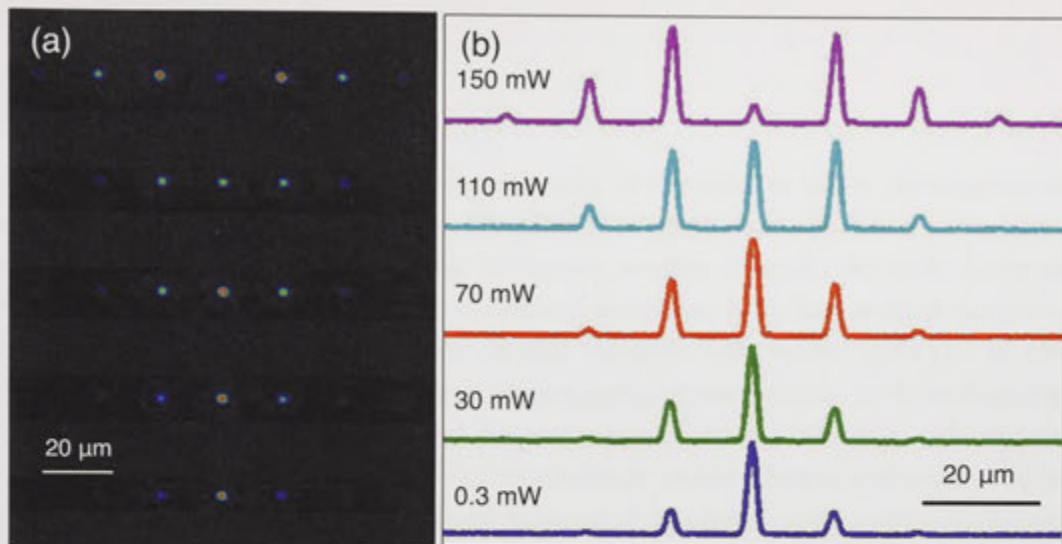
further into the array.

Figure 2.9: Demonstration of nonlinear defocusing as the input power is increased (a) at the fibre end face, and (b) profiles of the end face images.

I have successfully demonstrated a planar waveguide array in a selectively infiltrated PCF. The platform presented here can be expanded to other complex structures supported by the cladding of a chosen PCF, for example 2D networks with tuneable beam interaction [108]. More recent work has achieved highly sensitive refractive sensors [89], and other methods for the selective infiltration of PCFs [109]. While these methods require significantly more investment in equipment and techniques, they have been used to demonstrate high quality and repeatable selective infiltration. The platform presented here provides a quick and relatively inexpensive method of selective infiltration, which can be used to test the feasibility and properties of other selectively infiltrated structures.

While the demonstrated nonlinear beam propagation in these selectively infiltrated PCFs shows a defocusing effect, there are many other interesting nonlinear modes in 1D systems with defocusing nonlinearity. Gap solitons are one example, and have been shown in a variety of platforms with defocusing nonlinearity [39] including Lithium Niobate [51]. Nonlinear Bloch-waves have also been observed in 1D structures [9, 110]. Theoretical work and experimental observation in Bose-Einstein condensates have discovered a nonlinear mode in between a gap soliton and nonlinear Bloch-wave soliton [111, 112, 113]. I next show my observation of these truncated Bloch-wave solitons on Lithium Niobate waveguide arrays.

2.3 Truncated Bloch-Wave Solitons in Lithium Niobate Waveguide Arrays

2.3.1 Introduction

The coherent transport of nonlinear waves is essential in many phenomena in nature. In contrast to linear waves, the physics becomes complex when wave interactions start to play a role, making laboratory studies difficult. As such, many of the fundamental physical effects of nonlinear waves have been first studied in optics, where the advent of the laser as an intense coherent light source gave rise to the field of nonlinear optics. The recent experimental developments in Bose-Einstein condensates (BEC) opened the way for many analogous experiments with intense sources of coherent matter waves. Correspondingly, many effects earlier observed in nonlinear optics have been later found to occur in nonlinear atom optics, including four-wave mixing of matter waves [114] and matter-wave solitons [115].

A few years ago Anker *et al.* [111] reported the experimental observation of nonlinear self-trapping of Bose-condensed atoms in stationary periodic potentials. This trapping effect due to interaction between condensed atoms is manifested as a change from the diffusive regime, characterised by an expansion of the condensate, to the nonlinearity dominated self-trapping regime, where the initial expansion stops and the width of a matter-wave packet remains finite. This observation abrogates a seemingly obvious analogy between nonlinear optics and matter wave physics, because this type of nonlinearity-induced self-trapping in the presence of *repulsive interaction* has never been observed in optics.

In this section, I report on the first observation of nonlinear self-trapping of broad beams with zero transverse momentum in an array of defocusing optical waveguides. My results not only provide an optical analogue of the self-trapping effect of Bose-condensed atoms [111], but also reveal important new features of these localised states. In particular, I demonstrate that unlike conventional gap solitons known in defocusing photonic lattices [103] and BEC [25], the spatial extent of such self-trapped states is controlled by the width of the input excitation rather than by the input power. Since this observation these states have been shown as a useful form of image transmission in photonic lattices [116].

While a detailed intuitive explanation of the self-trapping effect in terms of wave tunnelling in a single Josephson junction has been provided in Ref. [111], this description was found incomplete as it did not account for the periodic nature of the trapping potential. Subsequent theoretical works [112, 117, 113] have extended the description of the wave localisation linking it to the Bloch modes in the system. However, this subsequent description remained untested experimentally, largely due

to the challenges in BEC experiments. By using an optical system, here I investigate the nature of the self-trapped state to a degree not attainable in the original BEC system. As such, I demonstrate experimentally *two new fundamental effects*: (i) Dependence of the width of the localised state on the input excitation, and (ii) independence of the localisation on the strength of the nonlinearity (beam power, or equivalently number of atoms in the BEC system), once above a critical value. This is due to the existence of a class of robust nonlinear states with arbitrary width which act as attractors in the system, with loss of excess power (or equivalently atom loss) able to occur through the edges of the localised state [117]. The latter point remained unnoticed in the earlier experiments which focused on the edge effects in a deep lattice. I reveal that the unique properties of the self-trapped states make them both highly robust and easily controllable.

2.3.2 Theoretical Exploration

I begin with the theoretical description of the beam localisation, and model beam propagation through lithium niobate (LiNbO$_3$) waveguide array by the nonlinear Schrödinger equation with a periodic potential and Kerr-type nonlinearity,

$$i\frac{\partial E}{\partial z} + D\frac{\partial^2 E}{\partial x^2} + \rho\Delta n(x)E - \gamma|E|^2 E = 0. \tag{2.1}$$

Here $D = z_s\lambda/(4\pi n_0 x_s^2)$, $\rho = 2\pi z_s/\lambda$. The transverse coordinate x and longitudinal coordinate z are normalised in units of $x_s = 1~\mu$m and $z_s = 1$ mm, respectively. While the complete description of the defocusing photovoltaic nonlinearity of LiNbO$_3$ involves a complex charge diffusion type description, this simplified model captures well the generic features of the nonlinear beam evolution, as was successfully demonstrated for gap solitons in Ref. [118]. The linear refractive index of the substrate material is $n_0 = 2.234$ at $\lambda = 532$ nm, leading to a diffraction coefficient of $D = 18.95$. The linear refractive index change $\Delta n(x)$ of the waveguides is taken as $\Delta n(x) = \epsilon\Sigma_n \exp[-(x - nd)^2/w^2]$, where ϵ defines the modulation depth [103]. I take the waveguide width and spacing to be $w = 7~\mu$m and $d = 14~\mu$m respectively, matching the experimental realisation of the waveguide array. The modulation depth is set at $\epsilon = 0.0003$ to provide a match between the theoretical and experimental linear output profiles. This is a shallow depth compared to the experimental regime of Ref. [111]. I find however that the general effects presented in this work are preserved over a wide range of depths ($\epsilon = 0.0002 \div 0.005$ have been considered).

I examine the stationary solutions of the system Eq. (2.1) using the ansatz $E(x, z) = U(x)\exp(i\beta z)$, where β is the propagation constant (typically related to the negative value of the chemical potential in BEC physics). In the linear limit the
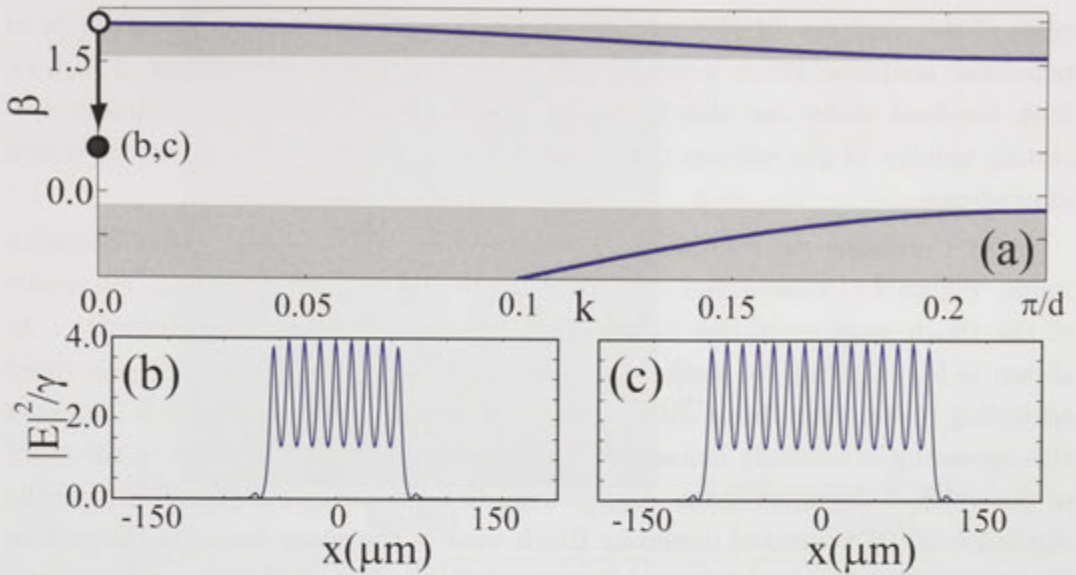
Figure 2.10: (a) Bandgap spectrum. (b,c) Examples of two truncated non-linear Bloch waves of different widths.

stationary wave solutions take the form of Bloch waves, $U_{n,k}(x) = A(x)\exp(ikx)$ where n denotes the band number and k the Bloch wavevector. The spectrum of these linear waves is divided into bands separated by gaps as shown in Fig. 2.10(a). In the presence of nonlinearity, stationary solutions may exist inside the linear transmission gaps in the form of either periodic nonlinear Bloch waves [119] or spatially localised states known as gap solitons [44]. A third type of state has recently been revealed as a bridge between these two classes of solution, the so-called *truncated nonlinear Bloch waves* [112]. Such a type of localisation occurs when the propagation constant of the Bloch wave is shifted into the gap, passing through the entire linear band, as shown with an arrow in Fig. 2.10(a). This crossing happens when a Bloch wave with zero transverse momentum is excited at the top of the first band and the defocusing nonlinearity decreases the propagation constant into the Bragg reflection gap. Intuitively this can be understood as confining a truncated piece of the Bloch wave between two Bragg reflectors, with no radiation into other linear waves due to the presence of the linear bandgap. Unlike conventional gap solitons in defocusing lattices, where the width of the soliton is proportional to the soliton power [44], the width of the truncated state is a control variable [113] in the sense that it selects the soliton family out of an infinite number of families (for an infinite lattice), each with a different number of occupied lattice sites. The particular family excited depends on the initial width of the incident optical beam. The families are all distinct, bifurcating near the upper gap edge above a critical

61

value of the nonlinear Bloch wave intensity [112, 113]. Two particular examples of truncated nonlinear Bloch waves of different widths are shown in Figs. 2.10(b,c). Such localised states can also be regarded as multi-soliton states composed of a certain number of gap solitons [120], however they are stable in their entire region of existence.

Next I examine the excitation of such localised Bloch waves from a Gaussian input. Figure 2.11 summarises the numerical results of a beam propagation model of the Bloch wave excitation for different values of the optical nonlinearity. As shown in Fig. 2.11(a), for weak defocusing nonlinearity the beam undergoes rapid spreading (faster than linear diffraction). However as the nonlinearity is increased this spreading is suddenly halted and the beam localises with a width of the order of the width of the input beam. As is evident in a comparison of Figs. 2.11(b,c) the signature of the truncated nonlinear Bloch wave is the sharp intensity drop-off in the wings of the beam. Additional features visible in Figs. 2.11(a,b) are the strong intensity modulations occurring within the localised state. The large diffraction coefficient leads to long-lived nonlinear excitations of the truncated nonlinear Bloch wave, which despite the strong modifications of the intensity profile do not lead to decay of the localised state. Most importantly, Fig. 2.11(a) shows that above a certain threshold for the optical nonlinearity ($\gamma \approx 0.15$), the width of the localised state remains practically independent of the input beam power.

Interestingly, the localisation occurs even when the nonlinearity is strong enough to detune the propagation constant of the beam into the higher band. The localisation in this latter case occurs through a rapid loss of power from the central part of the beam into higher-order low intensity nonlinear Bloch waves, effectively moving the propagation constant back into the linear gap [112]. This is an important feature not addressed in the earlier experiments using deep lattices [111]. The tight-binding limit considered there always considered generation of a state within the linear band gap. We see here that even if the nonlinearity (or intensity) is sufficient to drive the state outside the gap, localisation may occur through radiation of the excess power into higher-order low intensity nonlinear Bloch waves which can drain power through the sharp boundaries. It is also in contrast to the long-lived nonlinear excitations of the Bloch wave background [121].

An important feature of the generation process is that the output beam width is solely defined by the input width of the Gaussian beam, while being independent of the medium's nonlinearity. There is a linear dependence (Fig. 2.11(d)) between the input and output widths, while the different values of the nonlinearity lead to identical output beam widths (at least for moderate input beam widths). This can be understood as a consequence of the requirement of a critical intensity for generation [112]. As the nonlinearity (or equivalently beam power) is increased,
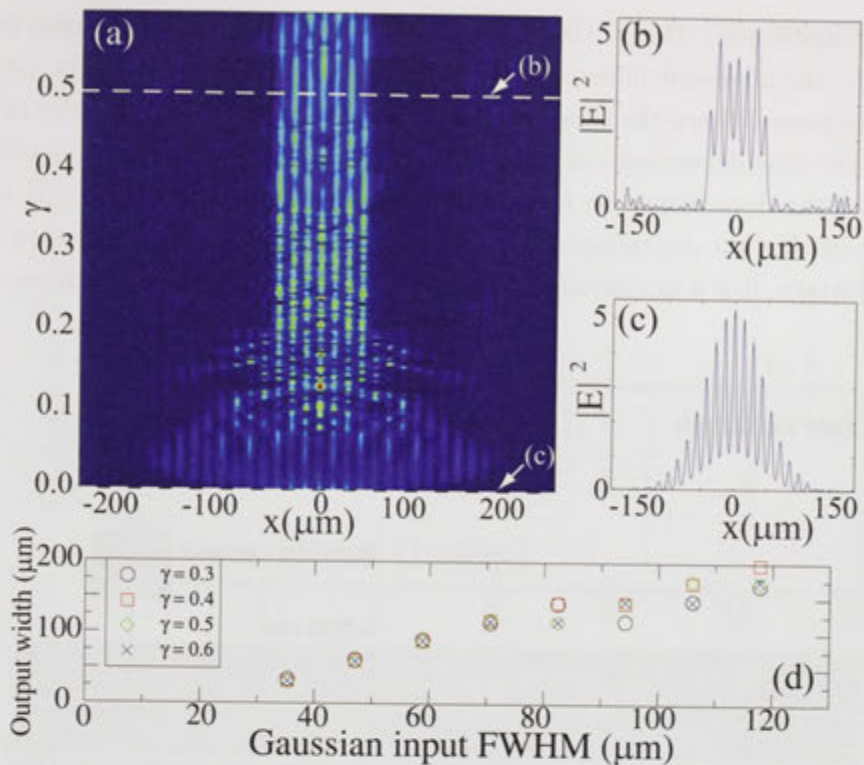
Figure 2.11: (a) Dependence of output intensity profile on the nonlinearity γ. The beam spreading is arrested at a critical nonlinearity, $\gamma \approx 0.15$. (b,c) Output beam profiles (as marked in (a)) showing localisation. (d) Variation of the output beam width (defined as the width between the sharp boundaries) with the input beam full width at half maximum (FWHM) for different values of the nonlinear coefficient γ.

the number of excited waveguides above the critical intensity does not change for moderate beam widths. At larger beam widths the nonlinear excitations of the truncated nonlinear Bloch state may lead to fluctuations in the measured width. This behavior arises due to the existence of independent families of arbitrary, but fixed, width which persist even into the higher order bands (where radiation occurs). Increasing the power of such states changes the maximum intensity, but not the width. Stable nonlinear localised states with arbitrary fixed widths have not been seen before in any physical context, and the existence of these nonlinear states as stable attractors is at the heart of the new results of this work.

2.3.3 Experimental Setup

Experimentally, I test the excitation of truncated Bloch waves by employing the defocusing nonlinearity of a LiNbO$_3$ waveguide array (6 cm long, fabricated by

Titanium indiffusion). Due to the slow nature of the photovoltaic nonlinear response in LiNbO$_3$, the nonlinear index change increases slowly with time under a constant input laser power. Since the time-scale of this index change is of the order of several minutes, the time dependence of the beam output intensity profile can be effectively mapped to the dependence on the nonlinear coefficient γ in Eq. (2.1). It is worth pointing out that the dependence $\gamma(t)$ is a nonlinear function that saturates at large times. However, it is a monotonic function and uniquely defines the nonlinear index change.
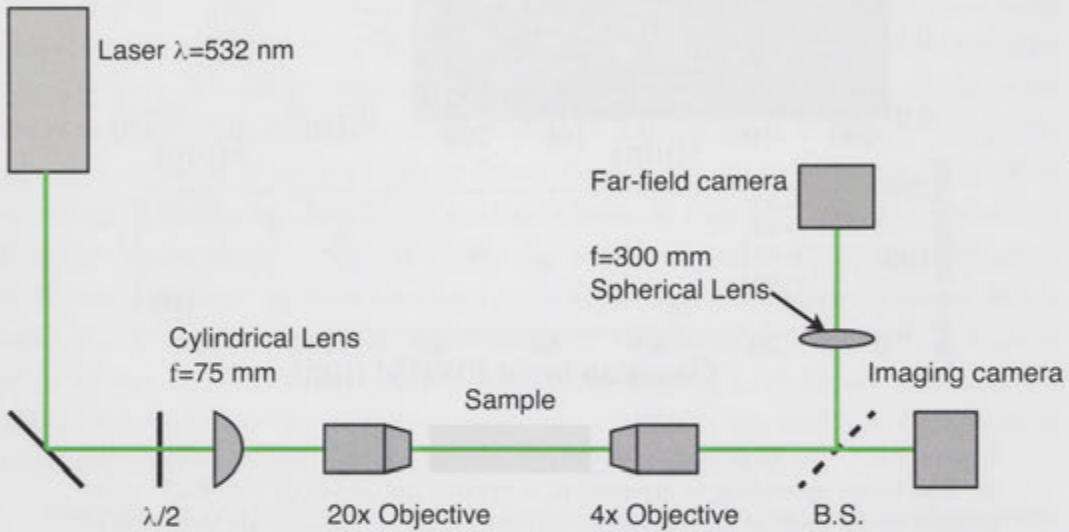
Figure 2.12: Experimental setup to excite truncated nonlinear Bloch waves. A laser beam with wavelength $\lambda = 532$nm is elliptically shaped with a cylindrical lens after being polarised parallel to the plane of the waveguides with a half wave ($\lambda/2$) plate. The cylindrical lens used has either $f = 50$ mm or $f = 75$ mm. A 20x objective lens is used to focus this beam onto the sample, which is imaged with a 4x objective lens. The output is split and imaged directly onto an imaging camera, as well as the passing through a lens to image the Fourier spectrum on a second camera (Far-field camera).

I excite the array with a broad Gaussian laser beam at 532 nm. The input beam (Fig. 2.13(a)) is elliptically shaped (Fig. 2.12) by a cylindrical lens ($f = 50$ mm) before a (20x) focusing objective. I monitor the beam output intensity profile with time for a typical input power of 1 mW and measure the variation of the beam width. We can note here that at these laser powers are far from nonlinearity saturation with intensity [118]. The width of the output beam (Fig. 2.13) is determined as the size of the area which contains 50% of the output light power. This allows us to filter out any noise in the diffraction pattern while maintaining a high degree of accuracy. Error bars are calculated as the asymmetry of the output profile with

Figure 2.13: Output beam width (estimated as the width containing 50% of the total light) vs. time (nonlinear index change). Dashed line – the width of 75% of the input beam, solid line – a fit to the experimental data. (a) Input beam profile; (b) linear diffraction at the output. (c) Nonlinear defocusing at low nonlinearity (time), (d) beam localization at high nonlinearity. Beam power, 1 mW.

respect to the center of the input beam.

2.3.4 Truncated Bloch-Wave Solitons

The linear diffraction in the array causes the beam to spread out and occupy nearly twice the number of waveguides in comparison to the input beam (Fig. 2.13(b)). Upon increase of the nonlinearity with time, we observe an initial defocusing of the beam (Fig. 2.13(c)) resulting from the weak negative nonlinearity. As the exposure time increases and the nonlinearity grows, the beam experiences gradual confinement and reduces its width (Fig. 2.13(d)). The dependence of the beam width with time is plotted in the main panel of Fig. 2.13, where we observe

that the beam localises and the width remains essentially constant. This localised state has a width equal to the width of the input beam containing 75% of the power, where the remaining 25% have been lost in radiation (filtered out in my method for beam-width estimation). Small oscillations around this value are observed at longer times, thus matching the numerical predictions in Fig. 2.11.
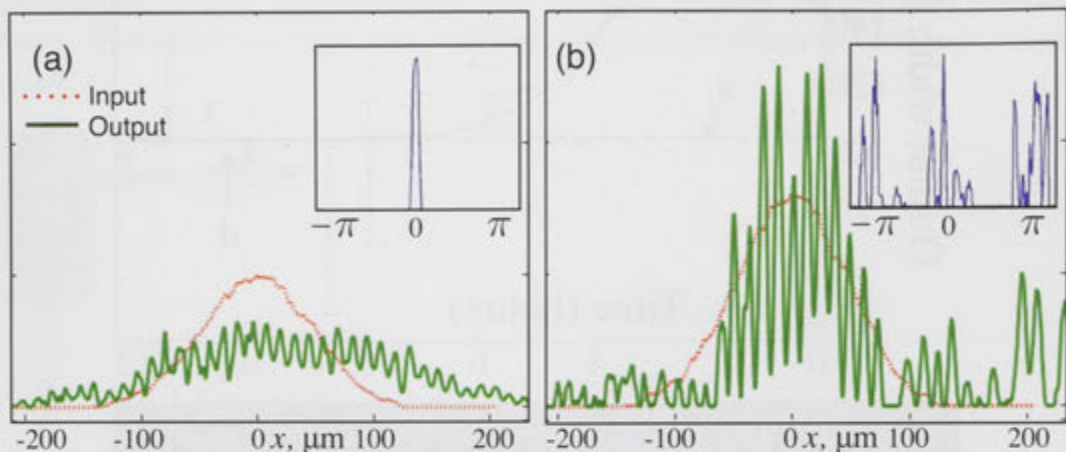
Figure 2.14: Beam profiles at the array input (dotted line) and output (solid) for (a) linear ($t \sim 0$) and (b) nonlinear ($t = 10$ hours) propagation, corresponding to Figs. 2.13(b,d). Insets: Fourier spectrum of the output beams. $\pm\pi$ indicate the edges of the Brillouin zone of the lattice.

Proof that the nonlinear localization is inside the Bragg reflection gap is the appearance of spatial frequencies at the edges of the Brillouin zone. This is seen in the insets of Fig. 2.14 together with the intensity profiles of the beam for linear and nonlinear propagation. We can note here that the intensity scale in the Fourier spectrum plots is nonlinear due to the nonlinear response of the camera.

A unique property of the optical system is the ability to control independently the width and the power of the input beam. This control allows us to test the new feature of nonlinear Bloch wave localisation – that it is parameterised by the input beam width rather than by the input power. For this purpose the input beam width in my experiment is reduced using a cylindrical lens with $f = 75$ mm. This arrangement results in an input beam nearly half the beam width in Fig. 2.13(a). The variations of the output beam width vs. the increase of the nonlinear response with time is shown in Fig. 2.15. Due to the strong diffraction in this case, the output beam profile acquires more noise and I therefore estimate the beam width as the area containing 30% of the total output power. Nevertheless, we can again identify similar behaviour of the output beam evolution. First we observe the initial beam defocusing with increase of the nonlinearity, while at longer times the beam confines
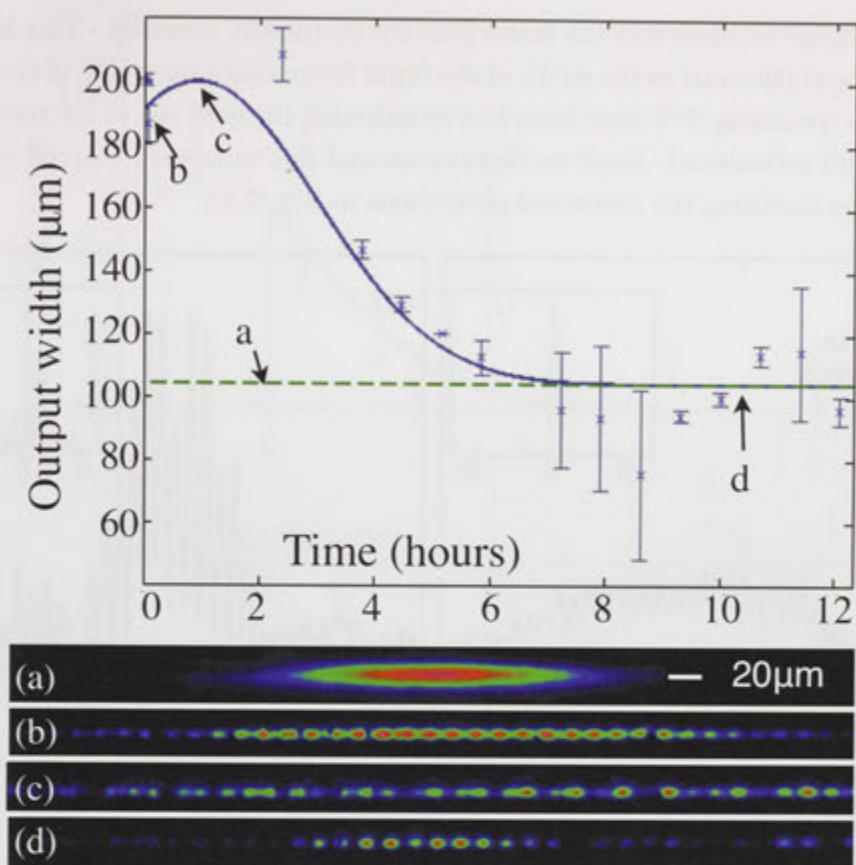
66
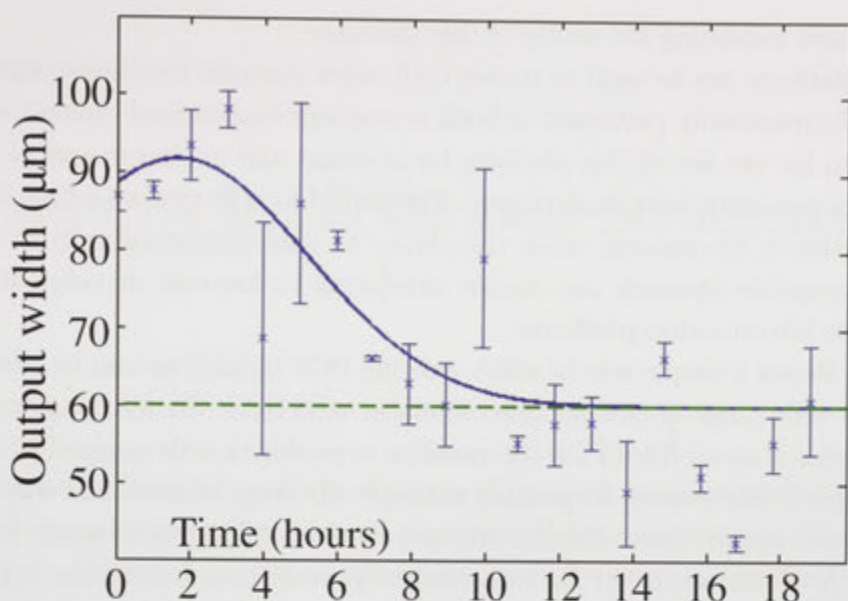
Figure 2.15: Output beam width (estimated as the width containing 30% of the total light) vs. time (nonlinear index change). Dashed line indicates the width of 65% of the input beam, solid line indicates a fit to the experimental data. Beam power, 1 mW.

to a narrower localised state equal to the width of the input beam containing about 65% of the total input power.

The higher loss in this localisation process can be intuitively understood since the narrower beam (of the same power) used in Fig. 2.15 has approximately twice higher intensity than the beam of Fig. 2.13. This higher intensity pushes the propagation constant into the higher order bands, leading to higher losses. Most importantly, however, the experiments shown in Fig. 2.13 and Fig. 2.15, confirm the unique property of the truncated Bloch wave localisation in comparison to any other nonlinear localised states known in nature, namely that the width of the localised state remains independent of the nonlinearity, but can be chosen by the width of the input excitation.

2.4   Chapter Summary

In this Chapter I have demonstrated a technique for the fabrication of one dimensional arrays of sealed, micron scale hollow channels using dry film lamination of SU8 polymer. The channels can be easily infiltrated with high refractive index fluid to enable optical waveguiding. Temperature tuned discrete diffraction has been

demonstrated validating the utility of this platform.

This platform can be used to realise high index contrast waveguide arrays that can be lithographically patterned in both lateral and longitudinal dimensions. The exploration for the use of this platform for resonant and nonlinear optical investigations are presently being undertaken. The ability to infiltrate with fluid suggests opportunities in bio-sensing, while the ability to photolithographically define the optical waveguide channels can enable interfacing to low-cost densely integrated opto-fluidic lab-on-a-chip platforms.

I have shown a simple way in which existing PCF technology can be adapted to produce a wide range of new periodic nonlinear structures. By blocking one end of selected holes of an air filled PCF it is possible to produce a wide range of structures. I have applied this process to produce a simple 1D array of nonlinear waveguides, and demonstrated 1D linear discrete diffraction, and nonlinear defocusing. I propose that this platform can easily be expanded to provide long interaction lengths (> 10 cm) with the infiltrating liquid with little, if any, alteration to the procedure described here. Such arrays can go beyond 1D planar structures, and can include 2D networks for tuneable beam interaction [108], ring structures for beam steering. Other infiltration patterns can be used to control birefringence [91]. 2D arrays can be adapted with complex surface structures and geometries, allowing for the study of surface states. This method can also be used with other nonlinear liquids without alteration, since the infiltrating liquid and blocking liquids never come into direct contact they will have no interaction. This allows for the selective infiltration of solvents with higher nonlinearity such as Toluene or CS_2, although the high index and low boiling point would make coupling between waveguides very weak [122]. Liquids with stronger nonlinear responses would enhance the nonlinear diffraction, and could be used to probe other nonlinear effects such as gap solitons.

I have observed nonlinear self-trapping of broad optical beams in defocusing waveguide arrays. I have revealed that these novel types of spatially localised modes can have an arbitrary width defined by the input beam, while the width is practically independent of nonlinearity. The origin of these effects lies in the existence of an infinite number of independent families of localised solutions with different, but fixed, widths, which persist into the higher order bands of the linear bandgap structure. My experimental results provide the first proof of the existence of the unique properties of such states. I believe that the robust nature of the truncated nonlinear Bloch states and their controllable generation will encourage further observation in other physical systems, along with recent observation in optically induced lattices [116], including higher dimensional ones.

Nonlinearity in 2D Periodic Structures

Having studied several nonlinear effects in 1D periodic arrays of nonlinear waveguides, we can now generalise some of these to 2D hexagonal arrays of nonlinear waveguides. Moving from 1D to 2D opens up new opportunities to study new physical effects and to further investigate light propagation in tuneable nonlinear periodic photonic structures.

I utilise liquid infiltrated Photonic Crystal Fibres as a 2D array of tuneable nonlinear waveguides in a hexagonal array. I begin by studying nonlocal gap solitons, where structure far from the light field influence soliton formation because of heat flow. I then study the point at which a 2D nonlinear periodic system crosses from focusing to defocusing. Solitons are no longer excitable in a waveguide array below a threshold index contrast, but before the index contrast reaches zero because the bandgap closes while the index contrast is still positive. Finally I study vortex states on the surface of the core of a photonic crystal fibre, their existence and stability in linear and nonlinear propagation.

3.1   Nonlocal Gap Solitons

3.1.1   Introduction

The study of nonlinear wave propagation in periodic photonic structures has attracted a lot of recent interest due to possibility to engineer both linear and nonlinear properties of the material. In such systems, self-localised beams or lattice solitons can exist due to the interplay between effective diffraction and nonlinearity. Lattice solitons have been observed in various physical systems including optics [38], but only with on-site nonlinearity. The consideration of long-range nonlinear interactions between lattice sites, on the other hand, have shown to lead to novel nonlinear phenomena [123]. Such interactions appear when the nonlinear response at a particular lattice site is affected by the light intensity not only at this site

but also at its neighbours. In periodic structures, long-range nonlinear interactions can naturally arise from nonlocal response. Nonlocality is common to many physical systems [35], occurring due to electrostatic interactions or diffusion processes, however, its effect in periodic structures has not been investigated experimentally.

In this section of my thesis I study nonlinear localised states in a two-dimensional (2D) periodic system with nonlocal nonlinear interaction between the lattice sites and demonstrate, for the first time to my knowledge, the formation of *nonlocal gap solitons*.

I utilise the hexagonal lattice of the cladding of a photonic crystal fibre (PCF), where the holes are infiltrated with a high-index weakly absorbing oil. The nonlinearity in my system is *defocusing* and has thermal origin that arises due to the negative thermo-optic coefficient of the oil, while the nonlocality originates from the diffusive nature of heat transfer [124].

Nonlocal solitons have been experimentally studied in homogeneous media [125], but in periodic structures only theoretical studies in the one-dimensional (1D) case can be found [126, 127, 128, 129]. In defocusing materials, however, no nonlocal bright solitons have been observed to date. Only recently, it has been theoretically shown that 1D nonlocal solitons can exist in periodic structures with defocusing nonlinearity through localisation in the Bragg gap. In two dimensions, however, the situation can become dramatically different, since a complete Bragg gap only exists above a threshold value of the refractive index contrast [43, 53].

3.1.2 Theoretical Studies

I first study theoretically the existence of 2D nonlocal gap solitons in hexagonal lattices [53]. I consider the paraxial beam propagation in a periodic system with diffusive thermal nonlocal nonlinearity described by the equations,

$$i\frac{\partial A}{\partial z}(x, y, z) + \nabla_\perp^2 A(x, y, z) - p^2 A(x, y, z)$$
$$= -[n_0(x, y) - \tau(x, y, z)F_n(x, y)]^2 q^2 A(x, y, z), \tag{3.1}$$
$$\nabla_\perp^2 \tau(x, y, z) = -|A(x, y, z)|^2, \tag{3.2}$$

where $A(x, y, z)$ stands for the normalised envelope of the electric field, and $\tau(x, y, z)$ is the normalised nonlinearly-induced temperature change. The transverse dimensions are scaled to the pitch Λ, which is the distance between two adjacent holes (Fig. 3.1(a)). q is the normalised vacuum wavenumber, p is the normalised propagation constant, and $n_0(x, y)$ is the linear periodic refractive index. $F_n(x, y)$ is a normalised nonlinear coefficient with $F_n(x, y) = 1$ in the holes and zero elsewhere. This is justified since the thermal nonlinear response of the liquid dominates the

thermal response of the glass. Due to scaling $-\tau(x, y, z)n(x, y)$ can be interpreted as the light induced index change.

My structure (Fig. 3.1(a)) consists of high-index cylinders placed in a hexagonal pattern inside a circle with radius $R_0 = 5\Lambda$. R_0 must be large enough to encompass all the high-index cylinders and my results do not depend on its value. Away from the core the electric field decays rapidly, and we can therefore assume that a vanishes at the boundary of our computational domain R_0. The boundary condition for the temperature field requires a more careful analysis since commercially available PCFs often contain a large homogeneous region of silica outside the last ring of holes. If we assume that the physical fibre has a radius $R_1 = sR_0$ ($s \geq 1$), and that the temperature at the outer boundary is constant, $\tau(r = sR_0/\Lambda) = 0$, it can be shown that $\tau(R_0/\Lambda)/\tau_r(R_0/\Lambda) = -\log(s)R_0/\Lambda$. Here τ_r denotes differentiation with respect to radial coordinate. The above relation is derived under the condition that the heat distribution in the region from R_0 to R_1 is radially symmetric, and that there is no heat source in this region. The meaning of this relation is that one can practically control the electric field inside the lattice by varying the homogeneous spatial extent of the fibre (where the field is zero). This is a clear signature of the nonlocal thermal response, where the degree of nonlocality in the system is measured by the parameter $s = R_1/R_0$. The larger s relates to stronger nonlocality.
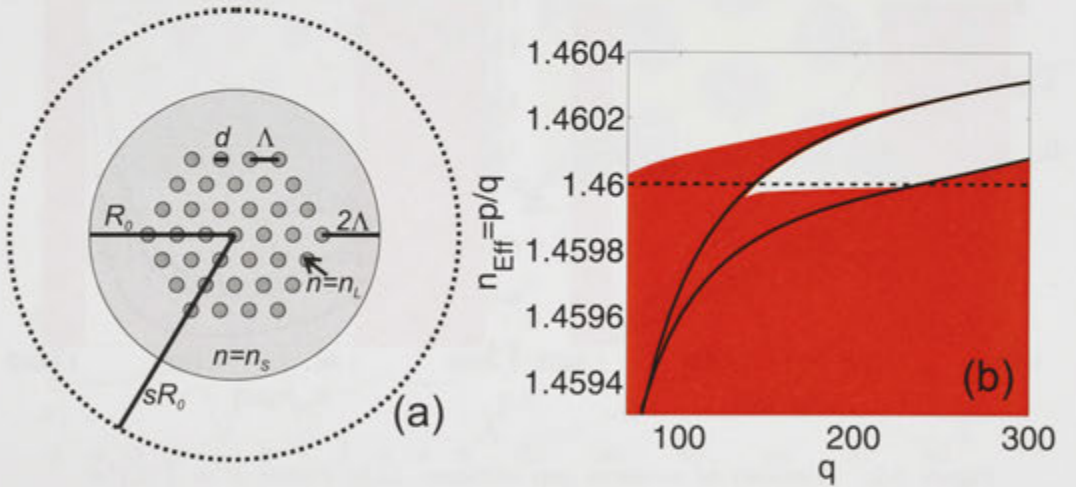
Figure 3.1: (a) System geometry. (b) Bandgap structure for $n_S = 1.46$, $n_L = 1.4605$, and $d/\Lambda = 0.5$. Shaded regions correspond to the bands of the finite structure in (a), while the solid lines show the edges of the first bandgap of an infinite lattice. The dashed line indicates the index of the solid material n_S.

The 2D lattice with thermal nonlinearity is inherently finite because the nonlinearity relies on the boundaries [124]. Therefore, I find the eigenmodes of Eq. (3.1)

on the finite domain shown in Fig. 3.1(a). The discrete spectrum of eigenvalues is divided into bands of closely spaced values separated by large jumps, similarly to the Bloch states of an infinite periodic lattice as shown in Fig. 3.1(b) ($d/\Lambda = 0.5$). In these calculations $n(x, y) = 1.4605$ in the holes, and 1.46 elsewhere. A bandgap is seen to open up at $q \approx 140$. In Fig. 3.1(b) the edges of the first finite bandgap of the corresponding infinite periodic lattice are also plotted with solid lines. At large q the edges of the first gap for the finite and the infinite structure almost coincide, while at smaller values there are propagation constants where a gap exists in the infinite, but does not exist in the finite structure.

The presence of the bandgap allows for existence of nonlinear localised states which for defocusing nonlinearity bifurcate from the bottom of the first band. I find these modes by looking for self-consistent z-independent solutions of Eqs. (3.1-3.2). Importantly, my calculations presented in Fig. 3.2 show that the gap solitons occupy the whole bandgap, regardless of the degree of nonlocality. I have tested this for different relative hole-diameters and outer boundaries, and every time the gap solitons occupy the whole bandgap. This is in contrast to earlier studies of asymmetric nonlocal response where solitons cease to exist at large nonlocality [127].
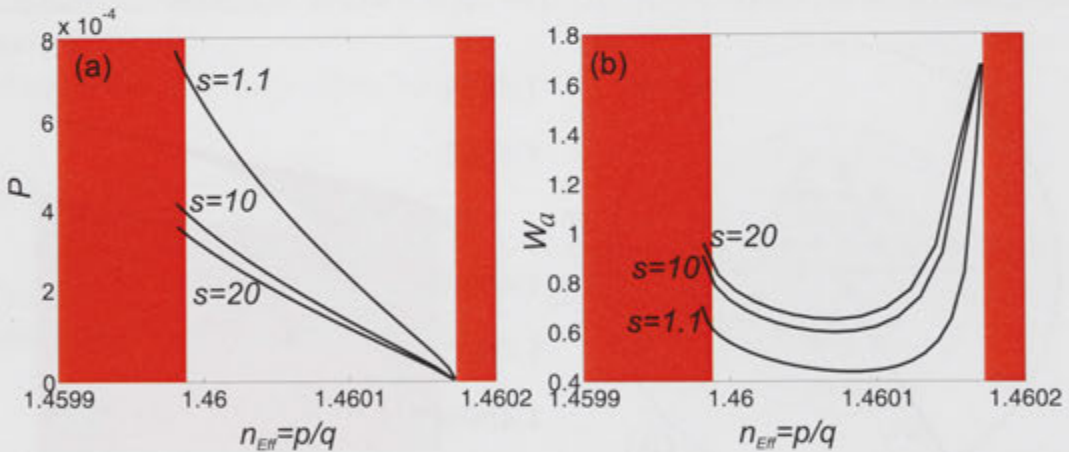
Figure 3.2: Families of nonlocal gap solitons. (a,b) Power $P = \int |E|^2 dr$ and soliton width vs. effective index for different values of s. The normalised wave number is $q = 200$. The dots correspond to the example in Fig. 3.3.

In Fig. 3.2(a), I show the soliton power vs. effective index for different values of nonlocality s. Notice that at high powers even solitons with propagation constants inside the second band of the corresponding linear structure exist. This apparent contradiction is a result of the finite size of my system which enables the temperature response to perturb the whole lattice, and thereby change the linear dispersion

bands. The same behaviour was also recently reported for a 1D system [129]. Another interesting feature seen in Fig. 3.2(a) is the decrease of the soliton power at increased degree of nonlocality. This is somewhat counter-intuitive, as one might expect that with increase of the thermal mass of the fibre (larger s) one would need to inject more power in order to achieve the same nonlinear effect.

In Fig. 3.2(b) I plot the soliton width $w_a = (\int r^2 |A|^2 dx dy / \int |A|^2 dx dy)^{1/2}$ as a function of $n_{\text{Eff}} = p/q$ for different values of the nonlocality parameter s. The solitons are seen to localise as they move further into the bandgap, until the effective index reaches approximately the middle of the bandgap. Then the solitons start to delocalise again. This behaviour is similar to what has been observed for gap solitons with local nonlinearity [130]. The main effect of nonlocality in the system is the spatial broadening of the solitons with increasing parameter s. This behaviour is typical to other nonlocal nonlinear systems [35].
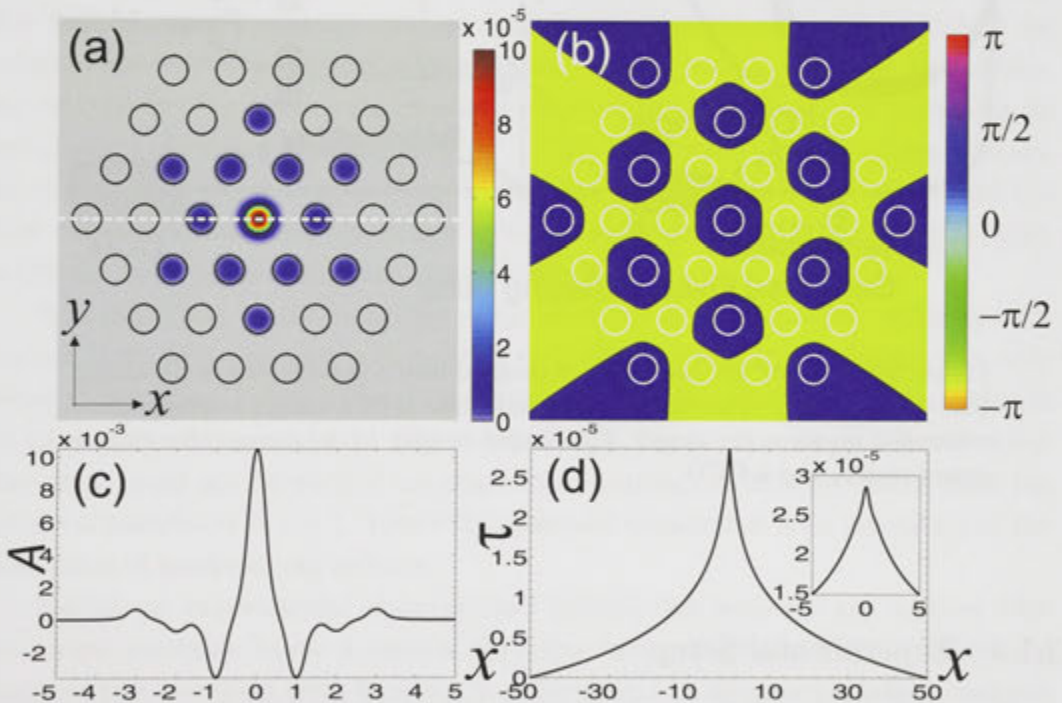
Figure 3.3: Numerically calculated nonlocal gap soliton for power $P = 4 \cdot 10^{-5}$ and $s = 10$, marked with a dot in Fig. 3.2. (a) Intensity and (b) corresponding phase distribution. (c) Soliton profile and (d) induced temperature change along the symmetry line shown white dashed line in (a).

An example of a gap-soliton profile is shown in Fig. 3.3(a). An inherent signature of the localisation in the Bragg gap is the staggered phase structure shown in Fig. 3.3(b). This staggered structure is in the form of concentric rings around the central

hole and resembles the electric field profile of one-dimensional gap solitons [39]. An important difference from gap solitons with local nonlinearity is the actual induced index change. In the thermal nonlocal case, this is represented by the induced temperature response (Fig. 3.3(d)) that is extended fully towards the boundaries of the structure.
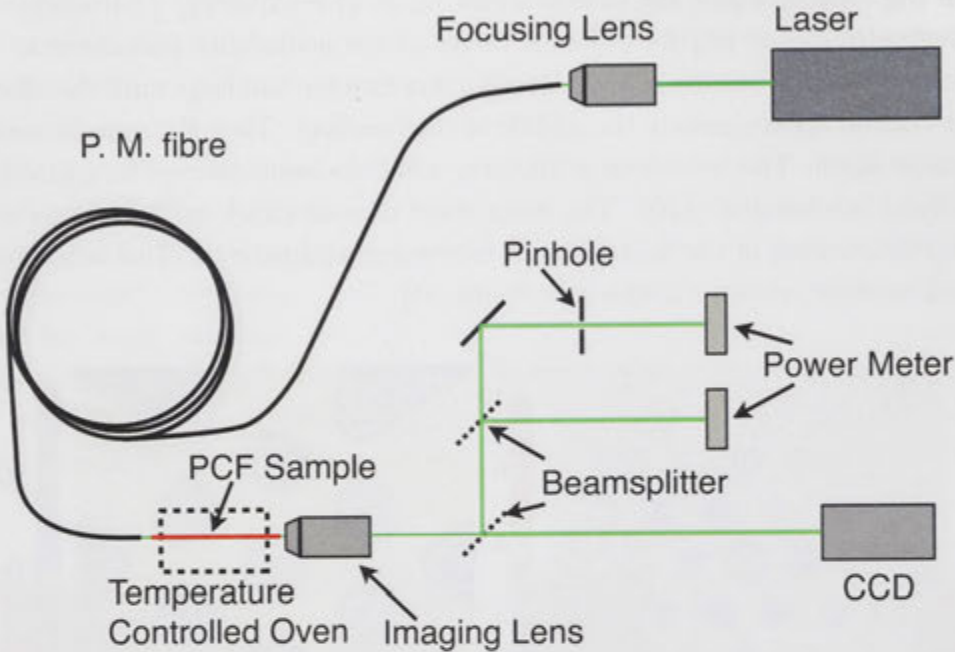
Figure 3.4: λ=532 nm laser light is coupled into a polarisation maintaining fibre (P. M. fibre). This butt-couples light into a PCF inside a temperature controlled on an x, y, z stage. The output is split by a beamsplitter to two power meters and a CCD.

3.1.3 Experimental Setup

To verify experimentally my predictions that gap solitons exists in nonlocal 2D lattice, I employ a system comprising the liquid-infiltrated PCF cladding, similar to our earlier experiments [85]. I use a commercially available fibre LMA-15(7) (from Crystal Fibre) with a relative hole diameter $d/\Lambda \approx 0.498$ and $s \approx 1$. The cladding holes are filled by capillary action with an index matching oil ($n = 1.48$). The fibre is placed in a temperature controlled oven (Fig. 3.4 and heated to 76°C such that the refractive index of the oil is reduced closer to the index of silica. 532 nm light is butt coupled into a single infiltrated hole in the cladding, well away from the core, using a single-mode fibre. The output is split to two power meters and a CCD. A

74

pinhole is placed in the imaging plane in front of one power meter, allowing light from the input waveguide to pass through to the power meter. The other power meter measures power for the entire output image. This allows us to measure the fraction of light in the input waveguide.

3.1.4 Observation and Characterisation of Nonlocal Gap Solitons

In this system, we can see linear diffraction at low input power ($\sim 3\,\mathrm{mW}$) (Fig. 3.5(a)), corresponding to propagation of approximately three diffraction lengths. At high laser power ($\sim 100\,\mathrm{mW}$) (Fig. 3.5(b)) we observe nonlinear self-localisation to almost a single lattice site. Utilising a pinhole (Fig. 3.4) I also measure the amount of light in the input hole as a function of the power injected in the fibre (Fig. 3.5(c)). This dependence effectively represents the degree of localisation achieved experimentally, and it corresponds to the theoretical predictions in Fig. 3.2. Indeed, my experiments confirm that the amount of localisation is highest for intermediate powers, while the soliton is delocalised at both band edges. In addition, we can observe the alternating phase structure of the gap solitons by producing an interference of the nonlinear mode (Fig. 3.5(b)) and a wide inclined reference beam. In the resulting interferogram (Fig. 3.5(d)), the input hole is out of phase with the first ring (upper line, expressed in a half-a-period shift in the interference fringes), while the first ring has constant phase (lower line).

It is important to mention that in my previous experiments [85] utilising infiltrated fibres with stronger nonlocality $s \approx 2$, we observed no localisation but only beam defocusing. This is a direct consequence of the fact that the nonlocal solitons in those fibres are much wider (due to the larger degree of nonlocality) and therefore they could not be excited via single site coupling. In this presented work the nonlocal parameter is $s = 1$. Hence the observed localisation is an indication of the formation of nonlocal gap solitons.

During my experimental observations I noticed that nonlocal gap solitons were no longer excitable below a certain refractive index contrast. This is interesting because this switching from focusing to defocusing in nonlinear periodic structures occurs before the index contrast is zero, meaning light is still guided in the liquid waveguides.
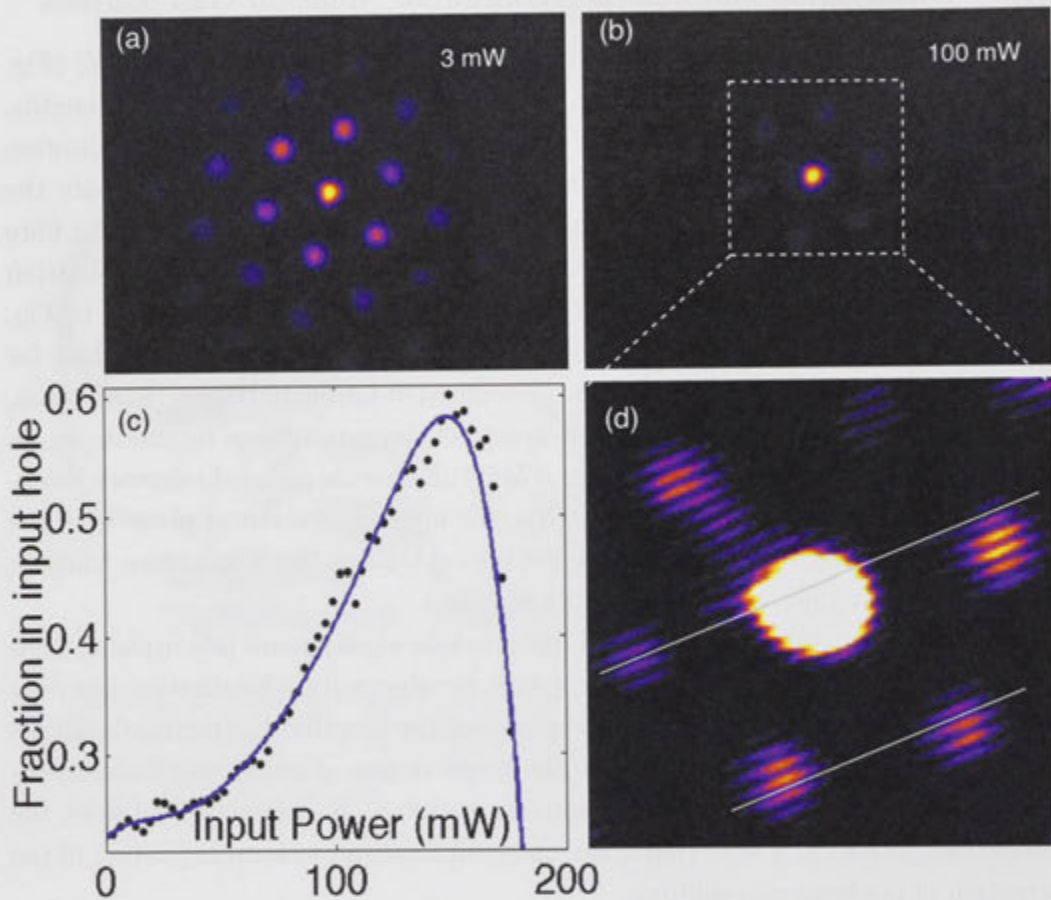
Figure 3.5: (a, b) Experimentally observed output diffraction pattern and soliton localisation in a liquid infiltrated PCF, at low and high input power, respectively. (c) Fraction of light in the input hole vs. input power. (d) Measured interference pattern of the output beam with an inclined reference beam.

3.2 Focusing to Defocusing Crossover in Nonlinear Periodic Photonic Structures

3.2.1 Introduction

Self-action of light in nonlinear periodic structures is a rich physical phenomenon giving rise to a range of fundamental phenomena which can only be observed due to the medium periodicity and have no analogue in homogeneous systems. Periodic structures in optics introduce dramatic changes in the linear wave spectrum through the the appearance of photonic band-gaps, and subsequent qualitative and quantitative modification of wave transport [131]. These features furthermore have a dramatic effect on nonlinear wave dynamics, in particular enabling localisation of slow-light pulses in the form of gap solitons [132] and supporting new types of spatial solitons and breathers [133].

A remarkable effect demonstrating a key difference between homogeneous and periodic nonlinear structures is the laser beam self-action. When an optical medium features Kerr-type nonlinear response such that the optical refractive index is decreased in the region of high optical intensity, then such nonlinearity is traditionally called "self-defocusing", since the nonlinear beam self-action leads to accelerated beam diffraction in such homogeneous medium [16]. However, in periodic photonic lattices or waveguide arrays the same type of nonlinearity can lead to beam focusing and self-trapping as was predicted theoretically [39, 134, 135] and subsequently observed experimentally [43, 44, 103]. Such reversal of nonlinear self-action can appear due to the transition of wave transport from continuous to discrete tunnelling between the waveguides [28] and the simultaneous opening of photonic band-gaps.

Whereas the nonlinear beam self-action is well understood in the extreme cases of purely homogeneous structures and strongly modulated periodic lattices, the beam dynamics in the intermediate regime is less studied. It was predicted theoretically for 1D lattices that there is a threshold (non-zero) value of modulation where the nonlinear beam response sharply switches its behavior [103], however this was not observed experimentally.

In this section, I employ a photonic structure with highly tuneable index modulation and present the first experimental demonstration of crossover from nonlinear self-focusing to defocusing when the refractive index modulation is gradually decreased. In my experiments I utilise the cladding of an liquid-infiltrated photonic crystal fibre (PCF) [85, 106] (see inset in Fig. 3.6) and use precision control of the fibre temperature to tune the index modulation of the two-dimensional (2D) periodic structure. In addition, the weak absorption of laser light in the liquid results in thermal defocusing nonlinearity. In such a way, my system enables detailed studies
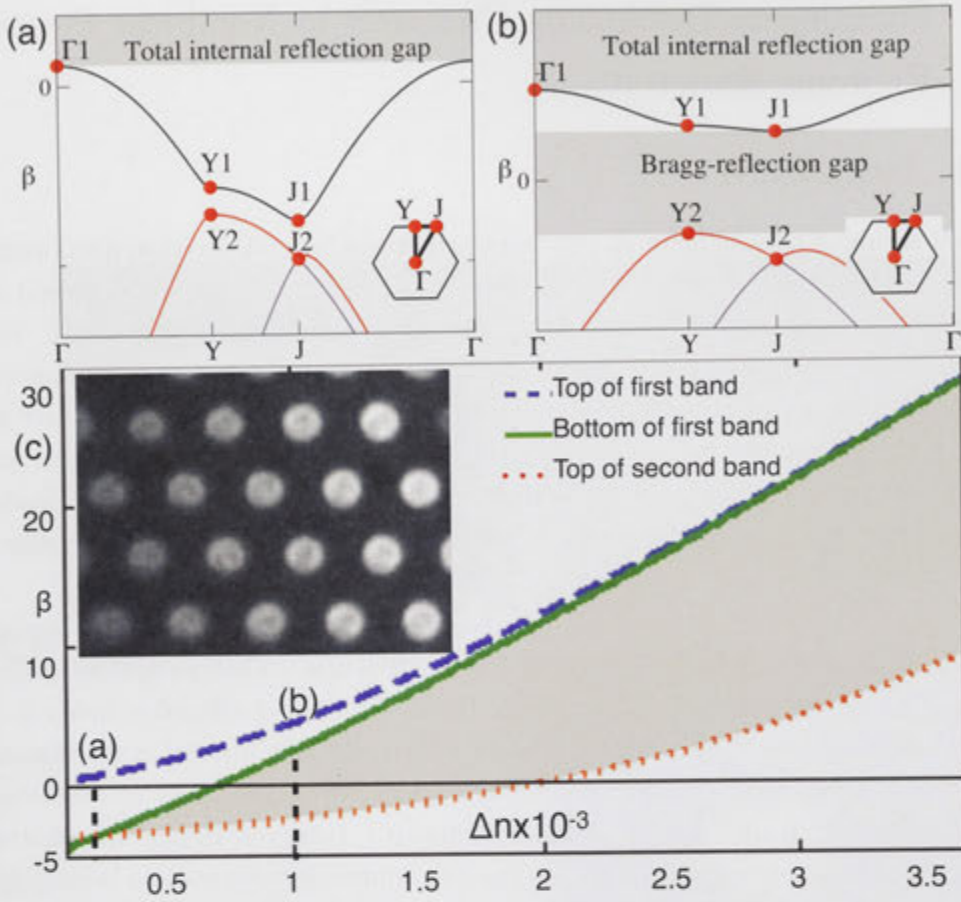
Figure 3.6: (a, b) Bandgap diagrams for refractive index modulation of 0.2×10^{-3} and 10^{-3}, respectively. (c) Propagation constants of the top (dashed line) and bottom (solid line) of the 1st and top of the 2nd band (red dashed line) vs. index modulation. Shading marks the position of the bandgap. Inset: hexagonal array of infiltrated holes in the PCF cladding.

of the interplay between periodicity and nonlinearity.

3.2.2 Theoretical Studies

First I characterise my system theoretically. The use of a 2D periodic structure brings some richer physics in the process of light localisation [43] in comparison to the 1D case [44, 103]. In particular, because for defocusing nonlinearity the propagation constant of localised states resides in the Bragg reflection gap, it is important that such gap exists. However, a property of the 2D lattices is that below a certain lattice depth the structure does not support a complete photonic bandgap anymore and only partial gaps in specific directions are allowed. This is

illustrated in Fig. 3.6(a,b) showing the bandgap structure (propagation constant vs. transverse wavenumber) of the hexagonal lattice for two different refractive index modulations. While in the case of $\Delta n = 10^{-3}$ there is a complete 2D bandgap in the system, for smaller index modulation, $\Delta n = 0.2 \times 10^{-3}$, the gap is only indirect and no localised states can exist.

To illustrate the closing of the 2D photonic gap with index modulation, in Fig. 3.6(c) I plot the propagation constants of the top ($\Gamma 1$ point) and bottom (J1 or Y1 points) of the first band together with the propagation constant of the top of the second band (Y2 point). With the decreasing of the index contrast of the structure, the gap (shaded area in Fig. 3.6(c)) gets narrower and completely closes for $\Delta n = 2.3 \times 10^{-4}$. Obviously, the localisation of beams in the 2D system is not possible when the gap is completely closed. This is in contrast to the 1D case where the Bragg reflection gap always exists.

Next, I simulate the beam evolution in my structure by solving the 2D nonlinear Schrödinger equation for the slowly varying electric field envelope A:

$$i\partial_z A + D\nabla_\perp^2 A + (2\pi\gamma/\lambda)|A|^2 A + (2\pi/\lambda)F(x,y) = 0. \qquad (3.3)$$

Here $\nabla_\perp^2 = \partial_x^2 + \partial_y^2$ is the transverse Laplacian, $D = \lambda/4\pi n_b$ is the diffraction coefficient, γ is the nonlinear coefficient, λ is the wavelength of light, n_b is the background refractive index, and $F(x,y)$ is the refractive index profile defined numerically as a hexagonal lattice of circular holes with a diameter of $5\,\mu$m, period $10\,\mu$m and refractive index contrast Δn. The notation ∂_i, $i = x, y, z$ stands for partial derivative on i. While the general description of the thermal nonlinearity is nonlocal [106], here I use the simpler approximation of Kerr type nonlinearity. As we will see below this model describes well the effect of crossover.

I characterise the beam evolution by calculating the fraction of light in the input waveguide after propagation of $2\,$cm. In Fig. 3.7(middle) I show a 2D plot of this fraction ($\log_{10}$ scale) versus linear (horizontal axis) and nonlinear (vertical axis) index modulation in the lattice. A larger fraction of light in the input hole indicates a stronger beam confinement. In the linear regime ($\gamma = 0$) we observe increased beam diffraction and correspondingly decreased amount of light in the input waveguide as the index contrast is reduced. This is clearly visible in the output intensity distribution shown Fig. 3.7(i,iii,v). In the nonlinear regime ($\gamma < 0$) we can observe high degree of beam localisation and soliton formation for large index contrast ($\Delta n > 2 \times 10^{-3}$), see Fig. 3.7(ii) and (iv). Below an index contrast of $\Delta n = 1.8 \times 10^{-3}$ we can see only beam defocusing with increased light intensity (Fig. 3.7(vi)). This crossover is indicated in Fig. 3.7 by the white dashed line, after which any increases in nonlinear coefficient γ leads to no increase in the fraction of light in the input waveguide. Interestingly, for the obtained threshold index modulation,

the photonic Bragg-reflection gap is fully open (Fig. 3.6(c)), suggesting that the crossover is a fundamental phenomena appearing equally in any periodic structures regardless its dimensionality.
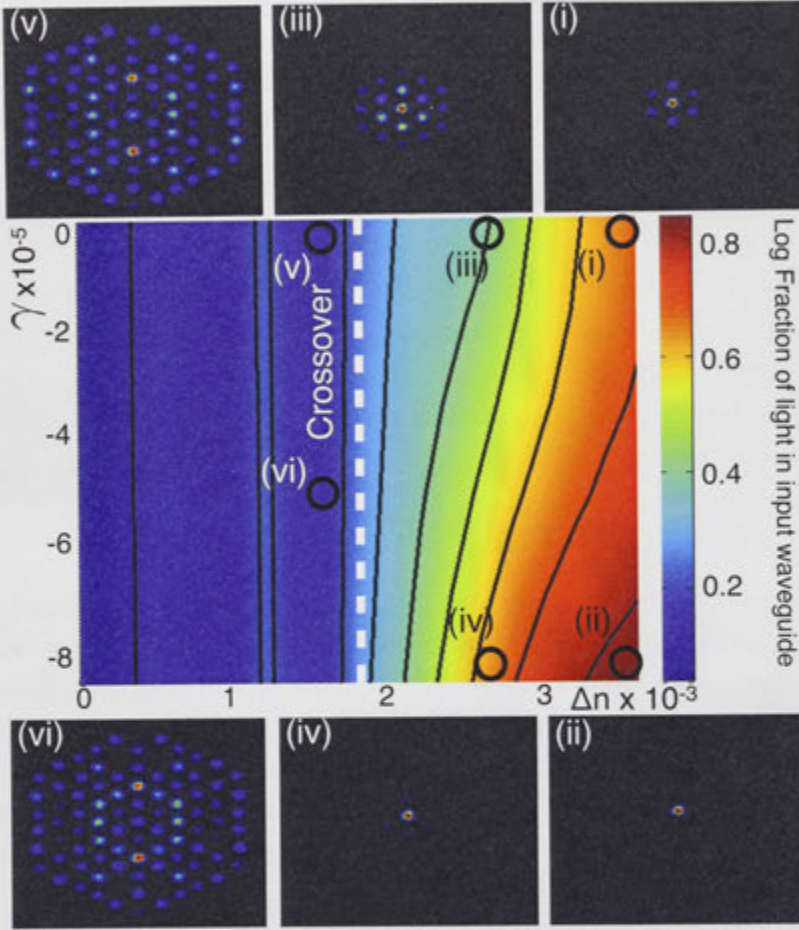
Figure 3.7: Calculated fraction of light in the input waveguide (log scale) over a range of index contrasts (Δn) and nonlinear coefficients (γ). Linear (i,iii,v) and nonlinear (ii,iv,vi) output beam profiles corresponding to the marked points. The white dashed line corresponds to the crossover from focusing to defocusing, black lines indicate contours.

3.2.3 Experimental Setup

For the experimental demonstration of the predicted crossover, I use the cladding of a PCF with a hexagonal arrangement of holes with diameter $\sim 5\,\mu$m and period $\Lambda \approx 10\,\mu$m (see the inset in Fig. 3.6) [106]. The holes are infiltrated with a high-refractive index Cargille oil ($n = 1.48$) which makes them act as optical waveguides.

The fibre is placed inside a temperature stabilised oven (Fig. 3.4), where its temperature is tuned such that the difference in the refractive indices of the infiltrating oil and the surrounding silica is $\sim 10^{-3}$. For sufficiently small refractive index difference between the liquid and the glass matrix the waveguides are coupled together, forming a hexagonal photonic lattice. To probe the structure, I use the light from a CW laser at 532 nm and focus it to one input channel in the array. The output of the fibre is imaged onto a CCD camera, in order to analyse the output beam intensity distributions. The thermal defocusing nonlinearity of the liquid arises due to weak light absorption and the accompanying heating of the liquid channels. This heating leads to expansion of the liquid and a corresponding decrease of its refractive index.

3.2.4 Experimental Observation of Focusing to Defocusing Crossover in Nonlinear Periodic Photonic Structure

I couple light into a single hole of the infiltrated PCF cladding and measure a fraction of light in the central (input) channel of the array as a function of the transmitted total laser power (Fig. 3.4). In Fig. 3.8 I show the measured (points) power dependencies for three different sample temperatures. An increase of the light transmitted through the input channel indicates light beam localisation. For temperatures $76 - 77°C$, the fraction of light in the input waveguide increases as the input power is increased. At high enough powers the beam is localised to a single waveguide (see Fig. 3.8(i-iv)), forming a gap soliton [106]. This strong beam localisation indicates that the system behaves as a discrete one.

Increasing the fibre temperature, hence reducing the refractive index contrast, we observe that the system sharply switches its behaviour. For temperature of $78°C$, with increase of beam power the output beam starts to defocus (Fig. 3.8(v-vi)). The focusing-defocusing transition occurs between $77°C$ and $78°C$ when the refractive index contrast is low enough and the system looses its discreetness. The observed crossover agrees well with my numerical simulations shown by solid curves in Fig. 3.8.

From these experimental and theoretical studies we can conclusively determine the point at which nonlinear periodic photonic structures switch from focusing to defocusing. This switching occurs before the bandgap closes, while the index contrast is still positive. Around this point the beam is very sensitive to changes in index contrast and nonlinearity. Having characterised the coupling and nonlinear properties of these tuneable nonlinear periodic photonic structures (liquid infiltrated PCFs), we can now move on to more advanced beam propagation in this system, including interactions with the boundary of the array.
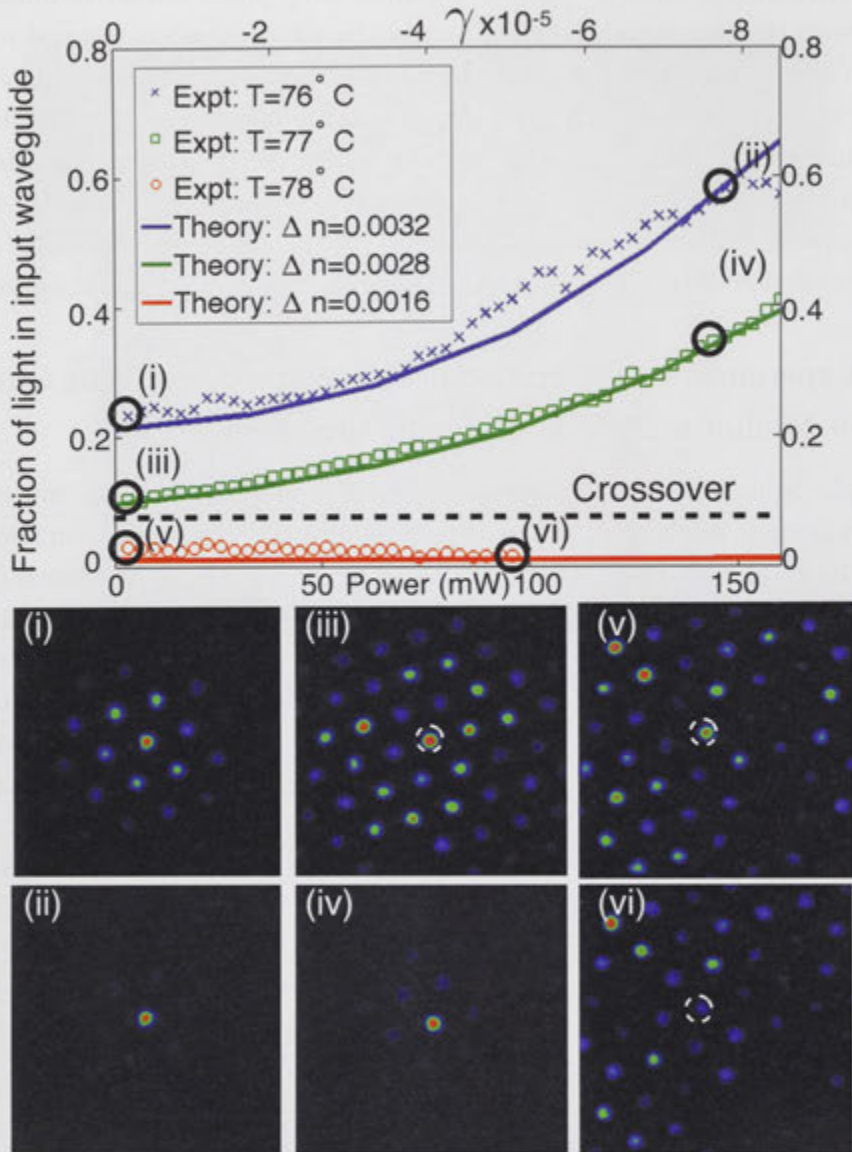
Figure 3.8: (top) Fraction of light in the input waveguide vs. input power/nonlinear coefficient: experiments (points) and numerical simulations (solid lines). (i,iii,v) Experimental images of the output beam in the linear, and (ii,iv,vi) nonlinear regime corresponding to marked points on the top plot and temperatures (i,ii) 76°C, (iii,iv) 77°C, and (v,vi) 78°C.

3.3 Surface Vortex States

3.3.1 Introduction

Until now this thesis has detailed experiments and numerics for nonlinear states in a periodic array without any defects. A defect in such an array can be any disruption to the otherwise regular periodicity of the array, they add new and interesting physics and uses to a system. For example one waveguide could be missing, as is the case in a PCF in the form of a core defect. This core defect is usually used to guide light along the PCF inside the core.

Perhaps the most common defect in any periodic system is the edge of the array. While in theory it is possible to have infinite arrays, such devices are practically difficult to achieve, and usually unnecessary. In both one and two-dimensional systems we find some interesting effects for modes at the edge of an array, when looking at previously well understood linear and nonlinear optical effects in periodic systems. These nonlinear surface states have been extensively studied in both 1D and 2D periodic arrays [136, 32, 137, 138, 57, 139]. Observed discrete and gap solitons occur for lower nonlinearity when on a surface, than when in an extended array [140, 141].

The surface at the edge of a 2D hexagonal array can form a number of angles between 60° and 300° (Fig. 3.9(a)). The excitation of nonlinear states at such angles has been studied in such an array [141], where Szameit *et al.* show that the nonlinearity required for soliton formation depends on the face angle.
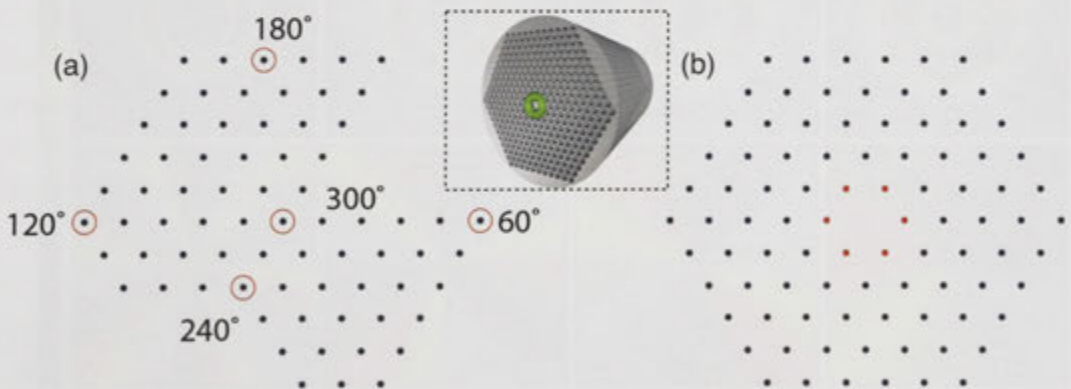

Figure 3.9: (a) A 2D hexagonal array of waveguides, shaped to show surface angles at the intersection of two planar edges with angles between 60° and 300°. (b) The hexagonal array of waveguides in an liquid infiltrated PCF with a vortex beam incident on the waveguides surrounding the core defect (red dots). Inset shows an illustration of the input mode incident on a PCF.

Nonlinear propagation of fundamental Gaussian optical beams has produced a rich variety of physical phenomena such as discrete and gap solitons in positive and negative periodic nonlinear media [27, 38, 39]. We can uncover an even wider range of novel nonlinear optical propagation, by studying modes with different symmetries. One such mode is an optical vortex, which is an optical mode including a phase singularity at its centre.

In this section I describe the work I performed with vortex surface states: vortex beams propagating in a liquid infiltrated PCF around the core defect (Fig. 3.9(b)). I studied such a system theoretically and experimentally.

A vortex mode in optics is an optical mode whose phase is radially uniform, and angular dependant. Such modes have the form:

$$A(z) = A(0)r^{|m|}e^{\left(-\frac{r^2}{w^2}+im\theta\right)}, \tag{3.4}$$

where $A(z)$ is the amplitude of the field, r is the radial coordinate from the centre of the beam, θ is the angular coordinate, m is the charge of the vortex, and w is the width of the beam. An optical vortex therefore has a mode profile with zero amplitude at its centre ($r = 0$), necessitated by the angular phase dependance (a photon cannot have more than one phase, yet a photon at $r = 0$ must have all phases $(0 - m2\pi)$. The toroidal mode profile of vortex modes with charge $m = 1, 2, 3, 6$ are shown in Fig. 3.10.
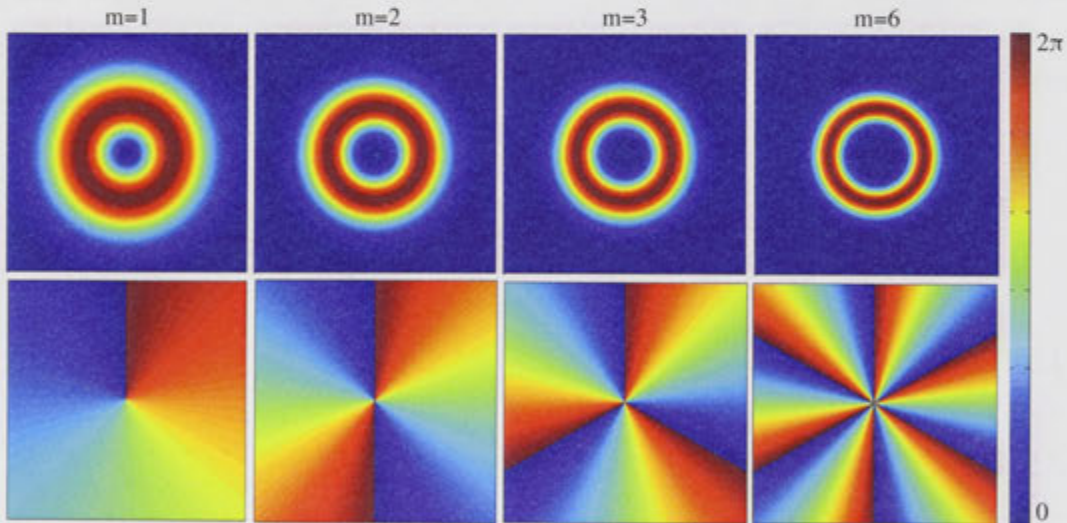

Figure 3.10: Mode profiles (top line) and phase profile (bottom line) for optical vortex modes with charge $m = 1, 2, 3$, and 6.

Optical vortices and their propagation have been studied for their ability to trap and manipulate particles [142], and in the production of waveguides in atomic

vapour [143]. The nonlinear propagation of vortex modes in the core of a photonic crystal fibre (PCF) have been studied theoretically [144, 145, 146, 54, 147], and there have been theoretical and experimental study of vortex solitons in optically induced lattices [148, 149, 29] and bulk nonlinear media [31, 150, 151]. The propagation [152] and reflection [153] of a vortex mode from a nonlinear-linear interface in a bulk media has also been studied for multi-charge vortices, and single charge vortices in semi-infinite optically induced lattices [154].

I take a new approach to the study of optical vortex propagation. Using an hexagonal array of nonlinear waveguides surrounding a solid core, I propagate an optical vortex in the waveguides adjacent to the core. I theoretically study the nonlinear propagation of vortex modes in this system, using both discrete and continuous models.

Such structure is analogous to a liquid infiltrated photonic crystal fibre (PCF), which have been used to study nonlocal gap solitons [106], the crossover from focusing to defocusing in a periodic array (Sec. 3.2), as well as the possibility for selective infiltration for a range of interesting structures and applications (Sec. 2.2) [89, 109].

By propagating a vortex mode in waveguides around the solid core of a PCF we can study vortex modes interacting with a surface, where the periodic structure meets a homogenous dielectric. Such states have been studied and observed in similar structures for single site excitation with Gaussian modes [155, 141]. Similar work has been done at the boundary of an optically induced lattice [154], showing the instability of some propagated vortex modes.

This section is organised as follows: Section 3.3.2 introduces the discrete model for an infiltrated PCF structure with an hexagonal geometry and a central defect making a solid core, in section 3.3.3 I introduce the continuous model of the same structure, focussing on the dynamical evolution of vortex excitations. Section 3.3.4 introduces the experimental setup, and section 3.3.5 discusses experimental results.

3.3.2 Discrete Model

I consider a finite two-dimensional array of weakly-coupled nonlinear (Kerr) waveguides with hexagonal geometry, with a missing waveguide at its center (Fig. 3.11 (a)). In the framework of coupled-modes theory, the electric field $E(x, y, z)$ is presented as a superposition of (single) transverse modes $\phi(x, y)$ with amplitudes $A(z)$ that vary slowly along the longitudinal direction: $E(\mathbf{r}, z) = \sum A_{\mathbf{n}}(z)\phi(\mathbf{r} - \mathbf{n})$, where $\mathbf{r} = (x, y)$ and $\mathbf{n} = (n_x, n_y)$. These amplitudes obey the discrete nonlinear

Schrödinger equation,

$$i\frac{dA_n}{dz} + V\sum_{m\neq n} A_m + \gamma|A_n|^2 A_n = 0,$$ (3.5)

where the sum is restricted to nearest-neighbors. The stationary solutions of Eq.(3.5) have the form $A_n(z) = A_n \exp(i\beta z)$, where A_n obeys

$$-\beta A_n + V\sum_{m\neq n} A_m + \gamma|A_n|^2 A_n = 0.$$ (3.6)

Figure 3.11: Hexagonal waveguide array with central hole. (a) Example of a fundamental inner surface mode ($\beta = 7.5, P = 8.33$). Amount of shading denotes the distribution of optical intensity. (b) Power vs. propagation constant curve for this kind of mode. Solid (dashed) curve denotes stable (unstable) portions.

I am interested in localised modes centred around the boundary of the solid core of the array. The simplest of these 'surface' modes is one centred on any of the six equivalent sites surrounding the missing guide. It is found by solving Eq. (3.6) using a direct extension of the Newton-Raphson method, starting from the decoupled (high-amplitude) limit, and performing a continuation process towards finite coupling values. For each mode found, I perform a standard linear stability analysis. Fig. 3.11(a) shows an example of a spatial profile for this kind of mode, along with its power content $P = \sum |A_n|^2$ vs propagation constant β curve (Fig. 3.11(b)). The curve obtained is typical of surface modes [156] and obeys the Vakhitov-Kolokolov stability criterion. In order to approach something resembling a vortex-like mode, I
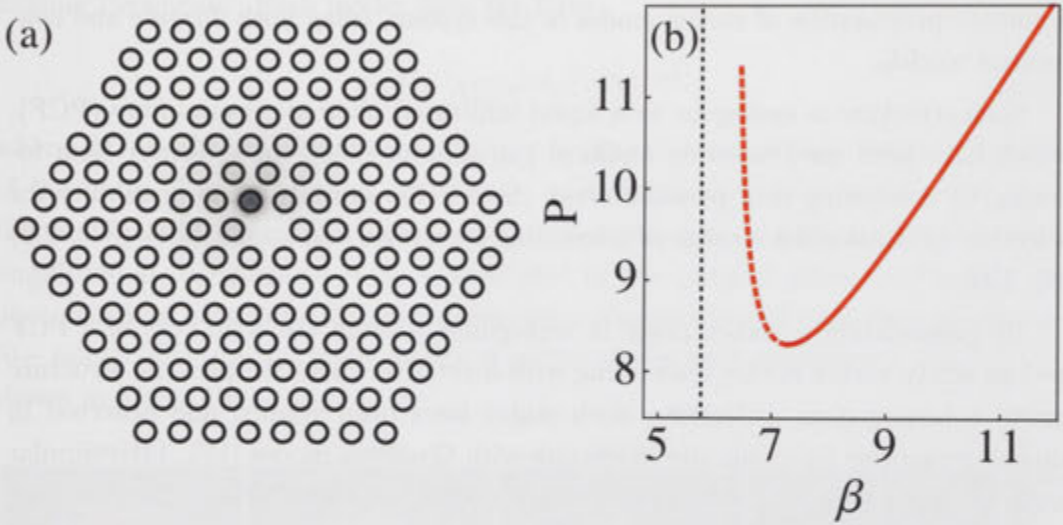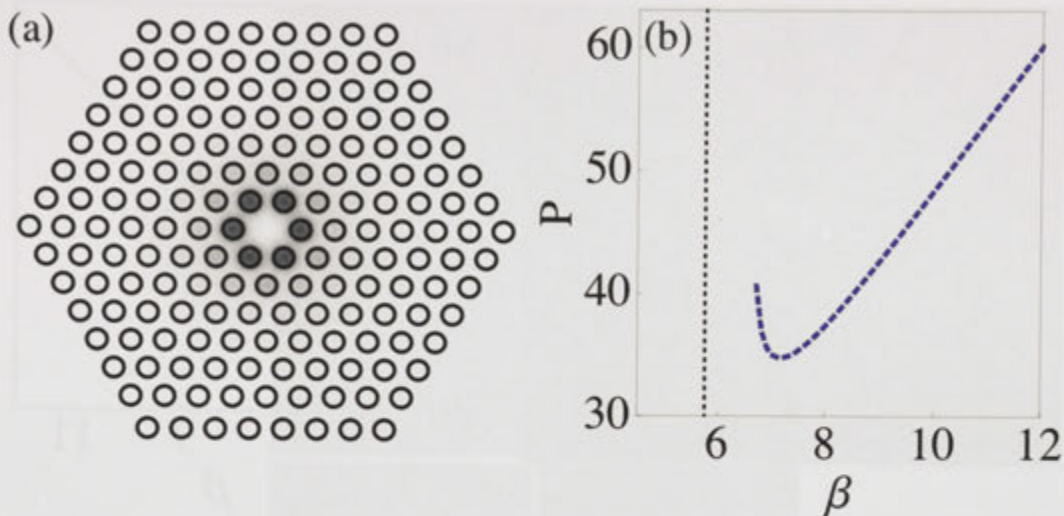
Figure 3.12: Hexagonal waveguide array with central hole. (a) Example of an unstaggered 'ring' surface mode ($\beta = 8.0, P = 37.4$). Amount of shading denotes the distribution of optical intensity. (b) Power vs. propagation constant curve for this kind of mode. This mode is always linearly unstable.

consider next a higher-order mode, in the form of an unstaggered 'ring' around the 'hole', with no phase difference (i.e., zero vorticity). An example of this high-power mode is shown in Fig. 3.12 along with its power vs. propagation constant curve. In this case, the mode is unstable for all values of its propagation constant. In fact, I find that most higher-order surface mode configurations are indeed unstable, with the exception of one: The staggered version of the ring mode (Fig. 3.13(a)), where all amplitudes around the hole are identical initially, but with a phase difference of π between nearest-neighbours around the ring. In this case, the mode is stable for initial amplitudes (Fig. 3.13(b)) exceeding a given threshold.

One interesting question at this points is: If we excite dynamically the unstaggered (i.e. unstable) ring configuration, what are the decay channels for this mode? Will it transition to the low-power, single-site stable mode, or will it change into the staggered (stable) ring, or perhaps it will dissipate as radiation? To look for an answer, I follow the dynamical evolution of an initially completely localised ring mode configuration: $A_n = A_0$ around the six sites surrounding the missing guide, $A_n = 0$ otherwise. Long-time evolution of this mode over large propagation distance for a finite sample of $N = 168$ sites is shown in Fig. 3.14. Clearly, after a long transient behaviour, where the diffracted beam bounces several times from the boundaries of the array, the beam becomes eventually self-trapped in one of the six possible fundamental mode configurations. It is interesting to note that this self-trapping
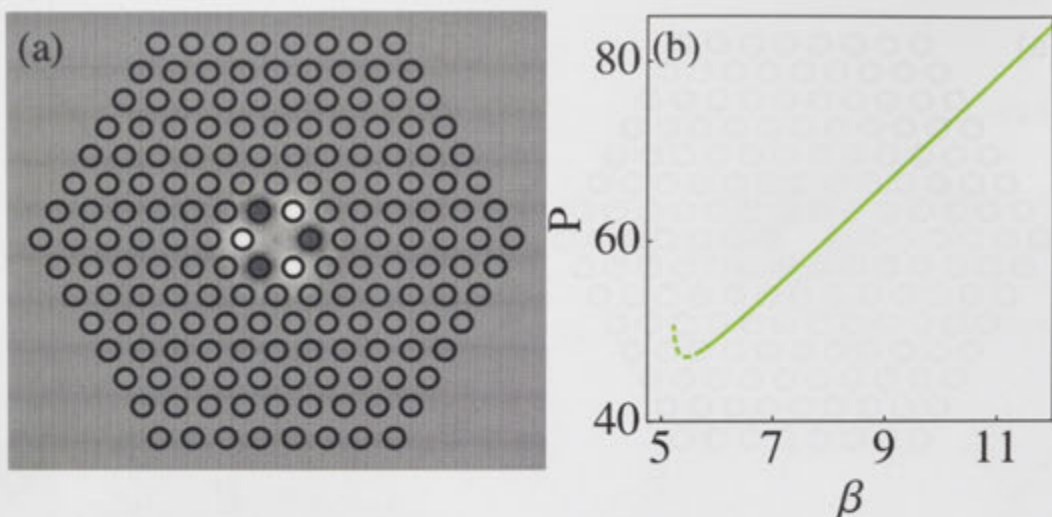
87

Figure 3.13: Hexagonal waveguide array with central hole. (a) Example of an staggered 'ring' surface mode ($\beta = 5.75, P = 47.95$). Amount of shading denotes the distribution of the mode amplitude, going from white (amplitude=−3) to dark grey (amplitude=+3). (b) Power vs. propagation constant curve for this kind of mode. Solid (dashed) curve denotes stable (unstable) portions.

transition is quite abrupt, as evidenced in Fig. 3.15.

3.3.3 Continuous Model

Given the geometry of the array, it is conceivable that the addition of vorticity could stabilise this (unstable) ring mode. After all, we know that in two-dimensional square arrays, the addition of vorticity can stabilise some low-power modes that are otherwise, unstable [54].

In order to test this idea in conditions that are closer to an actual experiment, I simulate next the beam evolution in the structure by solving the *continuous* 2D nonlinear Schrödinger equation for the slowly varying electric field envelope A:

$$i\frac{\partial A}{\partial z} + D\left(\frac{\partial^2}{\partial x^2} + \frac{\partial^2}{\partial y^2}\right) A + \frac{2\pi\gamma}{\lambda}|A|^2 A + \frac{2\pi}{\lambda} F(x,y) = 0 \qquad (3.7)$$

Where $\nabla_\perp^2 = \partial_x^2 + \partial_y^2$ is the transverse Laplacian, $D = \lambda/4\pi n_b$ is the diffraction coefficient, γ is the nonlinear coefficient, λ is the wavelength of light, n_b is the background refractive index, and $F(x,y)$ is the refractive index profile defined numerically as a hexagonal lattice of circular holes with a diameter of d, pitch Λ which is the distance between the centre of two adjacent holes, and refractive index

88
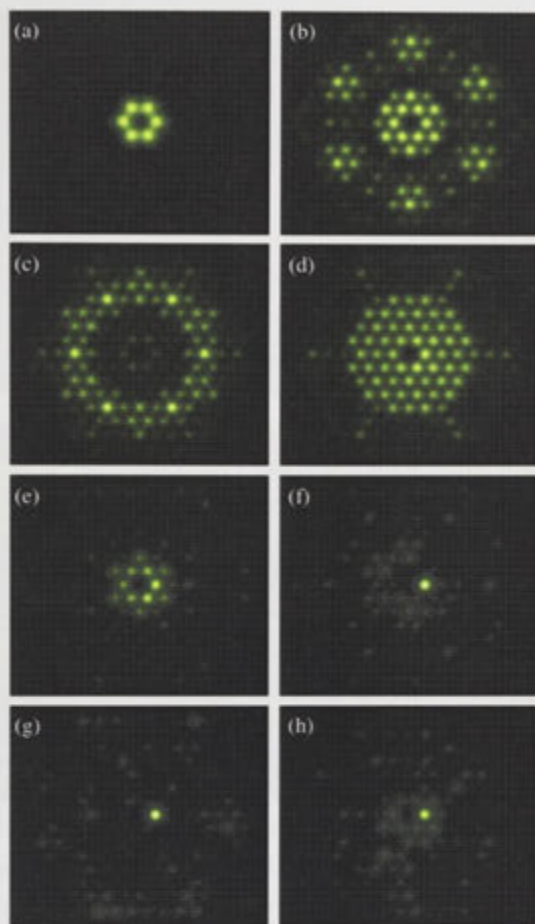
Figure 3.14: Evolution of unstable ring mode configuration over large propagation distance (a) $z = 0$, (b) $z = 50$, (c) $z = 100$, (d) $z = 136$, (e) $z = 137$, (f) $z = 138$ (g) $z = 150$, (h) $z = 200$. The initial amplitude in all six sites around the 'hole' is 2, with no phase differences.

contrast Δn. While the general description of the thermal nonlinearity is nonlocal (Sec. 3.1), here I use the simpler approximation of Kerr type nonlinearity.

Such model is commonly used to investigate guidance properties in periodic arrays [27]. Using a hole diameter of $d = 5\mu m$ and pitch $\Lambda = 10\mu m$, closely matching a commercial fibre (F-SM 15 by Newport) I am able to provide a theoretical basis for experimental observation.

I propagate an input mode with profile $A(z) = r^{|m|} \exp(-\frac{r^2}{w^2} + im\theta)$, where A is the amplitude of the mode, $m = 1$ is the charge of the vortex, r, θ and z are the cylindrical coordinates of the system, and $w = \sqrt{2/|m|}\Lambda$ is the width of the vortex mode.

I find that even though the input mode is symmetric, linear diffraction causes
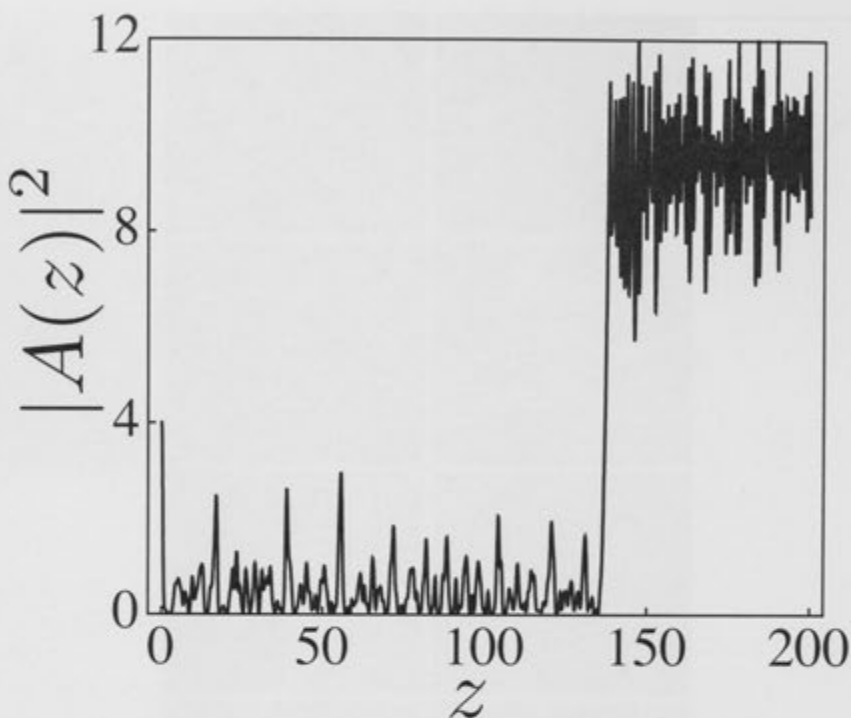
Figure 3.15: Evolution of unstable ring mode configuration over large propagation distance: Power content vs. longitudinal evolution distance, at the position of the center of the eventually self-trapped beam.

some asymmetry in the output mode after $z = 2$ cm of propagation (Fig. 3.16(a)) and index contrast $\Delta n = 0.0032$. The vortex phase is somewhat maintained at the output for linear propagation (one can pick a point in the cladding, and trace the phase in a circle around the core from 0 to 2π). This linear beams diffracts in the array as it propagates. Nonlinear output with $\gamma = 1 \times 10^{-4}$ shows localisation of the beam to the first ring of waveguides surrounding the solid core defect (Fig. 3.16(b)), and the loss of vorticity in the phase. Similar to the discrete model, we can see that the vortex mode is unstable when adjacent waveguides are not out of phase. These nonlinear modes are surface modes, largely confined to waveguides around the core for large propagation distance ($z = 20$ cm).

To test the stability in the continuous model I next propagate a beam with $m = 3$, which satisfies the condition of staggered phase between adjacent waveguides in the six waveguides surrounding the core. We can see that linear propagation is indeed more stable, and even more confined in the form of a ring mode, even though the vortex phase is lost (Fig. 3.17(a)). The linear beam diffracts as it propagates in a similar fashion to $m = 1$ modes. In the nonlinear regime we see the mode begins

Figure 3.16: (a) Linear propagation of an optical vortex mode with $m = 1$ at $z = 2$ cm (upper) and its phase (lower) in an hexagonal array of nonlinear waveguides. This linear mode diffracts as it propagates. (b) Nonlinear propagation of the same mode at $z = 2$ cm (upper) and its phase (lower) with $\gamma = 1 \times 10^{-4}$. The nonlinear mode propagates as a surface mode around a solid core defect. Pale dots on lower plots indicate waveguide location.

to break up as the staggered phase is lost (Fig. 3.17(b)). Again these nonlinear modes are surface modes, although this time more confined to waveguides around the core over large propagation distance ($z = 20$ cm), due to the initial staggered phase profile.

The linear and nonlinear modes produced with this $m = 3$ input mode are more strongly confined to the waveguides adjacent to the core defect, when compared to modes produced with an input with $m = 1$. While the π staggered phase between all six waveguides around the core is lost in the nonlinear propagation, the sites which have the highest intensity maintain this staggered phase. The initial vorticity of the $m = 3$ beam seems to stabilise the linear output into a vortex which survives for long propagation distances. In the nonlinear regime the vorticity is lost, but the ring mode structure is maintained with a somewhat staggered phase between some
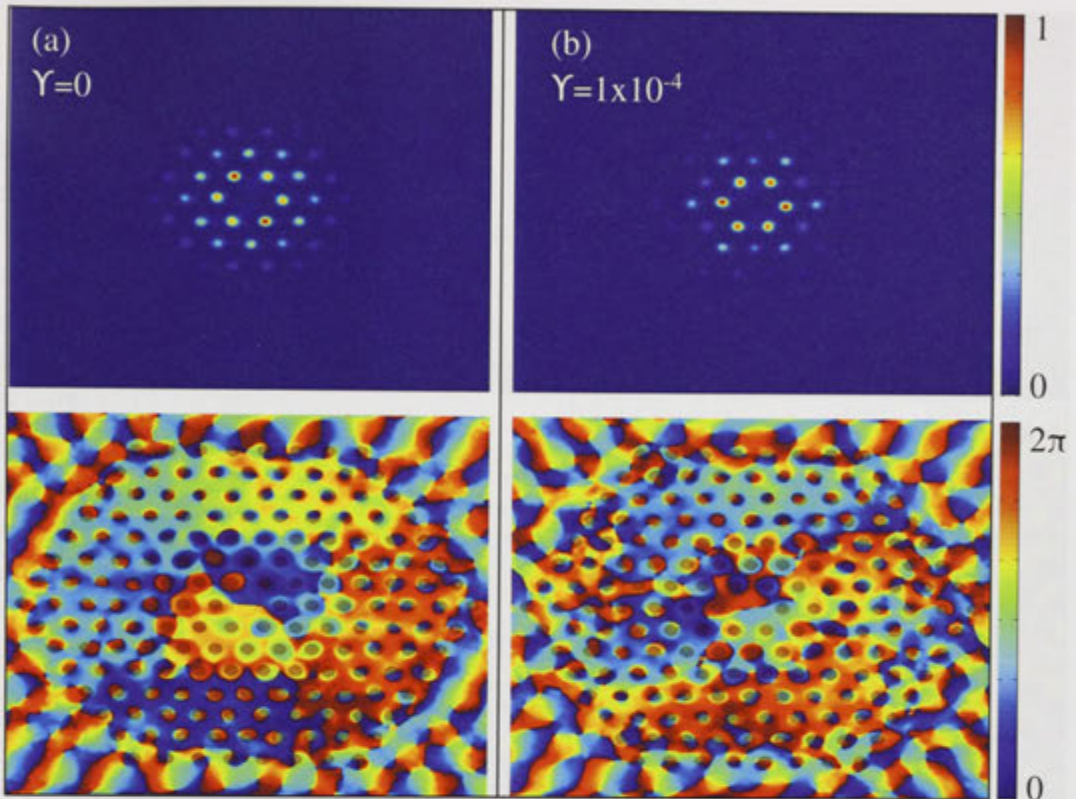
91
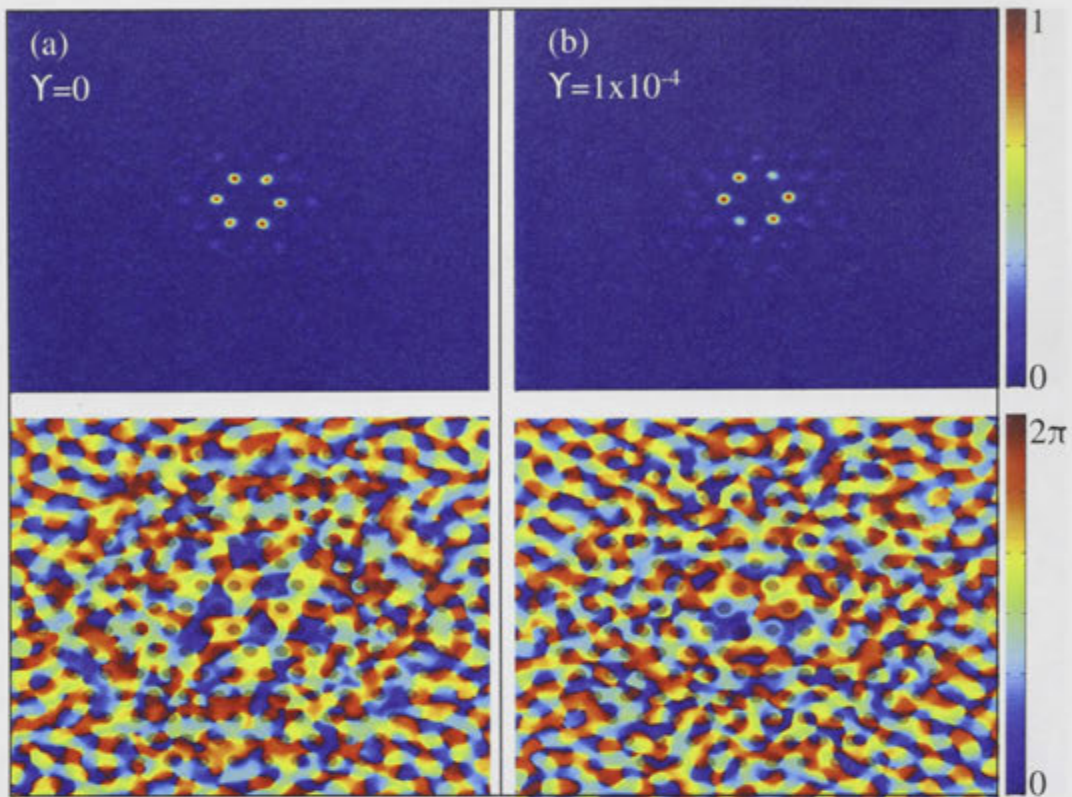
Figure 3.17: (a) Linear propagation of an optical vortex mode with $m = 3$ at $z = 2$ cm (upper) and its phase (lower) in an hexagonal array of nonlinear waveguides. This linear mode diffracts as it propagates. (b) Nonlinear propagation of the same mode at $z = 2$ cm (upper) and its phase (lower) with $\gamma = 1 \times 10^{-4}$. The nonlinear mode propagates as a surface mode around a solid core defect. Pale dots on lower plots indicate waveguide location.

waveguides.

3.3.4 Experimental Setup

The propagation of these surface vortex states was also tested in an experimental setup utilising liquid infiltrated PCFs as an array of tuneable nonlinear waveguides. A CW laser with $\lambda = 532$nm was split by a polarising beamsplitter (PBS) into a probe beam and a reference beam (Fig. 3.18). The probe beam is focused by a $f = 25$ mm lens through a 50 μm pinhole and recollimated to a larger size (diameter of about 15 mm) with a lens of $f = 250$ mm. This larger beam is given a horizontal polarisation and reflected off the spatial light modulator (SLM) at a very shallow angle ($\approx 10^{-4}$ rad). This modulated beam is then focused by a lens of $f = 125$ mm

and passed through a 30 μm pinhole to remove any pixilation noise caused by the SLM. This beam is recollimated by a $f = 50$ mm lens, passed through an iris and focused onto the sample fibre by a lens of $f = 75$ mm. The iris before the focusing lens is used to remove any noise outside the vortex, and make fine adjustments to its size.

The liquid infiltrated fibre sample is held at a constant temperature inside a temperature controlled oven. The fibre is pressed between two glass plates, with a small drop of the infiltrating oil on each end of the fibre to improve coupling into the fibre and imaging. After propagating through the fibre the output beam is collected by a 20× microscope objective and focused onto a camera. The output beam is passed through an iris to remove higher order modes from the image. An unmodified beam from the laser (which is not reflected by the PBS) is used as a reference beam to test the phase at the output of the fibre. It is combined with the output beam on the camera using a beamsplitter (BS).
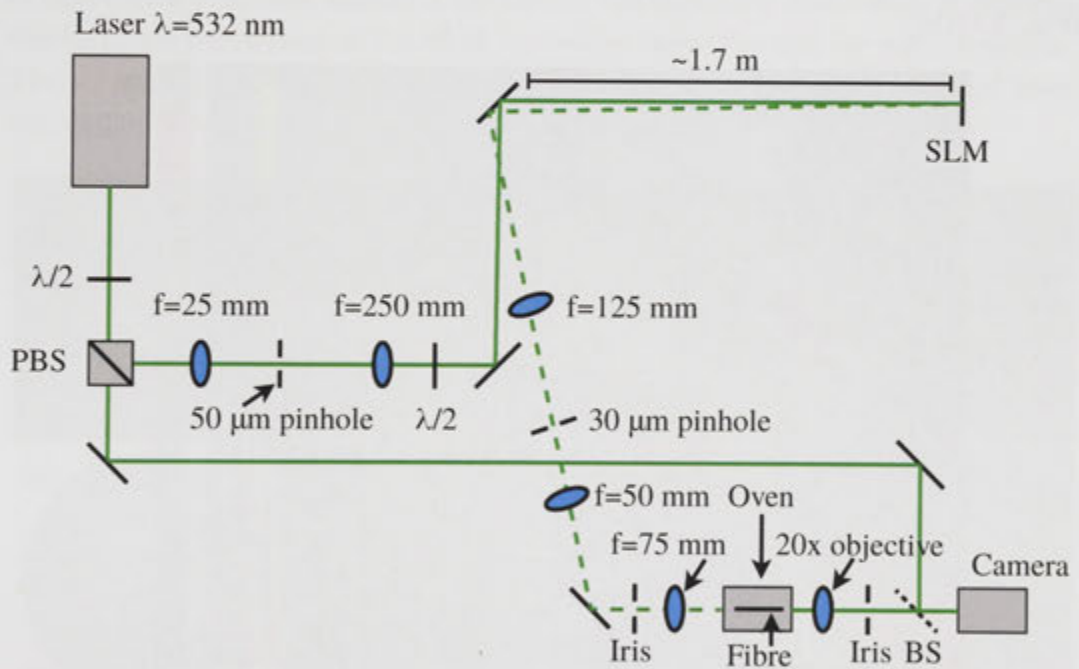
Figure 3.18: Experimental setup for propagating a vortex mode inside a liquid infiltrated PCF. Key: PBS- polarising beamsplitter; SLM- spatial light modulator; BS- beamsplitter.

This vortex beam is coupled into a liquid infiltrated PCF such that the minimum at the centre of the vortex is positioned on the core of the fibre (Fig. 3.9(inset)). The width of the vortex is adjusted using the $f = 50$mm collimating lens before the input lens. Any noise in the beam is removed with the iris before the input lens. Not

all inhomogeneity can be removed due to consideration of the transmitted power through the iris, as well as enlargement of the vortex mode caused by diffraction from the iris.

The vortex was generated on the SLM in phase modulation mode, with the laser polarisation parallel to the nematic axis. Examples of the phase used to generate a vortex beam are shown in Fig. 3.19. The phase is generated with a function:

$$\phi(r,\theta) = m\theta \qquad (3.8)$$

where ϕ is the phase, m is the vortex charge, and r, θ are the cylindrical coordinates. The vortex charge can be altered to suit the application, charge one (Fig. 3.19(a)) has a single phase jump (from 0 to 2π), while charge two has two phase jumps (Fig. 3.19(c)). Some distortion appears in the reflected modulated beam due to protective coatings and glass in front of the modulating liquid crystals. This can be corrected by adding a corrective phase to the beam, provided by the manufacturer (Fig. 3.19(b)).
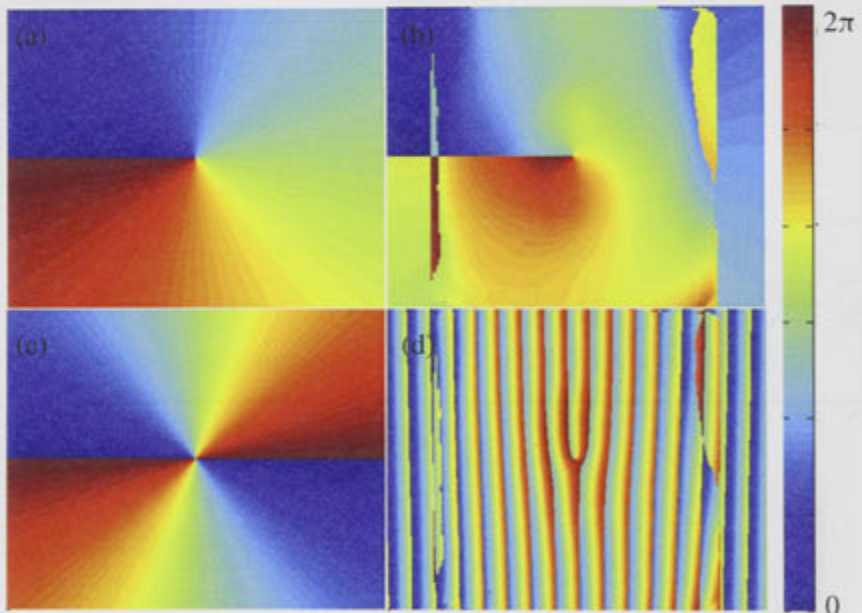
Figure 3.19: Phase profile used to generate vortex beams with (a),(b),(d) charge 1, and (c) charge 2. (b) and (d) contain a phase correction for the shape of the protective glass plate on the modulator. (d) Adds a small angle to the modulated beam so it can be separated from any unmodulated light.

Some unmodulated light is reflected from a protective glass plate on the SLM, situated in front of the liquid crystals which modulate the phase. This unmodulated reflection distorts the vortex and adds noise to the modulated beam. The vortex

94

phase was modulated by adding a constant phase gradient (Fig. 3.19(d)), effectively adding a small angle to the modulated beam. These two images are then separated by a spatial filter in the form of a 30 μm pinhole. The result of this is to separate any unmodulated reflection from the modulated beam from the SLM, in order to improve the vortex quality. Combined with the correction for any non-uniformity (Fig. 3.19(d)) in the SLM it is possible to produce a vortex beam of high quality.

3.3.5   Linear and Nonlinear Beam Interactions With PCF Core

Experimentally a vortex beam is launched into a liquid infiltrated PCF. The central minimum of the vortex mode is placed on the core defect of the fibre. The maximum of the vortex mode coincides with the first ring of holes surrounding the core defect. The infiltrating liquid is castor oil doped with gold nanoparticles to increase absorption and nonlinearity. The nanoparticles absorb approximately 30% of light over a 1 cm bulk sample of the liquid. The increased nonlinearity is required due to power restrictions of the SLM, and other losses through the optical system. The input (Fig. 3.20(a)) is generated as a charge one vortex, and separated from any unmodulated light.
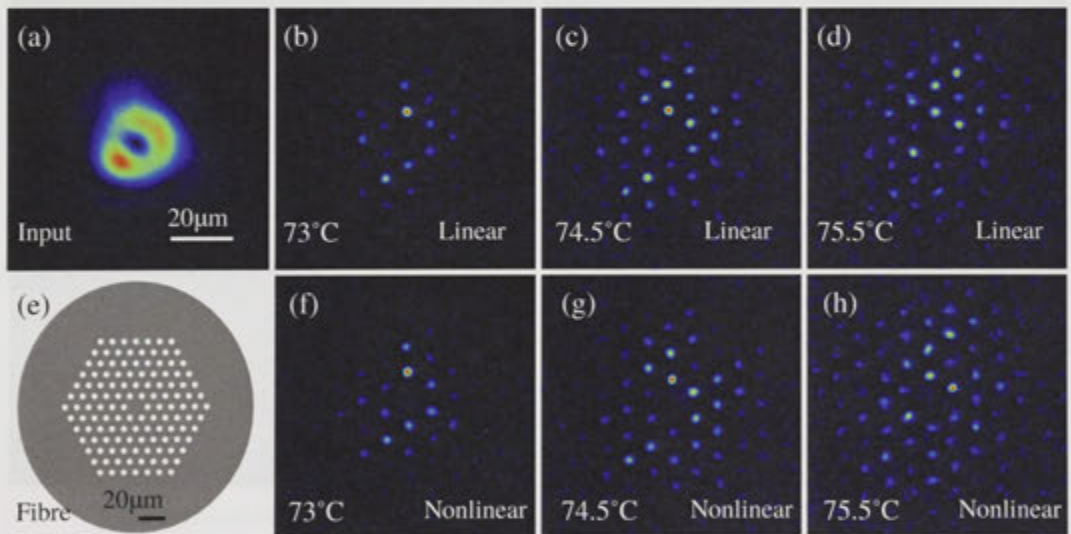
Figure 3.20:   (a) Vortex mode input, (b)-(d) linear output of vortex mode propagating around the core in liquid infiltrated fibre (e) at (b) 73°C, (c) 74.5°C, (d) 75.5°C. (f)-(h) Nonlinear output of vortex mode around the core in liquid infiltrated fibre (e) at (f) 73°C, (g) 74.5°C, (h) 75.5°C.

Fig. 3.20 shows the experimental linear and nonlinear propagation observed for a vortex mode propagating around the solid core. In the linear regime (Fig. 3.20(b)-

(d)) the output broadens as the coupling is increased due to smaller refractive index contrast caused by the higher temperature. In the nonlinear regime (Fig. 3.20(f-h)) the output is broader than in the linear case, for each temperature. This indicates self defocusing caused by the nonlinearity. This self defocusing in this case is caused by the nonlocal response, not considered in the theoretical model (Fig. 3.16). The nonlocal parameter of the fibre is close to 2 (the nonlocal parameter is the ratio between the cladding size and the size of the array (Sec. 3.1)) (Fig. 3.20(e)).

The asymmetry in the beam comes not only from the asymmetry in the input mode, but also from inhomogeneity in the fibre itself. While the cladding in general is quite homogenous the holes around the core are subject to further stresses during the drawing process due to the missing hole in the centre. When comparing an input beam such as that in Fig. 3.20(a) propagating in the cladding (such that the minimum at the centre of the beam falls on a single waveguide) seen in Fig. 3.21(a), and the same beam propagating around the core (Fig. 3.21(b)) it is obvious that the beam propagating in the cladding has a greater symmetry. This is most likely due to asymmetric coupling between the waveguides around the core due to inhomogeneity in the fibre structure around the core.
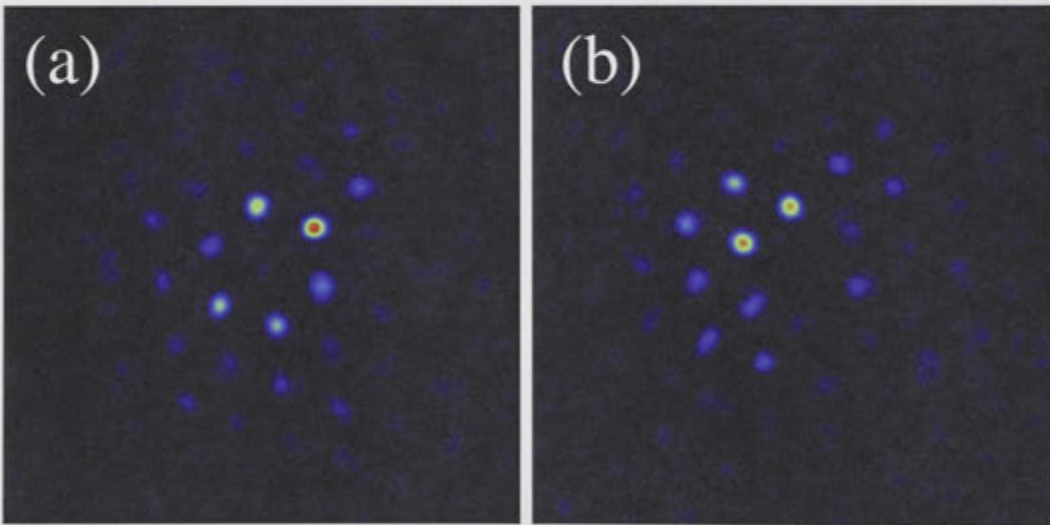
Figure 3.21: Linear output for a vortex produced by the SLM propagating (a) in the cladding of the infiltrated PCF at 74°C, away from the core, and (b) around the core.

This can also be shown using a highly symmetric vortex beam produced with a reflective phase plate (Fig. 3.22(a)) (a reflective piece of brass with a height profile producing the phase profile in Fig. 3.19(a)). When this beam is propagating around the core at 72°C when there is little coupling between the waveguides, the output

profile is symmetric (Fig. 3.21(b). As the coupling is increased to 74°C and the waveguides begin to couple, the output profile is seen to become less symmetric (Fig. 3.21(c)). This is due to asymmetric coupling between these waveguides and their neighbours, caused by inhomogeneity in the fibre structure. All symmetry is lost when the coupling is increased again at 76°C (Fig. 3.21(d)).
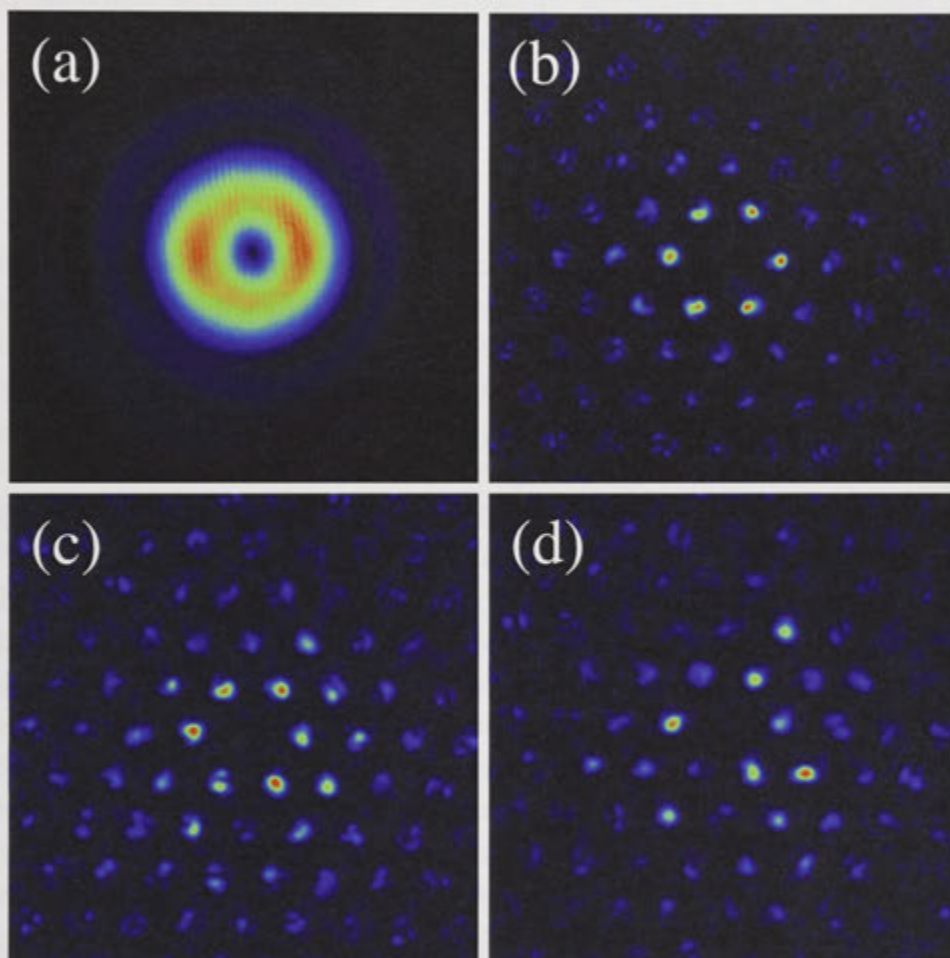
Figure 3.22: (a) A vortex produced by a reflective phase plate, and its output when propagated around the core of an infiltrated PCF at (b) 72°C, (c) 74°C, and (d) 76°C.

The observed asymmetry is most likely caused by inhomogeneity in the waveguides surrounding the core. During the fibre drawing process it is highly likely that structural stresses in the fibre preform can cause slight deviations in the structure around the core, and at the boundary of the cladding structure. This can occur because of the defect of a missing hole or the edge of the array, and was seen in many of the early fibres produced [62, 67].

Vortex modes propagating around the core defect of a hexagonal nonlinear periodic waveguide array can be stable, provided the mode symmetry matches natural Bloch modes of the system. Using the discrete and continuous model I have shown that a charge 3 vortex mode is stable because of its staggered phase profile for the six waveguides around the core. The discrete model shows that charge 1 surface vortex modes decay to a single site surface mode. I experimentally tested the propagation of linear and nonlinear vortex modes from the continuous model, and was able to show that asymmetry in the output is caused by inhomogeneity of the fibre.

3.4 Chapter Summary

In this chapter I have shown my theoretical and experimental work on nonlinearity in 2D periodic structures. I have utilised liquid infiltrated PCFs as an array of tuneable hexagonal nonlinear waveguides. I have studied theoretically and generated in experiment nonlocal gap solitons in liquid-infiltrated photonic-crystal fibres. I have shown a possibility to control nonlocality in a realistic periodic structure by varying its boundaries.

I have utilised a liquid infiltrated PCF as a 2D periodic structure with highly tuneable refractive index modulation to study the crossover behaviour of a the system from periodic to homogeneous. The crossover is observed as the point where the defocusing nonlinear response of the propagating beams abruptly switches from beam localisation to defocusing. Through numerical simulations and detailed experimental analysis I have determined the threshold index contrast for such crossover. Near this threshold point the output beam is highly sensitive to index modulations and power fluctuations in the system, and therefore this regime can be applied for high-sensitivity refractive index or temperature sensing. Furthermore, my results may have implications beyond the field of optics relating e.g. to the crossover behaviour of conductivity in graphene sheets [157].

I have examined the localised surface modes around the core defect of a PCF surrounded by a hexagonal array of nonlinear waveguides. I find that the stable modes in both the discrete and continuous models have a staggered phase profile for the six waveguides surrounding the core. Ring shaped surface modes are studied in the discrete model and shown to always decay to a single site fundamental surface mode. The continuous model shows a similar decay of the surface modes and loss of vorticity in the phase at high nonlinearity. These vortex states are explored experimentally but due to the nonlocal nature of the fibre and asymmetry in the structure, soliton formation was not achieved.

CHAPTER 4

Conclusions

The propagation of light in periodic photonic structures offers a new way to control light interactions, and opens new areas for research into how light can be used to control light. The invention of the laser opened up the possibility for the study of nonlinearity in optics, allowing high intensity beams of light to interact through a nonlinear medium. To further study and utilise nonlinear media to fit in with our current technological world we need to create new structures to further understand and explore the physics behind these systems, leading to real world applications.

In this thesis I have studied light propagation in tuneable nonlinear periodic photonic media. There are three main areas to my research: (i) the experimental development of 1D periodic platforms for liquid infiltration and their character-isation; (ii) the experimental and theoretical observation of truncated nonlinear Bloch-wave solitons in 1D waveguide arrays; (iii) and theoretical and experimental study of nonlinear cladding modes in liquid infiltrated Photonic Crystal Fibres.

I have developed platforms for the study of light propagation in 1D structures. SU8 polymer was used to photolithographically define square channels which were infiltrated with an index matching oil. By choosing an index matching oil it is possible to precisely control the refractive index of the waveguides, and hence their coupling. This refractive index can further be tuned by changing the temperature of the whole structure. I showed linear propagation in this system in the form of discrete diffraction. I was able to demonstrate temperature tuneable linear discrete diffraction and performed accompanying theoretical calculations from which I was able to estimate the temperature of the liquid inside the waveguides.

I expanded on these waveguides by utilising existing arrays of capillaries in Photonic Crystal Fibres. I developed a simple and cost effective method for the selective infiltration of a PCF, using a tapered glass fibre to convey droplets of liquid into place on one end of a PCF to be infiltrated. I blocked the inverse pattern to be infiltrated on one end of the fibre, then filled the unblocked holes by submerging

the other end of the fibre into a reservoir of infiltrating liquid. I demonstrated a 1D array of coupled waveguides, and showed linear temperature tuneable discrete diffraction and nonlinear defocusing.

I have studied truncated nonlinear Bloch-wave solitons in Lithium Niobate waveguide arrays. These states are excited with a broad Gaussian input beam. After propagation and above a threshold nonlinearity these beams maintain a stable width, even as the nonlinearity increases. This nonlinearity independent width is maintained as the width of the input is changed. These states have already been demonstrated in an application of image transmission in photonic lattices [116].

I also studied light propagation in hexagonal 2D arrays using liquid infiltrated Photonic Crystal Fibres. After infiltration I utilise the cladding structure of the fibre as a 2D periodic array of tuneable nonlinear waveguides. I used similar index matching oils from my experiments in 1D structures. I was able to observe nonlocal gap solitons, where the width of the soliton depends on the properties of the structure far from the light field due to heat flow and thermal nonlocality. Above a certain temperature these solitons are no longer excitable, leading me to discover the crossover from focusing to defocusing in periodic nonlinear waveguide arrays. This crossover occurs before the refractive index contrast is reduced to zero because the bandgap closes before this point.

I was able to show that vortex surface states can be stabilised by utilising a vortex charge which mimics natural Bloch modes of the system, where neighbouring waveguides are out of phase. Through theoretical studies of the discrete and continuous model the stability of vortex modes propagating around the surface of a core defect in a liquid infiltrated PCF were studied. Modes not matching the symmetry of the waveguide structure (such as charge 1) break up and confine to a single waveguide after long propagation distance. Other modes (such as charge 3) can propagate for long distances without breaking up because of their staggered phase structure.

This research can be used as a basis for the construction of devices based on refractive index sensitivity and beam propagation. Such devices have been suggested [158], but can benefit from larger interaction between the probe beam and infiltrating liquid. Using for example nonlocal gap solitons to confine light to a single infiltrated waveguide, it would be possible to increase the exposure of an infiltrating liquid to the probe light by orders of magnitude.

The point at which a system switches from focusing to defocusing is similar in many ways to a system switching from a higher dimensional behaviour, to different behaviour in lower dimensions. This has been studied in graphene sheets, as the thickness is increased and the material moves from 2D to 3D its conductivity changes [157]. By studying this in optics we have another method for studying other physical

problems involving system behavioural change.

More advanced structures such as 2D arrays of gold and silver nanowires have shown waveguiding and plasmon resonances properties [159], following on from earlier work on guided modes in arrays of metallic nanowires [160]. This could be expanded to include plasmonic effects in periodic structures, including coating the inside of a PCF with a thin layer of silver. This could be infiltrated with a liquid or not, and may show some interesting coupling effects between waveguides. These waveguides could even be modified using selective infiltration to produce a wide variety of structures or networks, perhaps allowing for some external (electric, magnetic etc.) interaction to control light propagation.

References

[1] B. Saleh and M. Teich, *Fundamentals of Photonics*, vol. 45. Wiley, second ed., 2007.

[2] J. Love and F. Ladouceur, *Silica-based Buried Channel Waveguides and Devices*. Chapman & Hall, 1996.

[3] A. W. Snyder, "Coupled-Mode Theory for Optical Fibers," *Journal of the Optical Society of America*, vol. 62, pp. 1267–1277, Nov. 1972.

[4] C. Kittel, *Introduction to Solid State Physics*. Wiley, eighth ed., 2005.

[5] A. Hardy and W. Streifer, "Coupled mode theory of parallel waveguides," *Journal of Lightwave Technology*, vol. 3, no. 5, pp. 1135–1146, 1985.

[6] P. Zhang, R. Egger, and Z. Chen, "Optical induction of three-dimensional photonic lattices and enhancement of discrete diffraction," *Optics Express*, vol. 17, pp. 13151–13156, July 2009.

[7] A. Szameit, I. Garanovich, M. Heinrich, A. Sukhorukov, F. Dreisow, T. Pertsch, S. Nolte, A. Tünnermann, and Y. S. Kivshar, "Polychromatic dynamic localization in curved photonic lattices," *Nature Physics*, vol. 5, pp. 271–275, Mar. 2009.

[8] E. Pawlowski, M. Ferstl, H. Hellmich, B. Kuhlow, C. Warmuth, and J. Salgueiro, "Fabrication of a multichannel wavelength-division multiplexing-passive optical net demultiplexer with arrayed-waveguide gratings and diffractive optical elements.," *Applied Optics*, vol. 38, pp. 3039–3045, May 1999.

[9] D. Mandelik, H. Eisenberg, Y. Silberberg, R. Morandotti, and J. S. Aitchison, "Band-Gap Structure of Waveguide Arrays and Excitation of Floquet-Bloch Solitons," *Physical Review Letters*, vol. 90, p. 053902, Feb. 2003.

[10] E. Fermi, J. Pasta, and S. Ulam, "Studies of nonlinear problems," *Los Alamos Scientific Laboratory*, vol. Tech. Rep., 1955.

[11] T. Maiman, "Stimulated Optical Radiation in Ruby," *Nature*, vol. 187, pp. 493–494, 1960.

[12] R. W. Terhune, P. D. Maker, and C. M. Savage, "Optical harmonic generation in calcite," *Physical Review Letters*, vol. 8, no. 10, pp. 404–406, 1962.

[13] M. Hercher, "Laser-induced damage in transparent media," *Journal of the Optical Society of America*, vol. 54, no. 563, pp. 559–584, 1964.

[14] N. Bloembergen, R. K. Chang, S. S. Jha, and C. H. Lee, "Optical Second-Harmonic Generation in Reflection from Media with Inversion Symmetry," *Physical Review*, vol. 174, pp. 813–822, 1968.

[15] R. Chiao, E. Garmire, and C. Townes, "Slef-trapping of optical beams," *Physical Review Letters*, vol. 13, pp. 479–482, 1964.

[16] R. W. Boyd, *Nonlinear Optics*. Academic Press, second ed., 2003.

[17] N. J. Zabusky and M. D. Kruskal, "Interaction of "solitons" in a collisionless plasma and the recurrence of initial states," *Physical Review Letters*, vol. 15, pp. 240–243, 1965.

[18] S. Maneuf, R. Desailly, and C. Froehly, "Stable self-trapping of laser beams: observation in a nonlinear planar waveguide," *Optics Communications*, vol. 65, no. 3, pp. 193–198, 1988.

[19] J. S. Aitchison, A. M. Weiner, Y. Silberberg, M. K. Oliver, J. L. Jackel, D. E. Leaird, E. M. Vogel, and P. W. Smith, "Observation of spatial optical solitons in a nonlinear glass waveguide.," *Optics Letters*, vol. 15, pp. 471–473, May 1990.

[20] J. Salgueiro, A. Sukhorukov, and Y. Kivshar, "Spatial optical solitons supported by mutual focusing.," *Optics Letters*, vol. 28, pp. 1457–1459, Aug. 2003.

[21] J. Salgueiro, A. Sukhorukov, Y. Kivshar, and S. Saltiel, "Parametric vector solitons in tetragonal crystals.," *Optics Letters*, vol. 28, pp. 828–830, May 2003.

[22] A. Hasegawa, "Transmission of stationary nonlinear optical pulses in dispersive dielectric fibers," *Applied Physics Letters*, vol. 23, no. 3, pp. 142–144, 1973.

[23] L. F. Mollenauer, R. H. Stolen, and J. P. Gordon, "Experimental Observation of Picosecon Pulse Narrowing and Solitons in Optical Fibres," *Physical Review Letters*, vol. 45, pp. 1095–1098, 1980.

[24] K. E. Strecker, G. B. Partridge, A. G. Truscott, and R. G. Hulet, "Formation and propagation of matter-wave soliton trains," *Nature*, vol. 417, pp. 150–153, May 2002.

[25] B. Eiermann, T. Anker, M. Albiez, M. Taglieber, P. Treutlein, K.-P. Marzlin, and M. Oberthaler, "Bright Bose-Einstein Gap Solitons of Atoms with Repulsive Interaction," *Physical Review Letters*, vol. 92, p. 230401, June 2004.

[26] A. S. Davydov, "The theory of contraction of proteins under their excitation," *Journal of Theoretical Biology*, vol. 38, pp. 559–569, Mar. 1973.

[27] D. Christodoulides and R. I. Joseph, "Discrete self-focusing in nonlinear arrays of coupled waveguides," *Optics Letters*, vol. 13, pp. 794–796, Sept. 1988.

[28] D. Christodoulides, F. Lederer, and Y. Silberberg, "Discretizing light behaviour in linear and nonlinear waveguide lattices," *Nature*, vol. 424, pp. 817–823, Aug. 2003.

[29] D. Neshev, T. J. Alexander, E. A. Ostrovskaya, Y. S. Kivshar, H. Martin, I. Makasyuk, and Z. Chen, "Observation of discrete vortex solitons in optically induced photonic lattices," *Physical Review Letters*, vol. 92, p. 123903, 2004.

[30] F. Jermann, M. Simon, and E. Krätzig, "Photorefractive properties of congruent and stoichiometric lithium niobate at high light intensities," *Journal of the Optical Society of America B*, vol. 12, pp. 2066–2070, Nov. 1995.

[31] Z. Chen, M. Segev, D. Wilson, R. Muller, and P. Maker, "Self-Trapping of an Optical Vortex by Use of the Bulk Photovoltaic Effect," *Physical Review Letters*, vol. 78, pp. 2948–2951, Apr. 1997.

[32] C. R. Rosberg, D. Neshev, W. Krolikowski, A. Mitchell, R. A. Vicencio, M. I. Molina, and Y. S. Kivshar, "Observation of surface gap solitons in semi-infinite waveguide arrays," *Physical Review Letters*, vol. 97, p. 083901, 2006.

[33] F. S. Chen, J. T. LaMacchia, and D. B. Fraser, "Holographic storage in lithium niobate," *Applied Physics Letters*, vol. 13, no. 7, pp. 223–225, 1968.

[34] C. Rotschild, O. Cohen, O. Manela, M. Segev, and T. Carmon, "Solitons in Nonlinear Media with an Infinite Range of Nonlocality: First Observation of Coherent Elliptic Solitons and of Vortex-Ring Solitons," *Physical Review Letters*, vol. 95, p. 213904, Nov. 2005.

[35] W. Krolikowski, O. Bang, N. I. Nikolov, D. Neshev, J. Wyller, J. J. Rasmussen, and D. Edmundson, "Modulational instability, solitons and beam propagation in spatially nonlocal nonlinear media," *Journal of Optics B*, vol. 6, pp. S288–S294, May 2004.

[36] M. Born and E. Wolfe, *Principles of Optics.* Cambridge University, Cambridge, 1999.

[37] S. A. Akhmanov, R. V. Khoklov, and A. P. Sukhorukov, *Laser Handbook.* 1972.

[38] H. S. Eisenberg, Y. Silberberg, R. Morandotti, A. R. Boyd, and J. S. Aitchison, "Discrete Spatial Optical Solitons in Waveguide Arrays," *Physical Review Letters*, vol. 81, pp. 3383–3386, 1998.

[39] Y. S. Kivshar, "Self-localization in arrays of defocusing waveguides," *Optics Letters*, vol. 18, pp. 1147–1149, July 1993.

[40] R. Morandotti, U. Peschel, J. S. Aitchison, H. Eisenberg, and Y. Silberberg, "Dynamics of discrete solitons in optical waveguide arrays," *Physical Review Letters*, vol. 83, pp. 2726–2729, 1999.

[41] H. S. Eisenberg, Y. Silberberg, R. Morandotti, and J. S. Aitchison, "Diffraction Management," *Physical Review Letters*, vol. 85, pp. 1863–1866, 2000.

[42] R. Morandotti, H. Eisenberg, Y. Silberberg, M. Sorel, and J. S. Aitchison, "Self-Focusing and Defocusing in Waveguide Arrays," *Physical Review Letters*, vol. 86, pp. 3296–3299, Apr. 2001.

[43] J. W. Fleischer, T. Carmon, M. Segev, N. K. Efremidis, and D. Christodoulides, "Observation of two-dimensional discrete solitons in optically induced nonlinear photonic lattices," *Nature*, vol. 422, pp. 147–150, Mar. 2003.

[44] J. Fleischer, T. Carmon, M. Segev, N. Efremidis, and D. Christodoulides, "Observation of Discrete Solitons in Optically Induced Real Time Waveguide Arrays," *Physical Review Letters*, vol. 90, p. 023902, Jan. 2003.

[45] D. Neshev, E. Ostrovskaya, Y. Kivshar, and W. Krolikowski, "Spatial solitons in optically induced gratings," *Optics Letters*, vol. 28, no. 9, pp. 710–712, 2003.

[46] Z. Chen, H. Martin, E. Eugenieva, J. Xu, and A. Bezryadina, "Anisotropic Enhancement of Discrete Diffraction and Formation of Two-Dimensional Discrete-Soliton Trains," *Physical Review Letters*, vol. 92, p. 143902, Apr. 2004.

[47] H. Martin, E. D. Eugenieva, Z. Chen, and D. Christodoulides, "Discrete Solitons and Soliton-Induced Dislocations in Partially Coherent Photonic Lattices," *Physical Review Letters*, vol. 92, p. 123902, 2004.

[48] D. Mandelik, R. Morandotti, J. S. Aitchison, and Y. Silberberg, "Gap Solitons in Waveguide Arrays," *Physical Review Letters*, vol. 92, p. 093904, Mar. 2004.

[49] D. Neshev, A. Sukhorukov, B. Hanna, W. Krolikowski, and Y. Kivshar, "Controlled Generation and Steering of Spatial Gap Solitons," *Physical Review Letters*, vol. 93, p. 083905, Aug. 2004.

[50] N. Efremidis, J. Hudock, D. Christodoulides, J. Fleischer, O. Cohen, and M. Segev, "Two-Dimensional Optical Lattice Solitons," *Physical Review Letters*, vol. 91, p. 213906, Nov. 2003.

[51] F. Chen, M. Stepić, C. Rüter, D. Runde, D. Kip, V. Shandarov, O. Manela, and M. Segev, "Discrete diffraction and spatial gap solitons in photovoltaic LiNbO3 waveguide arrays," *Optics Express*, vol. 13, pp. 4314–4324, May 2005.

[52] Z. Chen and K. McCarthy, "Spatial soliton pixels from partially incoherent light," *Optics Letters*, vol. 27, pp. 2019–2021, Nov. 2002.

[53] C. Rosberg, D. Neshev, A. Sukhorukov, W. Krolikowski, and Y. S. Kivshar, "Observation of nonlinear self-trapping in triangular photonic lattices," *Optics Letters*, vol. 32, no. 4, pp. 397–399, 2007.

[54] B. Malomed and P. Kevrekidis, "Discrete vortex solitons," *Physical Review E*, vol. 64, p. 026601, July 2001.

[55] B. Terhalle, T. Richter, A. S. Desyatnikov, D. Neshev, W. Krolikowski, F. Kaiser, C. Denz, and Y. Kivshar, "Observation of Multivortex Solitons in Photonic Lattices," *Physical Review Letters*, vol. 101, p. 013903, July 2008.

[56] B. Terhalle, T. Richter, K. Law, D. Göries, P. Rose, T. J. Alexander, P. G. Kevrekidis, A. S. Desyatnikov, W. Krolikowski, F. Kaiser, C. Denz, and Y. S. Kivshar, "Observation of double-charge discrete vortex solitons in hexagonal photonic lattices," *Physical Review A*, vol. 79, p. 043821, 2009.

[57] X. Wang, A. Bezryadina, Z. Chen, K. Makris, D. Christodoulides, and G. Stegeman, "Observation of Two-Dimensional Surface Solitons," *Physical Review Letters*, vol. 98, p. 123903, Mar. 2007.

[58] J. Yang, I. Makasyuk, P. Kevrekidis, H. Martin, B. Malomed, D. Frantzeskakis, and Z. Chen, "Necklacelike Solitons in Optically Induced Photonic Lattices," *Physical Review Letters*, vol. 94, p. 113902, Mar. 2005.

[59] H. Michinel, J. Campo-Táboas, M. Quiroga-Teixeiro, J. Salgueiro, and R. Garcia-Fernandez, "Excitation of stable vortex solitons in nonlinear cubic-quintic materials," *Journal of Optics B*, vol. 3, pp. 314–317, 2001.

[60] J. R. Salgueiro, A. H. Carlsson, E. Ostrovskaya, and Y. Kivshar, "Second-harmonic generation in vortex-induced waveguides," *Optics Letters*, vol. 29, pp. 593–595, Mar. 2004.

[61] R. Fischer, D. Träger, D. Neshev, A. Sukhorukov, W. Krolikowski, C. Denz, and Y. Kivshar, "Reduced-Symmetry Two-Dimensional Solitons in Photonic Lattices," *Physical Review Letters*, vol. 96, p. 023905, Jan. 2006.

[62] T. A. Birks, J. C. Knight, and P. S. Russell, "Endlessly single-mode photonic crystal fiber.," *Optics Letters*, vol. 22, pp. 961–963, July 1997.

[63] R. F. Cregan, B. J. Mangan, J. C. Knight, T. A. Birks, P. S. J. Russell, P. J. Roberts, and D. C. Allan, "Single-Mode Photonic Band Gap Guidance of Light in Air," *Science*, vol. 285, pp. 1537–1539, 1999.

[64] P. Yeh and A. Yariv, "Bragg Reflection Waveguides," *Optics Communications*, vol. 19, pp. 427–430, 1976.

[65] J. C. Knight, T. A. Birks, P. S. Russell, and D. M. Atkin, "All-silica single-mode optical fiber with photonic crystal cladding," *Optics Letters*, vol. 22, pp. 484–485, Apr. 1997.

[66] P. Russell, "Photonic crystal fibers," *Science*, vol. 299, pp. 358–362, Jan. 2003.

[67] J. C. Knight, J. Arriaga, T. A. Birks, A. Ortigosa-Blanch, W. J. Wadsworth, and P. S. J. Russell, "Anomalous dispersion in photonic crystal fiber," *IEEE Photonics Technology Letters*, vol. 12, pp. 807–809, July 2000.

[68] W. Reeves, J. Knight, P. Russell, and P. Roberts, "Demonstration of ultra-flattened dispersion in photonic crystal fibers," *Optics Express*, vol. 10, pp. 609–613, July 2002.

[69] J. K. Ranka, R. S. Windeler, and A. J. Stentz, "Visible continuum generation in air-silica microstructure optical fibers with anomalous dispersion at 800 nm," *Optics Letters*, vol. 25, pp. 25–27, Jan. 2000.

[70] F. Fogli, L. Saccomandi, P. Bassi, G. Bellanca, and S. Trillo, "Full vectorial BPM modeling of index-guiding photonic crystal fibers and couplers," *Optics Express*, vol. 10, pp. 54–59, Jan. 2002.

[71] L. Zhang and C. Yang, "Polarization splitter based on photonic crystal fibers.," *Optics Express*, vol. 11, pp. 1015–1020, May 2003.

[72] J. Salgueiro and Y. Kivshar, "Nonlinear dual-core photonic crystal fiber couplers.," *Optics Letters*, vol. 30, pp. 1858–1860, July 2005.

[73] J. Laegsgaard, "Gap formation and guided modes in photonic bandgap fibres with high-index rods," *Journal of Optics A*, vol. 6, pp. 798–804, Aug. 2004.

[74] B. T. Kuhlmey, K. Pathmanandavel, and R. C. McPhedran, "Multipole analysis of photonic crystal fibers with coated inclusions," *Optics Express*, vol. 14, pp. 10851–10864, Oct. 2006.

[75] B. T. Kuhlmey, T. P. White, G. Renversez, D. Maystre, L. C. Botten, C. M. de Sterke, and R. C. McPhedran, "Multipole method for microstructured optical fibers. II. Implementation and results," *Journal of the Optical Society of America B*, vol. 19, pp. 2331–2340, Oct. 2002.

[76] T. Grujic, B. T. Kuhlmey, C. M. de Sterke, and C. G. Poulton, "Modelling of photonic crystal fiber based on layered inclusions," *Journal of the Optical Society of America B*, vol. 26, pp. 1852–1861, Sept. 2009.

[77] T. M. Monro, D. J. Richardson, and P. J. Bennett, "Developing holey fibres for eanescent field devices," *Electronic Letters*, vol. 35, no. 14, pp. 1188–1189, 1999.

[78] J. B. Jensen, L. H. Pedersen, P. E. Hoiby, L. B. Nielsen, T. P. Hansen, J. R. Folkenberg, J. Riishede, D. Noordegraaf, K. Nielsen, A. Carlsen, and A. Bjarklev, "Photonic crystal fiber based evanescent-wave sensor for detection of biomolecules in aqueous solutions," *Optics Letters*, vol. 29, pp. 1974–1976, Sept. 2004.

[79] F. M. Cox, A. Argyros, and M. C. J. Large, "Liquid-filled hollow core microstructured polymer optical fiber," *Optics Express*, vol. 14, no. 9, pp. 4135–4140, 2006.

[80] B. Eggleton, C. Kerbage, P. Westbrook, R. Windeler, and A. Hale, "Microstructured optical fiber devices," *Optics Express*, vol. 9, pp. 698–713, Dec. 2001.

[81] T. Larsen, A. Bjarklev, D. Hermann, and J. Broeng, "Optical devices based on liquid crystal photonic bandgap fibres," *Optics Express*, vol. 11, pp. 2589–2596, Oct. 2003.

[82] T. Alkeskjold, J. Laegsgaard, A. Bjarklev, D. Hermann, A. Anawati, J. Broeng, J. Li, and S.-T. Wu, "All-optical modulation in dye-doped nematic liquid crystal photonic bandgap fibers," *Optics Express*, vol. 12, pp. 5857–5871, Nov. 2004.

[83] P. Steinvurzel, B. Kuhlmey, T. White, M. Steel, C. de Sterke, and B. Eggleton, "Long wavelength anti-resonant guidance in high index inclusion microstructured fibers," *Optics Express*, vol. 12, pp. 5424–5433, Nov. 2004.

[84] B. T. Kuhlmey, B. J. Eggleton, and D. K. C. Wu, "Fluid-Filled Solid-Core Photonic Bandgap Fibers," *Journal of Lightwave Technology*, vol. 27, no. 11, pp. 1617–1630, 2009.

[85] C. R. Rosberg, F. H. Bennet, D. N. Neshev, P. D. Rasmussen, O. Bang, W. Krolikowski, A. Bjarklev, and Y. S. Kivshar, "Tunable diffraction and self-defocusing in liquid-filled photonic crystal fibers," *Optics Express*, vol. 15, pp. 12145–12150, Sept. 2007.

[86] A. Fuerbach, P. Steinvurzel, J. A. Bolger, A. Nulsen, and B. J. Eggleton, "Nonlinear propagation effects in antiresonant high-index inclusion photonic crystal fibers," *Optics Letters*, vol. 30, pp. 830–832, Apr. 2005.

[87] S. Lebrun, P. Delaye, R. Frey, and G. Roosen, "High-efficiency single-mode Raman generation in a liquid-filled photonic bandgap fiber," *Optics Letters*, vol. 32, pp. 337–339, Feb. 2007.

[88] R. Zhang, J. Teipel, and H. Giessen, "Theoretical design of a liquid-core photonic crystal fiber for supercontinuum generation," *Optics Express*, vol. 14, pp. 6800–6812, July 2006.

[89] D. Wu, B. T. Kuhlmey, and B. Eggleton, "Ultrasensitive photonic crystal fiber refractive index sensor," *Optics Letters*, vol. 34, no. 3, pp. 322–324, 2009.

[90] P. Steinvurzel, C. Desterke, B. Eggleton, B. Kuhlmey, and M. Steel, "Mode field distributions in solid core photonic bandgap fibers," *Optics Communications*, vol. 263, pp. 207–213, July 2006.

[91] C. Kerbage, P. Steinvurzel, P. Reyes, P. S. Westbrook, R. S. Windeler, A. Hale, and B. J. Eggleton, "Highly tunable birefringent microstructured optical fiber," *Optics Letters*, vol. 27, no. 10, pp. 842–844, 2002.

[92] X. Zhang, R. Wang, F. M. Cox, B. T. Kuhlmey, and M. C. J. Large, "Selective coating of holes in microstructured optical fiber and its application to in-fiber absorptive polarizers," *Optics Express*, vol. 15, pp. 16270–16278, Nov. 2007.

[93] B. T. Kuhlmey, F. Luan, L. Fu, D.-I. Yeom, B. J. Eggleton, A. Wang, and J. C. Knight, "Experimental reconstruction of bands in solid core photonic bandgap fibres using acoustic gratings," *Optics Express*, vol. 16, pp. 13845–13856, Sept. 2008.

[94] C. R. Rosberg, I. L. Garanovich, A. A. Sukhorukov, D. N. Neshev, W. Krolikowski, and Y. S. Kivshar, "Demonstration of all-optical beam steering in modulated photonic lattices," *Optics Letters*, vol. 31, pp. 1498–1500, May 2006.

[95] H. Schmidt and A. R. Hawkins, "Optofluidic waveguides: I. Concepts and implementations," *Microfluidics and Nanofluidics*, vol. 4, pp. 3–16, Aug. 2007.

[96] D. Psaltis, S. R. Quake, and C. Yang, "Developing optofluidic technology through the fusion of microfluidics and optics," *Nature*, vol. 442, pp. 381–386, July 2006.

[97] P. Abgrall, C. Lattes, V. Conédéra, X. Dollat, S. Colin, and A. M. Gué, "A novel fabrication method of flexible and monolithic 3D microfluidic structures using lamination of SU-8 films," *Journal of Micromechanics and Microengineering*, vol. 16, pp. 113–121, Jan. 2006.

[98] L. Zhu, Y. Huang, and A. Yariv, "Integration of a multimode interference coupler with a corrugated sidewall Bragg grating in planar polymer waveguides," *Photonics Technology Letters, IEEE*, vol. 18, no. 6, pp. 740–742, 2006.

[99] F. Lederer, G. Stegeman, D. Christodoulides, G. Assanto, M. Segev, and Y. Silberberg, "Discrete solitons in optics," *Physics Reports*, vol. 463, pp. 1–126, July 2008.

[100] S. Somekh and H. L. Garvin, "Channel Optical Waveguides and Directional Couplers in GaAs-lmbedded and Ridged," *Applied Optics*, vol. 13, no. 2, pp. 327–330, 1974.

[101] A. L. Jones, "Coupling of Optical Fibers and Scattering in Fibers," *Journal of the Optical Society of America*, vol. 55, no. 3, pp. 261–269, 1965.

[102] K. M. Davis, K. Miura, N. Sugimoto, and K. Hirao, "Writing waveguides in glass with a femtosecond laser," *Optics Letters*, vol. 21, no. 21, pp. 1729–1731, 1996.

[103] M. Matuszewski, C. R. Rosberg, D. N. Neshev, A. A. Sukhorukov, A. Mitchell, M. Trippenbach, M. W. Austin, W. Krolikowski, and Y. S. Kivshar,

"Crossover from self-defocusing to discrete trapping in nonlinear waveguide arrays.," *Optics Express*, vol. 14, pp. 254–259, Jan. 2006.

[104] A. Fratalocchi, G. Assanto, K. A. Brzdakeiwicz, and M. A. Karpierz, "Optical multiband vector breathers in tunable waveguide arrays," *Optics Letters*, vol. 30, no. 2, pp. 174–176, 2005.

[105] P. Domachuk, H. C. Nguyen, B. J. Eggleton, M. Straub, and M. Gu, "Microfluidic tunable photonic band-gap device," *Applied Physics Letters*, vol. 84, no. 11, pp. 1838–1840, 2004.

[106] P. D. Rasmussen, F. H. Bennet, D. N. Neshev, A. A. Sukhorukov, C. R. Rosberg, W. Krolikowski, O. Bang, and Y. S. Kivshar, "Observation of two-dimensional nonlocal gap solitons," *Optics Letters*, vol. 34, pp. 295–297, Feb. 2009.

[107] U. Bog, C. L. C. Smith, M. W. Lee, S. Tomljenovic-hanic, C. Grillet, C. Monat, L. O. Faolain, C. Karnutsch, T. F. Krauss, R. C. Mcphedran, and B. J. Eggleton, "High-Q microfluidic cavities in silicon-based two-dimensional photonic crystal structures," *Optics Letters*, vol. 33, no. 19, pp. 2206–2208, 2008.

[108] D. Christodoulides and E. D. Eugenieva, "Blocking and Routing Discrete Solitons in Two-Dimensional Networks of Nonlinear Waveguide Arrays," *Physical Review Letters*, vol. 87, p. 233901, 2001.

[109] M. Vieweg, T. Gissibl, S. Pricking, B. Kuhlmey, D. Wu, B. Eggleton, and H. Giessen, "Ultrafast nonlinear optofluidics in selectively liquid-filled photonic crystal fibers," *Optics Express*, vol. 18, no. 24, pp. 25232–25240, 2010.

[110] A. Sukhorukov, D. Neshev, W. Krolikowski, and Y. Kivshar, "Nonlinear Bloch-Wave Interaction and Bragg Scattering in Optically Induced Lattices," *Physical Review Letters*, vol. 92, p. 093901, Mar. 2004.

[111] T. Anker, M. Albiez, R. Gati, S. Hunsmann, B. Eiermann, A. Trombettoni, and M. K. Oberthaler, "Nonlinear Self-Trapping of Matter Waves in Periodic Potentials," *Physical Review Letters*, vol. 94, p. 020403, 2005.

[112] T. J. Alexander, E. Ostrovskaya, and Y. Kivshar, "Self-Trapped Nonlinear Matter Waves in Periodic Potentials," *Physical Review Letters*, vol. 96, p. 040401, Jan. 2006.

[113] J. Wang, J. Yang, T. J. Alexander, and Y. Kivshar, "Truncated-Bloch-wave solitons in optical lattices," *Physical Review A*, vol. 79, p. 043610, Apr. 2009.

[114] L. Deng, E. W. Hagley, J. Wen, M. Trippenbach, Y. Band, P. S. Julienne, J. E. Simsarian, K. Helmerson, S. L. Rolston, and W. D. Phillips, "Four-wave mixing with matter waves," *Nature*, vol. 398, no. March, pp. 218–220, 1999.

[115] L. Khaykovich, F. Schreck, G. Ferrari, T. Bourdel, J. Cubizolles, L. D. Carr, Y. Castin, and C. Salomon, "Formation of a matter-wave bright soliton.," *Science*, vol. 296, pp. 1290–1293, May 2002.

[116] J. Yang, P. Zhang, M. Yoshihara, Y. Hu, and Z. Chen, "Image transmission using stable solitons of arbitrary shapes in photonic lattices," *Optics Letters*, vol. 36, pp. 772–774, Mar. 2011.

[117] M. Rosenkranz, D. Jaksch, F. Yin Lim, and W. Bao, "Self-trapping of Bose-Einstein condensates expanding into shallow optical lattices," *Physical Review A*, vol. 77, p. 063607, June 2008.

[118] D. Neshev, A. Sukhorukov, A. Dreischuh, R. Fischer, S. Ha, J. Bolger, L. Bui, W. Krolikowski, B. J. Eggleton, A. Mitchell, M. Austin, and Y. Kivshar, "Nonlinear Spectral-Spatial Control and Localization of Supercontinuum Radiation," *Physical Review Letters*, vol. 99, p. 123901, Sept. 2007.

[119] A. S. Desyatnikov, D. N. Neshev, Y. S. Kivshar, N. Sagemerten, D. Träger, J. Jägers, C. Denz, and Y. V. Kartashov, "Nonlinear photonic lattices in anisotropic nonlocal self-focusing media," *Optics Letters*, vol. 30, pp. 869–871, Apr. 2005.

[120] G. L. Alfimov, V. V. Konotop, and M. Salerno, "Matter solitons in Bose-Einstein condensates with optical lattices," *Europhysics Letters*, vol. 58, pp. 7–13, Apr. 2002.

[121] V. V. Konotop and M. Salerno, "Small-amplitude excitations in a deformable discrete nonlinear Schrodinger equation," *Physical Review E*, vol. 55, pp. 4706–4712, 1997.

[122] A. Samoc and I. Introduction, "Dispersion of refractive properties of solvents: Chloroform, toluene, benzene, and carbon disulfide in ultraviolet, visible, and near-infrared," *Journal of Applied Physics*, vol. 94, no. 9, pp. 6167–6174, 2003.

[123] S. F. Mingaleev, Y. S. Kivshar, and R. A. Sammut, "Long-range interaction and nonlinear localized modes in photonic crystal waveguides," *Physical Review E*, vol. 62, pp. 5777–5782, 2000.

[124] A. Minovich, D. N. Neshev, A. Dreischuh, W. Krolikowski, and Y. S. Kivshar, "Experimental reconstruction of nonlocal response of thermal nonlinear optical media," *Optics Letters*, vol. 32, no. 12, pp. 1599–1601, 2007.

[125] C. Rotschild, B. Alfassi, O. Cohen, and M. Segev, "Long-range interactions between optical solitons," *Nature Physics*, vol. 2, no. November, pp. 769–774, 2006.

[126] Z. Xu, Y. V. Kartashov, and L. Torner, "Soliton mobility in nonlocal optical lattices," *Physical Review Letters*, vol. 951, p. 113905, 2005.

[127] Z. Xu, Y. V. Kartashov, and L. Torner, "Gap solitons supported by optical lattices in photorefractive crystals with asymmetric nonlocality.," *Optics Letters*, vol. 31, pp. 2027–2029, July 2006.

[128] Y. Lin, I.-h. Chen, and R.-k. Lee, "Breather-like collision of gap solitons in Bragg gap regions within nonlocal nonlinear photonic crystals," *Journal of Optics A*, vol. 10, no. 4, p. 044017, 2008.

[129] N. K. Efremidis, "Nonlocal lattice solitons in thermal media," *Physical Review A*, vol. 77, p. 063824, 2008.

[130] P. J. Y. Louis, E. A. Ostrovskaya, C. M. Savage, and Y. S. Kivshar, "Bose-Einstein condensates in optical lattices: Band-gap structure and solitons," *Physical Review A*, vol. 67, p. 013602, 2003.

[131] J. D. Joannopoulos, R. D. Meade, and J. N. Winn, *Photonic Crystals: Modeling the Flow of Light*. Princeton: Princeton University Press, 1995.

[132] J. T. Mok, C. M. de Sterke, I. C. M. Littler, and B. J. Eggleton, "Dispersionless slow light using gap solitons," *Nature Physics*, vol. 2, pp. 775–780, Oct. 2006.

[133] Y. S. Kivshar and G. P. Agrawal, *Optical Solitons: From Fibres to Photonic Crystals*. San Diego: Academic Press, 2003.

[134] R. F. Nabiev, P. Yeh, and D. Botez, "Spatial gap solitons in periodic nonlinear structures," *Optics Letters*, vol. 18, pp. 1612–1614, Oct. 1993.

[135] J. Feng, "Alternative scheme for studying gap solitons in an infinite periodic Kerr medium," *Optics Letters*, vol. 18, pp. 1302–1304, Aug. 1993.

[136] K. G. Makris, S. Suntsov, D. Christodoulides, G. I. Stegeman, and A. Hache, "Discrete surface solitons," *Optics Letters*, vol. 30, pp. 2466–2468, Sept. 2005.

[137] E. Smirnov, M. Stepić, C. Rüter, D. Kip, and V. Shandarov, "Observation of staggered surface solitary waves in one-dimensional waveguide arrays.," *Optics letters*, vol. 31, pp. 2338–2340, Aug. 2006.

[138] G. Siviloglou, K. Makris, R. Iwanow, R. Schiek, D. Christodoulides, G. Stegeman, Y. Min, and W. Sohler, "Observation of discrete quadratic surface solitons," *Optics Express*, vol. 14, no. 12, pp. 5508–5516, 2006.

[139] A. Szameit, Y. Kartashov, F. Dreisow, T. Pertsch, S. Nolte, A. Tünnermann, and L. Torner, "Observation of Two-Dimensional Surface Solitons in Asymmetric Waveguide Arrays," *Physical Review Letters*, vol. 98, p. 173903, Apr. 2007.

[140] S. Suntsov, K. Makris, D. Christodoulides, G. Stegeman, A. Haché, R. Morandotti, H. Yang, G. Salamo, and M. Sorel, "Observation of Discrete Surface Solitons," *Physical Review Letters*, vol. 96, p. 063901, Feb. 2006.

[141] A. Szameit, Y. V. Kartashov, V. A. Vysloukh, and M. Heinrich, "Angular surface solitons in sectorial hexagonal arrays," *Optics Letters*, vol. 33, no. 13, pp. 1542–1544, 2008.

[142] K. T. Gahagan and G. A. Swartzlander, "Simultaneous trapping of low-index and high-index microparticles observed with an optical-vortex trap," *Journal of the Optical Society of America B*, vol. 16, no. 4, pp. 533–537, 1999.

[143] A. Truscott, M. Friese, N. Heckenberg, and H. Rubinsztein-Dunlop, "Optically Written Waveguide in an Atomic Vapor," *Physical Review Letters*, vol. 82, pp. 1438–1441, Feb. 1999.

[144] A. Ferrando, M. Zacares, P. Fernandez De Cordoba, D. Binosi, and J. A. Monsoriu, "Vortex solitons in photonic crystal fibers," *Optics Express*, vol. 12, no. 5, pp. 817–822, 2004.

[145] M. Johansson, S. Aubry, Y. B. Gaididei, P. L. Christiansen, and K. Rasmussen, "Dynamics of breathers in discrete nonlinear Schrödinger models," *Physica D*, vol. 119, pp. 115–124, Aug. 1998.

[146] P. Kevrekidis, B. Malomed, A. Bishop, and D. Frantzeskakis, "Localized vortices with a semi-integer charge in nonlinear dynamical lattices," *Physical Review E*, vol. 65, p. 016605, Dec. 2001.

[147] P. Kevrekidis, B. Malomed, and Y. Gaididei, "Solitons in triangular and honeycomb dynamical lattices with the cubic nonlinearity," *Physical Review E*, vol. 66, p. 016609, July 2002.

[148] J. Yang and Z. H. Musslimani, "Fundamental and vortex solitons in a two-dimensional optical lattice," *Optics Letters*, vol. 28, no. 21, pp. 2094–2096, 2003.

[149] T. J. Alexander, A. S. Desyatnikov, and Y. S. Kivshar, "Multivortex solitons in triangular photonic lattices," *Optics Letters*, vol. 32, no. 10, pp. 1293–1295, 2007.

[150] Z. Chen, M. F. Shih, M. Segev, D. W. Wilson, R. E. Muller, and P. D. Maker, "Steady-state vortex-screening solitons formed in biased photorefractive media.," *Optics Letters*, vol. 22, pp. 1751–1753, Dec. 1997.

[151] J. Salgueiro and Y. Kivshar, "Single- and double-vortex vector solitons in self-focusing nonlinear media," *Physical Review E*, vol. 70, p. 056613, Nov. 2004.

[152] H. Michinel, J. Salgueiro, and M. Paz-Alonso, "Square vortex solitons with a large angular momentum," *Physical Review E*, vol. 70, p. 066605, Dec. 2004.

[153] M. Paz-Alonso, D. Olivieri, H. Michinel, and J. Salgueiro, "Collisional dynamics of vortices in light condensates," *Physical Review E*, vol. 69, p. 056601, May 2004.

[154] D. Song, C. Lou, K. J. H. Law, L. Tang, Z. Ye, P. G. Kevrekidis, J. Xu, and Z. Chen, "Self-trapping of optical vortices at the surface of an induced semi-infinite photonic lattice," *Optics Express*, vol. 18, pp. 5873–5878, Mar. 2010.

[155] A. Szameit, Y. V. Kartashov, M. Heinrich, F. Dreisow, and T, "Observation of two-dimensional defect surface solitons," *Optics Letters*, vol. 34, no. 6, pp. 797–799, 2009.

[156] M. I. Molina, R. A. Vicencio, and Y. S. Kivshar, "Discrete solitons and nonlinear surface modes in semi-infinite waveguide arrays," *Optics Letters*, vol. 31, pp. 1693–1695, June 2006.

[157] S. Ghosh, W. Bao, D. L. Nika, S. Subrina, E. P. Pokatilov, C. N. Lau, and A. a. Balandin, "Dimensional crossover of thermal transport in few-layer graphene," *Nature Materials*, vol. 9, pp. 555–558, May 2010.

[158] L. Rindorf, P. Hoiby, J. Jensen Bo, L. Pederson, O. Bang, and O. Geschke, "Towards biochips using microstructured optical fiber sensors," *Analytical and Bioanalytical Chemistry*, vol. 385, pp. 1370–1375, 2006.

[159] M. Schmidt, L. Prill Sempere, H. Tyagi, C. Poulton, and P. Russell, "Waveguiding and plasmon resonances in two-dimensional photonic lattices of gold and silver nanowires," *Physical Review B*, vol. 77, p. 033417, Jan. 2008.

[160] C. G. Poulton, M. A. Schmidt, G. J. Pearce, G. Kakarantzas, and P. S. J. Russell, "Numerical study of guided modes in arrays of metallic nanowires," *Optics Letters*, vol. 32, pp. 1647–1649, June 2007.